Rechargeable Aqueous Zn-based Energy Storage Devices

Yiyang Liu[a], Xu Lu[b], Feili Lai[c], Tianxi Liu[d], Paul R. Shearing[a, g], Ivan P. Parkin[e], Guanjie He[a,e,f]* and Dan J. L. Brett[a, g]*

a Electrochemical Innovation Lab (EIL), Department of Chemical Engineering, University College London (UCL), London WC1E 7JE, UK.

b Clean Combustion Research Center, Division of Physical Sciences and Engineering, 4700 King Abdullah University of Science and Technology (KAUST), Thuwal 23955-6900, Kingdom of Saudi Arabia

c Department of Chemistry, KU Leuven, Celestijnenlaan 200F, Leuven 3001, Belgium

d The Key Laboratory of Synthetic and Biological Colloids, Ministry of Education, School of Chemical and Material Engineering, Jiangnan University, Wuxi 214122, P. R. China

e Christopher Ingold Laboratory, Department of Chemistry, University College London (UCL), 20 Gordon Street, London WC1H 0AJ, UK.

f School of Chemistry, University of Lincoln, Brayford Pool, Lincoln, LN6 7TS, UK.

g The Faraday Institution, Quad One, Becquerel Avenue, Harwell Campus, OX11 ORA, UK.

E-mail: g.he@ucl.ac.uk; d.brett@ucl.ac.uk.

Abstract

Since the emergence of the first electrochemical energy storage (EES) device in 1799, various types of aqueous Zn-based EES devices (AZDs) have been proposed and studied. The benefits of EES devices using Zn anodes and aqueous electrolytes are well-established and include competitive electrochemical performance, low cost, ease of manufacture, good safety, and environmentally benign characters. Over 50 different types of AZDs (the combination of electrodes and configurations) have been invented; some of them have dominated the current primary battery market, while others are considered promising next-generation EES devices.

While most of the existing reviews in this area consider the progress of a particular device or single component, this work adopts a holistic perspective to summarize and review all types of key devices and representative AZDs. First, this work will discuss electrochemical charge storage mechanisms and interface properties in AZDs. Next, the classification, challenges, recent progress and promising strategies of each key component will be provided. Finally, the way in which components can be assembled to meet the requirements of specific scenarios, including high

capacity, (ultra)high power or high-energy applications, will be considered. This work does not attempt to introduce all recent progress, but only discuss the most representative work with a view to figure out suitable directions for the advancement of this field.

1. Introduction

The megatrend of electrification will continue to expand for achieving regional and global carbon neutrality.[1,2] Therefore, the development of advanced electrochemical energy storage (EES) technologies and their employments in applications including grid-scale energy storage, portable electronics and electric vehicles, have become increasingly important in recent years.[3,4] Since the first commercialization in 1990, lithium-ion batteries (LIBs) have successfully dominated the EES market.[5] In particular, the past ten years have witnessed the unit energy storage cost decrease by ~9 times to 137 USD per kWh due to the device performance improvement and manufacturing cost reduction, which has significantly promoted the electrification process based on high energy density devices.[6] However, LIBs still face a series of endogenous challenges, such as: a) flammable organic electrolytes increase potential safety risks, especially for grid-scale applications; b) the uneven geographical distribution of raw materials leads to potential shortage of supply chains; c) limited raw material reserves induce the difficulty to further reduction of costs.[7–9]

1.1 Market demand and gaps of EES devices

Figure 1 provides a map of the range of performance requirements for EES applications. The quarter-circle is divided into nine parts: from top to bottom, it is divided into three parts, representing the areas where high energy density, high power density, and ultrahigh power density applications are located. From the inside to the outside, it is also divided into three regions, which respectively represent the performance requirements of the outdated, current and future EES devices. Although commercial LIBs currently occupy ~95% of the EES market share, their performance characteristics

are mainly concentrated in the 'current high energy density' and lower position of 'current high power density' regions. LIBs possess relatively good energy density (150~300 Wh kg^{-1}) and durability; however, despite years of improvements, their poor power density (160~340 W kg^{-1}) and long response times (minutes to hours) make them difficult to be competitive in future ultra(high) power applications.[10] Hence, there exists a technology gap and huge market potentials for (ultra)high power density devices.

The adaptability of various EES technologies in representative scenarios is shown in Figure 2. Older generation EES technologies, such as lead-acid (Pb-acid) and nickel-metal hydride (Ni-MH) batteries are gradually being withdrawn; meanwhile, evolving application requirements means that LIBs are struggling to meet the demands of various scenarios.[11]

1.2 Aqueous Zn-based EES devices (AZDs)

Rechargeable aqueous Zn-based EES devices (AZDs) have proven to be promising candidates in multiple application scenarios (Figure 2). Compared with non-aqueous systems, aqueous electrolytes possess certain attractive features, including: a) higher ionic conductivity (1~100 S m^{-1}) compared with organic electrolytes (10^{-6}~10^{-3} S m^{-1}), such as 1 M KOH (18.4 S m^{-1}), thus providing higher power densities and fast-charging capabilities; b) minimized potential risks due to low-volatile, non-toxic, and non-flammable characteristics; c) lower manufacturing costs by excluding oxygen-free and drying production lines; d) high tolerance against electrical and mechanical mishandling[7,12]. Also, compared with mainstream EES technologies, the use of Zn anodes has merits such as: a) high redox potential (-0.763 V $vs.$ SHE), high density (7.140 g cm^{-3}), and two-electron transfer process, which leads to a large theoretical volumetric energy density (5855 mAh cm^{-3} compared to 2061 mAh cm^{-3} for Li-metal anodes); b) much lower cost of Zn-metals (~3,000 USD per ton) than that of Li (~18,000 USD per ton), due to their high abundance in the Earth's crust and the convenience of refining and recycling; c) lower toxicity and improved safety.[4,13]

Research on AZDs has lasted for over 200 years (Figure 3). At the initial stage of industrialization (1784~1870), the voltaic pile (Zn-Cu) was invented in 1799 and gave birth to a series of other important discoveries, such as the electrolysis to separate sodium (1807), potassium (1807), and calcium (1808).[14] Subsequently, Daniel cells (1836) and Grove cells (1839) derived from the voltaic pile, provided the power for the entire 19th-century industry until the advent of the generator in 1870.[15] In the Industry 2.0 stage (1870~1969), when mass production began, primary Zn-C dry batteries (1886), primary Zn-MnO$_2$ alkaline batteries (1932) and primary Zn-Ag batteries (1952) were invented and are still in use today.[16–18] Thomas Edison also explored rechargeable Zn-Ni batteries (1901), but the commercialization process was interrupted due to the self-discharge issue and the formation of Zn dendrites.[19] The major breakthroughs in microelectronics in the 1970s marked the prelude to Industry 3.0 (1969-2010) and gave birth to the emergence of portable electronics; these also put forward higher requirements of energy/power densities and durability for EES devices.[20] From 1970 to 1980, although numerous studies have focused on the rechargeable Zn-MnO$_2$ alkaline batteries, including charge storage mechanisms, electrode materials and electrolytes, these efforts did not make them commercially viable.[21,22] In 1986, Yamamoto *et al.* first proposed a rechargeable mildly acidic Zn|ZnX|MnO$_2$ battery (X = SO$_4$, Cl, NO$_3$, BF$_4$, SiF$_6$, *etc.*), which demonstrates good reversibility.[12] Subsequently, in 2011, Kang *et al.* proved the presence of reversible Zn^{2+} (de)intercalation in the mildly acidic Zn-MnO$_2$ battery; therefore, these types of AZDs are also known as aqueous Zn-ion battery (AZIB).[23] In addition, a variety of Zn-based redox flow batteries (ZRFBs) with long cycling stability and high depth-of-discharge (DoD) have been invented, such as Zn-Br$_2$ flow batteries and Zn-Ni flow batteries, whose overall performance cannot match that of LIBs.[24,25]

In the Industry 4.0 era (since 2010), the further acceleration of the electrification process has spawned various application scenarios of next-generation EES devices with different demands. In this context, LIBs will not be able to dominate all markets. Fortunately, building on the accumulation of AZD research, in recent years a series of breakthroughs have put AZDs at a critical point that marks a renaissance in this technology. First, the advances in the electrolyte and Zn anodes have successfully

enhanced the durability of rechargeable AZDs to thousands or even tens of thousands of cycles.[26] Moreover, several promising strategies to increase the operating potential window of aqueous electrolytes have been proposed, such as 'water-in-salt' (WIS) electrolytes and the double-membrane configuration.[27,28] Additionally, a number of emerging high-performance AZDs have been designed, including: a) Zn-based solid-phase conversion-type batteries (ZSCBs) using Zn anodes and chalcogen (S, Se, and polysulfides) or halogen-based (I) cathodes with ultra-high specific capacity; b) Zn-ion hybrid supercapacitors (ZHSCs, or 'supercapatteries') with both high energy and high power densities; c) novel ZRFBs based on MnO_2, V and I_2 redox chemistry.[29–35]

1.3 Challenges of AZDs

Currently, AZDs are facing following major obstacles:

(a) **Zn anode issues** include uneven electrodeposition, limited reversibility, hydrogen evolution, Zn dendrite formation, low Zn utilization rate and passivation, causing low Coulombic efficiency (CE);

(b) **Low operating voltage** results from the narrow electrochemical stable potential window (ESPW) of water (1.23 V *vs.* SHE), limiting the energy density of AZDs;

(c) **Sluggish Zn-ion diffusion** associated with the high charge density of the Zn ion increases difficulties in developing high-performance cathode materials and limits the utilization rate of cathode active materials, which leads to an inadequate areal capacity;

(d) **Poor cathode stability** in aqueous media caused by active material dissolution, phase change, and structure collapse;

(e) **Expensive and non-persistent membrane materials** cause active substance crossover, self-discharge, reduce CE and increase the cost of AZDs containing membranes;

(f) **Limited electrolyte energy density** results from limited solubility of active substances, which leads to low energy efficiency (EE) and voltage efficiency (VE);

(g) **Insufficient electrocatalytic activities** in air cathodes for ZABs and electrodes for some ZRFBs raise the overpotential and limit device round-trip efficiency.

Usually, each type of AZDs simultaneously faces 3~7 of above-mentioned major obstacles, which dramatically increases the difficulty to commercialization. Since the performance of EES devices is mainly relevant to the electrochemical characteristics of the key components and their mutual interactions; hence, solving these issues requires breakthroughs in both materials discovery (anode, electrolyte, cathode and membrane materials) and cell configuration innovation (the combination of membranes and flow systems).

Currently, numerous reviews on AZDs merely focused on a specific component or device. On one hand, it is difficult to provide researchers with a view of the device development level, which inhibits the further commercialization of AZDs; on the other hand, the completed knowledge of the entire AZDs field has not been provided, thus restricting researchers from being inspired by researches on other similar Zn electrochemical systems. Therefore, this work uses a holistic perspective to review all types of key devices and representative AZDs. First, this work will discuss the electrochemical charge storage mechanisms and interface properties in AZDs. Then, the classification, challenges, recent progress and promising strategies of each key component will be provided. Next, conventional and emerging devices for four major application scenarios (high-capacity, (ultra)high power density, and high energy density) are summarized. Since the AZD is a broad topic, this review will not attempt to consider the progress in all aspects, but rather an in-depth discussion of representative examples for each device or individual component. Finally, future prospects and possible reconstruction strategies of key components for boosting overall performance are provided.

2. Fundamental electrochemistry of Zn-based EES devices

2.1 Energy storage mechanisms of Zn-based EES devices

From the perspective of classical electrochemical theories, charge storage mechanisms in AZDs can be classified as: a) capacitive process that creates an electrical double-layer (EDL), where charge is stored electrostatically; b) Faradaic process (battery-type behavior) that results from the valence electron transfer, the thermodynamics of which is governed by the Nernst equation; c) capacitive-Faradaic process (pseudocapacitive behavior), which is caused by the fast and reversible redox reactions at the surface or near-surface of active materials.[2,36] Figure 4a and 4b exhibit the electrochemical characteristics of the devices with the above three mechanisms, in the form of cyclic voltammogram (CV) curves and galvanostatic charge-discharge (GCD) profiles, respectively. A standard capacitive process comes with a rectangular CV curve and a linear GCD profile with respect to time, while a typical Faradaic process has obvious redox peaks in CV curves and detectable plateaus from GCD profiles. For a capacitive-Faradaic process, it generally possesses an approximately rectangular CV curve, as well as an almost linear GCD profile, without obvious plateaus.

However, merely observing charge/discharge behaviors, such as redox peaks in the CV curves and plateaus in the GCD profiles, may not be sufficient to identify energy storage mechanisms. For instance, as the size of $LiCoO_2$ is reduced to nanoscale, its plateaus on the potential-capacity (PC) curve gradually disappear and lead to an approximately linear shape, which is indicative of pseudocapacitive behavior (Figure 4d).[37] However, $LiCoO_2$ is a typical battery-type material with a Faradaic process and (de)insertion mechanisms; one possible explanation is that nanoscale effects rapidly increase the surface area of $LiCoO_2$ and make the redox reactions less restricted by the diffusion process, thus leading to a pseudocapacitive profile. Since (de)insertion is a unique mechanism, whose host lattice has undergone a very small structural transformation, thus resulting in negligible differences between pseudocapacitive electrodes and insertion-typed electrodes.[38] In 1999, Levi and Aurbach recognized the mechanistic similarity between surface adsorption and ion insertion into a host material.[39] After 16 years, by observing the electrochemical capacitive paradox of 2D

$Ti_3C_2T_x$ MXene electrodes, they proposed the concept of shallow *vs.* deep "adsorption" sites to identify pseudocapacitive materials and insertion-type materials.[40]

The kinetic analysis could be a more accurate identification method. As shown in the Nyquist plot (Figure 4c), an ideal capacitive process is surface-controlled, and an ideal Faradaic process is diffusion-controlled[41]. It is worth noting that the capacitive-Faradaic behavior possesses all regions (semi-circle, 45° and 90° straight line), which exhibits both EDLC and battery-type characteristics. However, distinguishing energy storage mechanisms from the Nyquist plot can be confusing due to factors such as measurement errors or contact resistance between collectors and electrodes. Simon and colleagues also proposed a quantitative method for the differentiation, based on the relationship between peak currents (i, A) and scan rates (v, mV s^{-1})[42]. For a capacitive process with surface-controlled kinetics, the peak current (i, A) varies with the scan rate (v, mV s^{-1}); while for a Faradaic process limited by semi-infinite diffusion, i varies as $v^{1/2}$. This relationship could be expressed as $i = av^b$,[37] where the value of b helps identify the charge storage mechanisms: a) $b = 1$ for ideal EDLC behavior; b) $b \approx 1$ for pseudocapacitive behavior; c) $0.5 < b < 1$ for battery-type dominated behavior. It is noted that the value of b could be > 0.5 when the redox process is not limited by the diffusion process.

Although the capacitive-Faradaic behavior can be caused by the fast and reversible redox reactions, it cannot be simply explained and predicted by the Nernst equation.[2,36] For instance, there is a continuous and constant influence in a noticeable potential range from the CV curve (Figure 4d). Chen *et al.* suggested that this behavior could be explained by a semi-conductor model, which is based on metals from separated and non-interactive atoms to weighable clusters with $> 10^{20}$ atoms (Figure 4e).[9] With the increase of the number of atoms in the cluster, the bandgap between the valence band (VB) and the conduction band (CB) will decrease, and the degree of electron delocalization will increase, which leads to a transformation from an insulator to a semiconductor or conductor. Currently, a wide range of semiconductors have been reported to possess pseudocapacitive properties, such as RuO_2 and MnO_2.[43] In general, a semiconductor has many orbitals with close energy levels

over a wide range; hence, a small potential change may cause an electron transfer, which leads to the linearly varying potential under a constant current.

For the convenience of discussion, the charge and energy storage mechanisms in this article are divided into non-Faradaic capacitive (NFC), non-capacitive Faradaic (NCF) and capacitive-Faradaic (CF) processes[9]. It can be further subdivided according to different components of AZDs, which will be discussed in the following sections.

2.2 Interfaces and interphases in aqueous Zn-based EES devices

The ESPW is highly relevant to electrode-electrolyte interfaces (EEI) consisting of the cathode–electrolyte interface (CEI) and anode–electrolyte interface (AEI). The electrolyte ESPW (E_s) is the difference between the energy of the lowest unoccupied molecular orbital (LUMO) and the highest occupied molecular orbital (HOMO); μ_A and μ_C are electrochemical potentials of the anode and cathode, respectively.[44] Theoretically, increasing the potential difference between the anode and the cathode can improve the energy density. However, when μ_A is higher than the LUMO energy, it will reduce the electrolyte; similarly, if the μ_C is lower than the HOMO energy, it will oxidize the electrolyte. For batteries using organic electrolytes (Figure 5a), the former and the latter will cause the formation of CEI and solid–electrolyte interface (SEI) films, respectively. Nevertheless, there are no SEI or CEI films in aqueous batteries (Figure 5b); instead, hydrogen evolution reaction (HER) and oxygen evolution reactions (OER) occur at the anode and the cathode, respectively. Practically, the output voltage (E) is generally higher than the ESPW of pure water (~ 1.23 V *vs.* SHE), due to the sluggish kinetics of HER and OER and their corresponding high overpotentials.

Figure 5c and d demonstrate possible interfaces in AZDs based on liquid electrolytes (LEs) and solid electrolytes (SEs), respectively. It should be noted that the interfaces involving gas molecules are also taken into consideration, which are available only for AZDs with gas-phase reactions such as Zn-air batteries (ZABs). Inspired by A. Banerjee *et al.*, this review identifies these interfaces into following four categories:[45]

1) **Void.** The existence of voids has following hazards: (a) hinder mass transfer; (b) increase contact resistance and deteriorate the charge transfer; (c) increase battery volume, thus reducing volumetric energy density; (d) reduce the utilization rate of active materials. For LEs, the formation of voids is mainly related to the battery fabrication process. For instance, when the ratio of active materials, conductive additives, and binders in the cathode is not appropriate, the generation of voids may be aggravated. To reduce voids, higher pressure can be applied during the manufacturing process; however, excessive pressure may cause the crack formation. Generally, SE cannot flow or penetrate into the gaps and pores in AZDs, which will produce more voids than LE. For example, the voids between the (coated) Zn metal anode and the SE will cause uneven current distribution, thereby exacerbating the growth of Zn dendrites and the formation of by-products. In addition, SE will generate intrinsic voids, further reducing its mechanical property and ionic conductivity.

2) **Chemical reaction.** When two materials with mismatched chemical potentials come into contact, a spontaneous chemical reaction will occur. Although AZDs do not produce SEI film during charge and discharge, spontaneous chemical reactions may occur when Zn metal and electrolyte are in direct contact, aggravating many problems such as self-discharge, hydrogen evolution, Zn dendrite growth, and formation of by-products. To suppress these issues, numerous efforts are devoted to constructing artificial SEI layers by coating polymers or inorganic substances on the Zn surface that are only conductive to Zn-ions.[46] Also, the deployment of hydrogel electrolytes could introduce the solid-solid interface between electrodes and electrolytes (instead of SEI) and reduce the water content, which can alleviate the growth of Zn dendrites, water-induced side reactions, and the dissolution of cathode materials.[44] In addition, the contact of the gas with the electrolyte may cause spontaneous chemical reactions. For example, in ZABs, CO_2 in the air may react with the alkaline electrolyte and form carbonate, which will block the pores of electrodes.

3) **Electrochemical reaction.** The regions where the electrolytes are in direct contact with the (coated) electrodes are the key interfaces where the electrochemical processes occur. Regardless

of the surface-controlled EDLC/pseudocapacitive process or the diffusion-controlled Faradaic process, the common strategies to improve the interface performance are: (a) improve the wettability of the electrolyte, and (b) optimize the electrode surface morphology. However, the contact between the electrolyte and the current collector or conductive additives may be harmful, which may lead to electrode passivation and parasitic side reactions such as hydrogen evolution and decomposition of the electrolyte. In addition, due to the limitation of the water electrolysis, the ESPW of most aqueous electrolytes is relatively narrow, which is lower than the entire voltage range of anode and cathode materials. Therefore, to reduce the electrochemical reactivity of the electrolyte, it is beneficial to couple the electrolyte and electrode with a matched operating voltage window and slow down the reaction kinetics.

4) **Grain boundary.** A grain boundary (GB) exists when two particles with different electrochemical potentials are in contact. Extensive investigations have revealed that the existence of GB will cause blocking effects and significantly reduce ion conductivity, which has been attributed to three potential causes: (a) ion transport barriers induced by structural distortions in the GB core area; (b) charge carriers near GBs are depleted, due to the space charge effect; (c) new phase formation with low ionic conductivity.[47,48] There are two types of GBs in AZDs: the first type is formed at the cathode active material/conductive additive interface, another type is present at the electrolyte-electrolyte interface in SE-based AZDs.

At present, the investigation of interface properties in AZDs is still in its infancy. Further research on interface properties in spatial and temporal scales (*e.g.*, mass transport, charge transfer, GB, phase transition, dynamic interface evolution) is highly recommended. Although many traditional *ex-situ* characterization techniques have provided basic understandings of the relationship between interfacial properties and electrochemical behaviors, it may not be possible to fully avoid the effects of potential contamination and artifacts. Hence, it is urgent to use *in-situ* or operando technologies to isolate and identify different interfacial components, thus tracking the evolution of the real-time interfaces and more effectively guiding the rational interface design. Subsequent novel material

discoveries and manufacturing improvements are also crucial to reducing voids, GBs and harmful chemical reaction interfaces. A perfect electrochemical reaction interface requires high ionic conductivity, excellent electrical insulation, good mechanical strength and electrochemical stability. The interfacial properties of AZDs are affected by multiple vital components, including electrodes, electrolytes, current collectors, membranes, and binders. Therefore, the research on multiple core components should be conducted simultaneously. The reasonable combination of various key components becomes more critical, which will be further discussed in subsequent sections.

3 Zn anodes for aqueous Zn-based EES devices

3.1 Fundamental electrochemistry and challenges

As discussed in Section 2.1, the energy storage mechanism of Zn anodes is a typical NCF process; namely, the reversible electrodeposition/dissolution process. Generally, this consists of four steps: mass transport, desolvation, nucleation and crystal growth (Figure 6b). As an amphoteric metal, the mechanism and equilibrium potential of Zn electrode reactions are strongly influenced by the electrolyte environment. Depending on the pH of the electrolytes, $Zn(OH)_2$, $Zn(OH)_3^-$ and $Zn(OH)_4^{2-}$ are often formed by the hydrolysis of Zn^{2+}.[49] Based on the Nernst equation (*Eqn.* 1a~d), the Pourbaix diagram (Figure 6a) can be drawn.

$$Zn^{2+}(aq) + 2e^- \leftrightarrow Zn(s) \quad E_1 = -0.762 + 0.0295 \, lg[Zn^{2+}] \quad \textbf{(1a)}$$

$$Zn(OH)_2(aq) + 2e^- \leftrightarrow Zn(s) + 2OH^-(aq) \quad E_2 = -0.439 - 0.0591 \, pH \quad \textbf{(1b)}$$

$$Zn(OH)_3^-(aq) + 2e^- \leftrightarrow Zn(s) + 3OH^-(aq) \quad E_3 = -0.54 - 0.0886pH + 0.0295 \, lg[Zn(OH)_3^-] \quad \textbf{(1c)}$$

$$Zn(OH)_4^{2-}(aq) + 2e^- \leftrightarrow Zn(s) + 4OH^-(aq) \quad E_4 = -0.441 - 0.1182pH + 0.0295 \, lg[Zn(OH)_4^{2-}] \quad \textbf{(1d)}$$
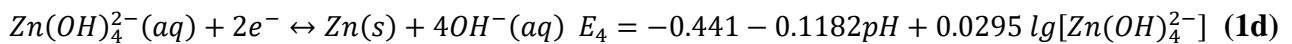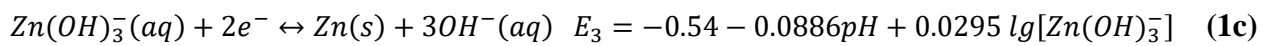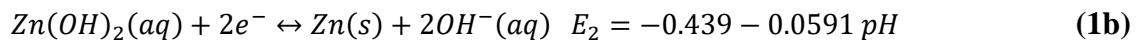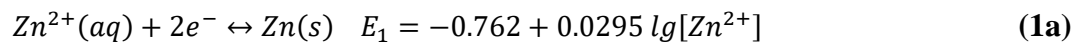
The Pourbaix diagram can be divided into four regions with different thermodynamically stable reactants in the reversible deposition/dissolution process. Since the $[Zn]_t$ in various AZDs may be different, the thermodynamically stable pH range of each reactant could be roughly given as follows:

a) Zn^{2+} in (mildly) acidic/near-neutral conditions (pH < 8); b) $Zn(OH)_2$ and $Zn(OH)_3^-$ in mildly alkaline/near-neutral conditions (pH = 8~12); c) $Zn(OH)_4^{2-}$ in the strong alkaline conditions (pH > 12).

The quality and granularity of the electrodeposition mainly depends on both the Zn nucleation and the growth process. A larger overpotential will lead to a higher nucleation rate and a finer crystal grain of deposition; when the overpotential is small, the crystal growth rate dominates, resulting in a coarser grain.[1] In addition, another notable factor is the (de)solvation of Zn-ions, whose coordination shell often changes with electrolyte ingredients[4]. Unfortunately, the electrodeposition/dissolution of the Zn is usually inhomogeneous and causes dendrite growth on the electrodes (Figure 6c). When influenced by unbalanced external forces (*e.g.*, gravity and non-uniform electric field), the migration of the Zn may lead to an irregular distribution of the concentration of active species, thus resulting in more nucleation in areas with a high Zn concentration. Then, the subsequent Zn will spontaneously nucleate and grow at the existing protrusion, which causes shape changes of the Zn anode and irreversible capacity loss.[50,51] As the cycle number increases, the continued nucleation and growth of the Zn-metal will gradually evolve into a Zn dendrite, which may penetrate into the separators and cause an internal short circuit and sudden drop of capacity/capacitance;[13] fortunately, unlike LIBs, there is no risk of explosion or combustion.

Besides, the corrosion and passivation of Zn anodes hinder the employment of secondary AZDs. Firstly, due to the poor thermodynamic stability in the aqueous solution, the parasitic self-discharge reaction may occur and generate H_2 (Figure 6d), thus corroding the electrode (*Eqn.* 2 a & b) and reducing the CE.[52] Meanwhile, the repeated deposition/dissolution process further intensifies the HER, owning to the high activity of freshly generated Zn nanocrystals. The HER in closed systems (*e.g.*, AZIBs and ZSCBs) should be of particular concern, since it may cause batteries to swell and the potential risk of electrolyte leakage and battery failure.[26]

$$Zn\,(s)\,+2H^+(aq) \leftrightarrow Zn^{2+}(aq) + H_2(g)\ (Acidic\ electrolyte) \tag{2a}$$

$$Zn\:(s)\:+2OH^-(aq)+2H_2O(l)\leftrightarrow Zn(OH)_4^{2-}(aq)+H_2(g)\:\:(Alkaline\:electrolyte)\quad\textbf{(2b)}$$
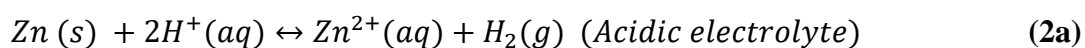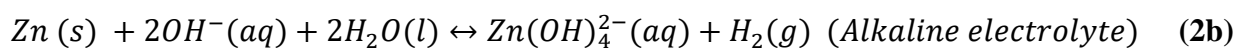
Secondly, when the $[Zn]_t$ in the electrolyte exceeds the saturation limit, solid precipitates will form in the cell, such as ZnO (in alkaline electrolyte) and $Zn_4(OH)_8SO_4$ (in the mildly acidic/near-neutral electrolytes), which may lead to the passivation of the electrode (Figure 6e). The formation of passivation films will block the transport of chemical species between electrodes and electrolytes, thus reducing the electrochemical performance and possibly causing the sudden death of batteries. Generally, the adoption of highly concentrated electrolyte and the water exhaustion due to evaporation or unfavorable reactions during cycling could exacerbate this issue.

Due to the existence of uneven deposition, dendrite growth, passivation, and hydrogen evolution, oversized Zn anodes are usually used to maintain the long-term cycling durability. Therefore, the design of AZDs should also consider the balance of cathode and anode capacity, thereby minimizing the mass and volume of the device. Depositing Zn on current collectors such as porous carbon and metal materials can achieve high DoD and Zn utilization rate. However, this strategy usually increases the volume of the battery and can only achieve a very limited Zn loading (1~8 mg cm^{-2}), which results in a low areal capacity (0.82~6.54 mAh cm^{-2}). Especially for ZRFBs, the cathode capacity is much larger than the anode, which makes it more challenging to achieve the same areal capacity as traditional liquid-liquid RFBs. The electrolyte optimization and configuration innovation can also improve the utilization rate and reversibility of Zn anodes, which will be discussed in Section 4 and 6, respectively.

3.2 Promising strategies

To address the challenges mentioned above, several strategies have been focused on the modification of electrodes and electrolytes, such as the anode structural design, interfacial modification and electrolyte engineering (*e.g.* WIS electrolytes).[53–55] The structural design of the new Zn anode promotes uniform Zn and current distribution, tolerates Zn dendrite growth and reduces the formation of by-products. These current collectors are usually carbon and metal materials with high electrical

conductivity and 3D porous nanostructured networks. Zheng and colleagues reported an epitaxial mechanism and deposited a graphene layer on the stainless steel, which epitaxially match the (002) basal plane of the Zn metal and minimize the lattice strain.[56] This strategy effectively regulates the Zn deposition with a locked crystallographic orientation, thus enabling Zn to form plates with preferential orientation parallel to the electrode. The as-prepared Zn anode yields noticeable reversibility (CE $\approx$ 99.7% over 2,000 cycles). Kang *et al.* prepared a highly stable Zn anode *via* electrodepositing Zn on a chemically etched 3D porous copper skeleton.[57] Benefiting from the open structure and high electrical conductivity of the 3D porous copper skeleton, the as-prepared Zn anode demonstrates high reversibility (CE = 99.53% over 350 h). Although the anode structural design improved the reversibility, the amount of deposited Zn on current collectors is still insufficient. For instance, the limited Zn loading on carbon (4~8 mg cm^{-2}, 3.28~6.56 mAh cm^{-2} anode) and metal networks (1~2 mg cm^{-2}, 0.82~1.64 mAh cm^{-2} anode) will lead to a poor areal capacity, which is inferior to high-capacity applications.

The second effective methodology is to construct an artificial SEI protective layer that allows ions to pass through and insulate water/electrons. These surface coatings avoid direct contact between the Zn metal and the electrolyte, thereby inhibiting self-discharge, preventing dendritic growth, reducing parasitic reactions, and facilitating uniform Zn deposition.[58] For instance, Cui and co-workers reported a "brightener-inspired'' polyamide coating layer, elevating the nucleation barrier and restricting Zn^{2+} 2D diffusion.[59] Due to the existence of hydrogen-bonding networks and the strong coordinating ability of the polyamide layer, the interfaces alleviate free water/O$_2$-induced corrosion and passivation. As a result, the as-prepared anode exhibits an ultrahigh areal capacity of 10 mA h cm^{-2} (10 mA cm^{-2}, 85% DoD) and high reversibility (CE > 99%, over 8,000 h). Unfortunately, the artificial SEI by coating inorganic materials or polymers on the Zn metal surface suffers from degradation and crack during the cycling; because these artificial interphases are not self-repairable compared to that of *in-situ* formed SEI layers.[46,60]

Rational electrolyte engineering is an effective strategy to *in-situ* construct a self-healing SEI. Wang *et al.* reported a trimethylethyl ammonium trifluoromethanesulfonate (Me$_3$EtNOTF) additive, engendering the *in-situ* formation of a Zn^{2+}-conducting and waterproof SEI.[60] This additive successfully improved Zn electroplating/deposition CE in trifluoromethanesulfonate (Zn(OTF)$_2$) electrolyte from 87.6% to 99.9% in a Ti||Zn asymmetric anode-free pouch cell for 1,000 cycles. Moreover, the as-assembled Zn||MnO$_2$ full battery exhibited a 100% DoD (based on Zn anode), remarkable energy density (218 Wh kg^{-1}, based on the weight of the cathode and anode) and high capacity retention (88.5% after 1,000 cycles). Afterwards, they further developed a Zn(OTF)$_2$-Zn(NO$_3$)$_2$ electrolyte, which will form a self-repairing Zn$_5$(OH)$_8$(NO$_3$)$_2 \cdot$ 2H$_2$O passivation layer, thus blocking water penetration and completely prevented the hydrogen evolution.[46] In addition to the intermediate passivation layer, this film consists of a highly flexible organic outer layer and a hydrophobic ZnF$_2$ inner layer. The outer layer can prevent SEI from crack, while the inner layer further removes solvated water and suppresses the water decomposition. However, this strategy will cause certain sacrifice to the rate performance and power density of AZDs. Besides, the adoption of SEs could alleviate the issues with Zn anodes, which will be discussed in Section 4.3.

Another promising countermeasure is derived from cell configuration innovations. For instance, flowing electrolytes can facilitate a more uniform distribution of Zn species, thus reducing the width of the Nernst diffusion layer (d_N) and enhancing the device durability.[61] This will be further discussed in Section 6.

4 Electrolytes for aqueous Zn-based EES devices

4.1 Conductive electrolytes

Most of the electrolytes in ZIBs, ZABs, ZSCs and anodic sides of ZRFBs are 'conductive electrolytes', which usually only serve as carriers for ion and charge transfer, and do not contribute to the capacity of entire devices. Generally, an ideal aqueous 'conductive electrolyte' should possess the following characteristics: a) high ionic conductivity; b) high ion transference number; c) wide

ESPW; d) high mechanical/chemical adaptability and wide working range (*e.g.*, temperature); e) low cost.[62]

An appropriate pH value is a prerequisite for a suitable electrolyte. First, it will greatly affect cell durability. Generally, strongly acidic electrolytes (pH < 3) are difficult to be applied to the Zn-based membrane-free EES devices owing to the intense HER on the anode; hence, the adoption of strongly acidic electrolytes is generally required to be paired with expensive ion-exchange membranes and noble metal electrocatalysts (for ZABs). Second, the pH value will significantly influence the ionic conductivity (σ), which can be expressed as:

$$\sigma = c(v_a\lambda_a^0 + v_c\lambda_c^0) \tag{3}$$

Where c is the concentration of the electrolyte; v_a and v_c represent the mole number of the dissociated cations and anions by dissolving 1 mol electrolyte, respectively; λ_a^0 and λ_c^0 relate to limiting molar conductivities of anions and cations, respectively.[62] As shown in Figure 7a and 7b, when the total Zn(II) concentration is constant (10^{-6} M), the concentration of Zn(II) soluble species is highly relevant to the pH value.[63] In the near-neutral and mildly alkaline solutions (pH = 7~13), a variety of Zn(II) soluble species will co-exist in the solution with a very small solubility; while in the acidic or alkaline electrolytes (pH < 6 or pH > 13), there is only a single type of Zn(II) species ($[Zn(H_2O)_6]^{2+}$ or $[Zn(OH)_4]^{2-}$) with a high solubility. The application of near-neutral electrolytes is challenging due to two major reasons: a) the co-existence of a variety of Zn(II) soluble species will make the electrochemical reaction more complicated and lead to the formation of various types of by-products, which will damage the performance; b) lower ionic conductivity and larger Ohmic loss, owning to their significantly lower H^+/OH^- concentration (10^{-8}~10^{-6} M) compared to strongly acidic or alkaline electrolytes (> 10^{-1} M). One strategy to enhance the ionic conductivity of neutral electrolytes is to add reducible anion species (*e.g.*, chlorides, perchlorates, nitrates) to form Zn-complexes, since Zn^{2+} can be complexed by different forms depending on the composition of the electrolyte.[64,65] A well-known example is the Leclanché electrolyte system ($ZnCl_2$-NH_4Cl), where many studies have shown the possible formation of Zn-complex and Zn anode discharge products,

such as $ZnCl_2 \cdot 2NH_3$ and $ZnCl_2$.[66,67] However, the adoption of electrolytes containing chlorides will inevitably lead to a chlorine evolution reaction (*Eqn.* 4a) in a similar potential range as the OER (*Eqn.* 4b), which will reduce the CE and cause safety issues.[68]

$$2Cl^-(aq) - 2e^- \rightarrow Cl_2\,(g) \quad E_{Cl}^0 = 1.36\,V \qquad \text{(4a)}$$

$$2H_2O(l) - 4e^- \rightarrow O_2\,(g) + 4H^+(aq) \quad E_O^0 = 1.23\,V \qquad \text{(4b)}$$
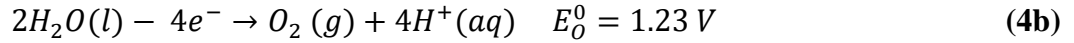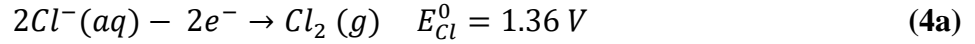
In an open system, ZABs generally use highly alkaline electrolytes, such as KOH, NaOH, LiOH solutions (typically 0.1~10 м).[69] Among highly alkaline electrolytes, KOH is the most extensively used because K^+ possesses superior transport kinetics, resulting from the lower dissociation heat and a higher limiting molar conductivity (λ_a^0, ~7.35 mS m^2 mol^{-1}) compared to Li^+ (3.869 mS m^2 mol^{-1}) and Na^+ (5.011 mS m^2 mol^{-1}).[62,70] However, with the further increase of KOH concentration, the solubility of Zn(II) species and the ionic conductivity will reach peak levels in ~30 *wt*% KOH solution (~7.78 м).[71] A major drawback of using highly alkaline electrolytes in open systems is the vigorous reaction with the acidic gases (*e.g.*, CO_2), thus producing the impurity ions (*Eqn.* 5a & b) and causing a series of issues such as a decline in ionic conductivity, cathode micropore blocking and an increase in electrolyte viscosity.[49,72]

$$CO_2\,(g) + OH^-(aq) \rightarrow HCO_3^-(aq) \qquad \text{(5a)}$$

$$CO_2(g) + 2OH^-(aq) \rightarrow CO_3^{2-}(aq) + H_2O(l) \qquad \text{(5b)}$$
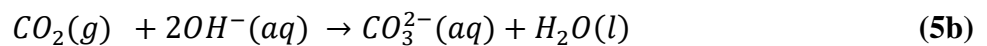
As for closed systems (ZIBs, ZSCBs, ZHSCs), the ability to adoption of a highly alkaline electrolyte depends on the tolerance of cathode materials. For ZHSCs using carbon-based cathodes, although the use of highly alkaline electrolyte is permissible, it still faces a series of issues, such as the rapid dissolution of Zn and sharp dendrite formation. However, extensively studied cathode candidates (MnO_2, V_2O_5, and Prussian blue analogs) for ZIBs are difficult to stabilize in highly alkaline solutions. It is worth mentioning that for batteries assembled with the KOH electrolyte, Zn anodes and the manganese dioxide cathodes are typical Zn-MnO_2 alkaline batteries, which are non-reversible

due to the formation of non-conductive Mn₂O₃ (*Eqn.* 6).[73] Forced charging would cause the water dissociation in the electrolyte, further risking battery failure.

$$2MnO_2\ (s)\ +2OH^-(aq)-2e^- \rightarrow Mn_2O_3(s)+H_2O(l) \tag{6}$$
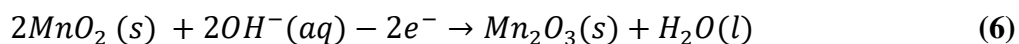
Currently, ZnSO₄ is the most widely used mildly acidic solutions; however, they're suffering from massive by-product formation (*e.g.*, $Zn_4(OH)_8SO_4$) and narrow voltage window (1.0~1.9 V *vs.* SHE) compared to that of organic electrolytes (2.5~4.0 V *vs.* SHE). Recently, a series of other mildly acidic electrolytes are used for AZDs, such as $Zn(CF_3SO_3)_2$ ($Zn(OTf)_2$), $Zn(N(CF_3SO_2)_2)_2$, and ($Zn(TFSI)_2$). This is primarily due to the following merits: a) ultra-stable anions; b) good compatibility with electrodes; and c) alleviation of the formation of byproducts.[74,75] With the increase of the salt concentration, many properties of electrolytes, such as solvation effect, ESPW and viscosity, will change significantly. Wang and colleagues reported a highly concentrated Zn-ion electrolyte (HCZE) consisting of $Zn(TFSI)_2$ and LiTFSI, which successfully extended the ESPW (~2 V *vs.* SHE) and enhanced the cycling stability of the Zn anode (80% capacity retention after 4000 cycles at 4C).[28] Through the structural and spectroscopic investigation, they proposed that the HCZE has changed solvation-sheath structures of Zn^{2+}, which forces anions into the vicinity of Zn^{2+} to form $(Zn-TFSI)^+$ and significantly suppress the formation of $[Zn(H_2O)_6]^{2+}$. Meanwhile, they observed that the pH value of the electrolyte elevated as the concentration of LiTFSI increased, and reached a near-neutral pH when the composition is 1 ᴍ $Zn(TFSI)_2$ + 20 ᴍ LiTFSI (Figure 7c and 7d). This is because water molecules can be severely confined within the Li^+ solvation structures, thus alleviating the Zn^{2+} hydrolysis effect. However, the adoption of highly concentrated electrolytes is exposed to several drawbacks: a) relatively high viscosity and low ionic conductivity; b) the increase in the overall weight, thus reducing the device energy density; c) salt precipitation under the low working temperature; d) high cost (*e.g.* $Zn(TFSI)_2$, 481.7 USD per 100 g) compared with commonly used electrolytes (*e.g.* ZnSO₄, 45.7 USD per 100 g).[7] Therefore, to some extent it is a strategy to sacrifice the energy density and increase the cost of the device for realizing better durability and reversibility. In addition to WIS electrolytes, the molecular crowding electrolytes are able to broaden the operating

voltage. In an aqueous Li-ion battery, Lu *et al.* developed a molecular crowding electrolyte using water-miscible poly(ethylene glycol) (PEG), which confines water molecules in the PEG networks, thus decreasing water activity and elevating electrolyte ESPW to 3.2 V.[76] However, this strategy has not been investigated in depth in AZDs.

4.2 Energized electrolytes

In addition to providing the ionic conductivity, the 'energized electrolytes' could serve as energy carriers and store the chemical energy *via* conversion reactions by active species (with different reduction potentials) dissolving or suspending in the electrolytes.[77] Generally, the common redox pairs for conversion reactions may involve the liquid-liquid transformation (*e.g.* Ce^{3+}/Ce^{4+}, V^{4+}/V^{5+}, $Fe(CN)_6^{4-}/Fe(CN)_6^{3-}$) and liquid-solid transformation (*e.g.* Pb^{2+}/PbO_2, Mn^{2+} or Mn^{3+}/MnO_2, $NiO(OH)/Ni(OH)_2$).[24,34,78–80] Some additives in the 'conductive electrolytes' can also serve as energy carriers, such as the reversible MnO_2 deposition in the AZIBs using Mn^{2+} pre-additive electrolytes[81]. However, the concentration of the Mn^{2+} additives is usually low and not the main source for contributing capacity; hence, the 'conductive electrolytes' involving these Mn^{2+} additives are not considered as 'energized electrolytes'. With the increase of Mn^{2+} concentration, the electrochemical deposition/dissolution processes of MnO_2 gradually dominate capacity contribution.[35] However, due to the poor electrical conductivity of MnO_2 ($\sim10^{-6}$ S m^{-1}), batteries based on Mn deposition are usually limited by surface area; therefore, it is challenging for them to achieve high areal capacity.[82]

The properties of 'energized electrolytes' would directly influence the device capacity and current output.[83] An ideal energized electrolyte is expected to possess the following characteristics: a) high reduction potential gaps between positive and negative electrolytes; b) high chemical/physical stability in the wide working range to inhibit the rapid degradation of active substances and capacity decay; c) high solubility of active substances in the electrolyte; d) small molecular weight and high electron-transfer number of active substances; e) low viscosity to reduce pump power and improve overall EE; f) low cost.[77,84] Among these, for ZRFBs, the energy density of energized electrolytes is the most important because it directly affects the reaction rate (power density), the volume of the

storage tank (device energy density) and the energy required by the pump (energy efficiency). The energy density of energized electrolytes is mainly affected by the solubility and existence form of active substances. The solubility of active substances in aqueous solution can be improved by active materials modification. For instance, to increase the solubility of TEMPO-containing polymer, Winsberg and co-workers synthesized a sulfate-potassium-salt-containing TEMPO derivative, which successfully improve the energy density of the electrolytes from 2.4 to 26.7 Ah L^{-1}.[85] Although the solubility of active materials elevated from ~0.091 м to ~ 1.016 м, it is still very limited.

In addition to improving the solubility of active materials, changing the existence form of active substances is an effective strategy to increase the energy density of energized electrolytes. For example, the solubility of Br$_2$ in aqueous solution is very low (3.58 g per 100 ml water at 25 °C), which leads to serious device corrosion problems. One viable strategy is to transform Br$_2$ into polybromide through the complexation reaction between Br$_2$ and complexing additives, such as 1-(carboxymethyl) pyridine-1-ium (QBr1) and N-ethyl-N-methyl pyrrolidinium bromide (MEP).[86] Moreover, the deployment of these large organic complexing additives can alleviate the crossover of active substances, thus enhancing the CE of the device. However, conventional complexing agents may lead to the deposition of dense polybromine oil phase, which may block the electrode and cause damage to the battery cycle life.[87] Therefore, the research in recent years is focusing on the development of complexing additives containing -OH and -COOH groups to maintain the polybromine components in the aqueous phase. This design concept has been validated in the electrolyte formulation of the Zn-Br$_2$ flow battery commercialized by Eos Energy Enterprises.[88] Moreover, this methodology has been employed in other chemistry systems, including Zn-I$_2$, and Zn-Fe batteries.[89,90]

4.3 Solid-state electrolytes

Compared with LEs, applying SEs to AZDs has following advantages: a) reducing the cell volume/mass and increase the volumetric/ gravimetric energy density; b) inhibiting the growth of Zn dendrites; c) providing the possibility of manufacturing membrane/separator-free and flexible

devices; d) extending the narrow ESPW.[44,91] However, due to the static nature of SEs, they cannot be used for involving forced flow system-assisted AZDs. In addition, the practical application of SEs faces a series of challenges; the improvements are urgent in electrical conductivity, mechanical properties, electro(chemical) stability, electrical insulation, and processability, *etc*.

According to the chemical composition of SEs, they can be divided into four categories: solid inorganic electrolytes (SIEs), solid polymer electrolytes (SPEs), hydrogel polymer electrolytes (HPEs) and hybrid solid-state electrolytes (HSEs). SIEs usually possess high moduli (*e.g.*, >1GPa for oxides), high thermal stability (> 100 °C) and wide ESPW (> 4V *vs.* SHE).[92] Most of SIEs possess a periodic structure with coordinated polyhedrons; the ions move in the defects within the framework, such as interstices and vacancies. Nevertheless, since the electrostatic force of Zn^{2+} is stronger than that for monovalent ions, Zn^{2+} is usually difficult to transport in SIEs, and the corresponding ionic conductivity is relatively low (< 1 S m^{-1}, at room temperature).[93] The investigation of Zn^{2+} diffusion in NASICON-type $ZnZr_4(PO_4)_6$ and β-Al_2O_3 have started 40 years ago; however, its diffusion is very slow (1.34×10^{-4} S m^{-1}) even at a high temperature of 500 °C.[94,95] Recently, See and colleagues reported an insulating and distorted honeycomb network of $ZnPS_3$, where Zn^{2+} is coordinated by $[P_2S_6]^{4-}$ polyanions. Although the existence of P-P bond in $[P_2S_6]^{4-}$ moiety could accommodate Zn^{2+} in the octahedral site and suppress the structural distortion, the ionic conductivity is still quite limited ($10^{-6} \sim 10^{-4}$ S m^{-1}).[96] In addition, the practical deployment of SIEs is restricted by several issues, such as inferior contact with the electrodes, high cost, and manufacturing difficulties arising from fragility.

Compared to SIEs, SPEs/HPEs possess many merits for AZDs, such as low density, low cost, easy synthesis, and good mechanical toughness. Unlike SIEs, the ions in SPEs/HPEs are stored in the framework with the free donor of the oxygen atoms and transmit to the neighboring site of free electron donors by segmental motions.[97] Zhi *et al.* constructed a hydrogen-free and dendrite-free SPE film *via* dissolving 1-ethyl-3-methyl-imidazolium tetrafluoroborate ([EMIM]BF$_4$) and zinc tetrafluoroborate (Zn(BF$_4$)$_2$) into the PVDF, which exhibits a high ionic conductivity (1.69 S m^{-1}).

Furthermore, they assembled the first all-solid-state AZIBs with long cycling durability (90% capacity retention, over 30,000 cycles) and wide temperature tolerance (20~70 °C).[98]

The research towards HPEs has become a hot spot in recent years, which could be identified as three types: natural biomass HPEs, synthetic porous HPEs, and oxide HPEs. Compared with SIEs/SPEs, the features of water absorption for HPEs is more compatible with chemical systems of AZDs, and exhibiting higher ionic conductivity (10^{-1}~10 S m^{-1}).[44] Generally, gel networks are mostly formed *via* hydrogen bonding, electrostatic, van der Waals interactions in the hydrophilic groups in the chain structures (*e.g.*, -COO, -NH$_4$, -NH, -CO, -OH, *etc.*); hence, they're easy to obtain from natural biomass of plants, animals and micro-organisms. Zhang and coworkers fabricated a flexible AZIB using a cellulose sodium hydrogel electrolyte, zinc hexacyanoferrate cathode and Zn anode, which exhibits a high areal capacity (100.2 mAh cm^{-3} at 0.1 mA cm^{-2}), high energy density (195.39 mWh cm^{-3}) and high capacity retention (93.2%) after bending 3,000 times.[99]

In addition to designability, synthetic porous HPEs are easier to eliminate undesirable impurities than natural biomass HPEs in large-scale production. Currently, a variety of 3D porous structured polymers are extensively studied for AZDs, such as poly(vinyl alcohol) (PVA), polyacrylamide (PAM), poly(acrylic acid) (PAA) and sodium polyacrylate (PANa).[100,101] For instance, Huang and coworkers fabricated a stretchable and compressible NiCo//Zn battery using PANa HPE, Zn anode, and Ni-Co hydroxide deposited on Au@CNT paper as a cathode.[102] The PANa HPE demonstrates an excellent ionic conductivity (20 S m^{-1}, at room temperature), and the as-assembled battery retains 87% and 97% of the initial capacity for 500 cycles stretching and 1500 cycles compression, respectively. However, due to the presence of water molecules in the HPE frameworks, undesirable by-products such as $Zn(OH)_2$ and ZnO increase the complexity of the electrode-electrolyte interface; in addition, the water-induced HER is more severe than that for SIEs/SPEs. Therefore, the interaction between water content and interface properties in HPEs should be further investigated, thus facilitating rational design and development of future HPEs.

By coupling distinctive merits of SIEs/SPEs/HPEs, HSEs have become promising candidates to obtain electrolytes with balanced properties. For example, adding inert inorganic particles into ion-conductive polymers could effectively enhance thermal stability and mechanical properties and facilitate salt dissociation.[103,104] However, this strategy has not made a breakthrough in AZDs in recent years, therefore this is also a promising direction for further development.

Above all, the development of SEs is highly beneficial to AZDs. From the perspective of device development, by reducing the electrolyte mass and volume and promoting the stability of the Zn anode, the application of SEs can offset many barriers to the commercialization of AZDs, such as limited energy density and durability. The current challenge of SEs is mainly focusing on the poor ionic conductivity caused by the high charge density of Zn^{2+}. Therefore, material innovation is urgent and essential. Meanwhile, the interface mechanisms of different electrolyte and electrode combinations should be further explored, and a universal methodology should be summarized to guide the development of SEs.

5 Cathodes for aqueous Zn-based EES devices

Based on the energy storage mechanisms, this work suggests a classification of cathodes (Figure 8). The classification includes four basic types of cathodes: EDLC (capacitive process), pseudocapacitive (capacitive-Faradaic process), insertion-type and conversion-type (Faradaic process). Cathodes with various mechanisms correspond to different performances. The EDLC cathodes (capacitive process) store the energy *via* the physisorption of ions at the EEI, which generally has a fast charge/discharge capability (ms-level), extremely high durability (> 100,000 cycles) and limited specific capacitance (50~350 F g^{-1}).[105] The cathodes with a Faradaic process will involve electron transfer *via* a reversible Zn^{2+} (de)insertion or the conversion reactions in the gas/liquid/solid phase. This type of material generally has a higher specific capacity, but a lower power density and cycling life (70%~90% capacity retention after 1,000 cycles). The pseudocapacitive cathode (capacitive-Faradaic processes) stores energy *via* rapid reversible redox reactions at the surface or near-surface of the electrode, which possesses the properties of both EDLC and battery-type behavior.

The research efforts in the past decades have found numerous promising materials for EDLC cathodes (*e.g.* activated carbon (AC), carbon nanotubes (CNTs) and graphene), insertion-type cathodes (*e.g.*, layered MnO_2 and V_2O_5), conversion-type cathodes (*e.g.*, $Ni(OH)_2$ and MnO_2), and pseudocapacitive cathodes (*e.g.*, RuO_2, MnO_2 and conductive polymers).[7,8,36,106,107] Some substances, such as MnO_2, can be used as active materials for different types of electrodes; however, they have completely different requirements. For instance, an EDLC or pseudocapacitive cathode is usually surface-controlled and therefore requires a larger specific surface area; nevertheless, the larger specific surface area created by micropores (< 2.0 nm) are not useful for insertion-type cathodes, since the large hydrated Zn-ions (4.3 Å, 0.43 nm) cannot enter all micropores. In addition, the consistency of electrode materials also provides the basis for the design of hybrid cathodes, which enables multiple charge storage processes to occur at the same electrode simultaneously. Theoretically, hybrid cathodes will possess a combination of properties and characteristics of the basic cathodes, leading to the design of promising electrode materials. The underlying mechanisms, challenges and opportunities will be introduced and discussed in Sections 5.1~5.4.

5.1 Insertion-type Cathodes

The reversible (de)insertion of ions is one of the charge storage mechanisms of LIBs, which can also be explained in AZDs. To date, a variety of insertion-type materials have been extensively investigated as cathode candidates for AZIBs, especially Prussian blue analogs (PBAs), Mn-based, V-based and organic compounds.[108–110] However, the development of insertion-type cathodes is facing several inherent challenges. Firstly, as a multivalent ion, Zn^{2+} possess a much larger charge density (112 C mm^{-3}) and hydrated ionic radius (4.3 Å) compared with those for monovalent ions such as Li^+ (52 C mm^{-3}, 3.82 Å), which lead to sluggish diffusion kinetics (or diffusivity) in mainstream cathode materials.[7] Secondly, the specific capacity of most insertion-type cathodes is still relatively low, and state-of-the-art high-performance cathode materials for ZIBs are usually based on oversized Zn anodes. Thirdly, the dissolution and the phase change or structural collapse of active materials during the cycling would aggravate the capacity decay and reduce the cycling stability of

the devices. For instance, due to the Mn^{3+} Jahn–Teller instability, the disproportionation (*Eqn.* 7) can cause the dissolution of Mn-based materials.[111,112] Although the pre-addition of Mn^{2+} may alleviate the dissolution, unstable Mn^{2+} may redeposit on the cathodes.[81]

$$2Mn^{3+}(s) \leftrightarrow Mn^{2+}(aq) + Mn^{4+}(aq) \tag{7}$$
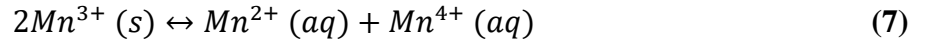
Current energy storage mechanisms are still controversial, which include three major hypotheses: a) Zn^{2+} (de)insertion; b) conversion reaction initiated by Zn^{2+} (de)insertion; c) H^+/Zn^{2+} co-(de)insertion. Take MnO_2 as an example, the most widely reported mechanism is the reversible Zn^{2+} (de)insertion (Figure 9a). Also, many researchers have observed that the Zn^{2+} insertion may trigger the structural transformation into layered Zn_xMnO_2 and/or $ZnMn_2O_4$ depending on the DoD (Figure 9b).[113] Besides, recent explorations have proven the existence of Zn^{2+} and H^+ co-(de)insertion in cathode materials (Figure 9c).[114] Through material characterizations and electrochemical analysis, Wang and colleagues first demonstrated the successive H^+ and Zn^{2+} insertion processes in the electrodeposited nanostructured akhtenskite MnO_2 (< 10 nm).[115] It is worth noting that most AZIBs involving H^+ and Zn^{2+} co-(de)insertion mechanisms have exhibited superior durability and rate performance.[116] For the sake of discussion, the above behaviors are classified as (de)insertion mechanisms in this review. Although the dissolution/deposition of active materials (*e.g.*, $Mn^{2+} + 2H_2O \leftrightarrow MnO_2 + 2e^- + 4H^+$) and complex electrochemical reactions (*e.g.*, formation of $Zn_4(SO_4)(OH)_6 \cdot nH_2O$) will also contribute additional capacity in AZIBs, they are not induced by the Zn^{2+} (de)insertion; hence, they will be further discussed in Section 5.2.3.[117]

To improve the performance of insertion-type cathodes, a variety of promising strategies have been proposed. The more in-depth discussion are provided in our recent review on insertion-type cathode design for aqueous multivalent-ion batteries, which have identified and discussed nine promising methodologies for the optimization of insertion-type cathodes, including: (a) cathode innovation *via* pre-intercalation strategy, defects engineering, heteroatom doping, size regulation, composites and freestanding configurations; (b) electrolyte innovation in terms of next-generation electrolyte additives and WIS electrolyte; (c) further theoretical investigations *via* advanced characterization and

computational techniques.[7] In essence, these strategies improve the cathode performance in one or more of the following aspects: a) enlarging the interlayer spacing; b) weakening the interaction between the Zn^{2+} and host materials; c) reducing the particle size to facilitate the mass transfer. In addition, conduction of more in-depth computational investigations (*e.g.* density-functional theory (DFT) and molecular dynamics (MD)) and advanced characterization (*e.g. in-situ* and synchrotron-based techniques) would further elucidate underlying mechanisms, thus providing fundamental guidance for the improvement of AZIBs.[108]

5.2 Conversion-type cathodes

In this review, conversion-type cathodes are defined as the cathodes that store charge and energy *via* non-insertion-type redox reactions, which commonly exist in ZSCBs, ZABs and ZRFBs. Based on the changes in physical states of matter, conversion reactions could be further classified as: a) liquid phase reaction (both reactants and products are liquid or solution state); b) solid-phase reaction (at least one of the reactants and products is the solid-state); c) gas reaction (at least one of the reactant and product is gas). For cathodes with liquid/gas phase reactions, the electrodes do not act as reactants, but participates in the reaction as current collectors or electrocatalysts; while for cathodes with solid reactions, the electrodes or the electrodeposited products on the electrodes will directly involve in conversion reactions. In this part, typical redox pairs are introduced to discuss the mechanisms of gas, liquid and solid phase conversion reactions, respectively.

5.2.1 Gas phase

Reversible oxygen reduction reactions (ORR) and OER are the most common gas-phase conversion reactions in AZDs. Both ORR and OER are multi-step and multi-electron transfer processes, which can occur in acidic, neutral and alkaline electrolytes. However, compared with polymer electrolyte membrane fuel cells (PEMFCs) operating at an acidic environment (pH ≈ 0), an alkaline environment (pH ≥ 13) may be a superior choice for AZDs from a perspective of commercialization: a) enable the

adoption of non-precious metal and metal-free catalyst; b) membrane-free configurations are allowed.[118,119] In addition, previous research has suggested that the thermodynamic barrier reduces as the pH increases, which leads to relatively faster ORR/OER kinetics (smaller overpotential and higher exchange current) in alkaline electrolytes.[120,121]

Since the OER is intrinsically the reverse process of ORR, this part will mainly discuss ORR mechanisms. Figure 10 exhibits ORR pathways in the alkaline electrolyte.[122] After the diffusion and adsorption of O_2 molecules at the surface of electrocatalysts, Nørskov and co-workers proposed two possible ORR mechanisms: a) the dissociative mechanism (*Eqn.* 8) that involves dissociation of oxygen and the formation of O_{ad}^*; b) the associative mechanism (*Eqn.* 9 and 10) that involves the formation of $HO_{2,ad}$ or $O_{2,ad}^-$.[123,124] In general, the associative mechanism is more energetically favorable than the dissociative mechanism, due to the high energy demand (498 kJ mol^{-1}) for cleavage of O-O bond in the O_2 molecule.[121]

$$O_2(g) + 2e^- \leftrightarrow O_{ad}^* + O_{ad}^* \tag{8}$$

$$O_2(g) + H_2O(l) + e^- \leftrightarrow OH^-(aq) + HO_{2,ad} \tag{9}$$

$$O_2(g) + e^- \leftrightarrow O_{2,ad}^- \tag{10}$$
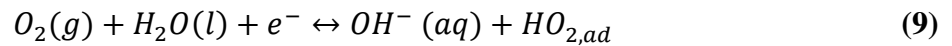
Its subsequent reduction to OH$^-$ ions proceeds through either an efficient 4e$^-$ pathway (one-step) or a sluggish 2e$^-$ pathway (two-steps). For a direct 4e$^-$ pathway, the reactions under dissociative (*Eqn.* 11) and associative mechanisms (*Eqn.* 12) are as follows:[122]

Dissociative 4e$^-$ pathway:

$$O_{ad} + O_{ad} + 2H_2O(l) + 2e^- \leftrightarrow 2OH_{ad} + 2OH^-(aq) \tag{11a}$$

$$2OH_{ad} + 2OH^-(aq) + 2e^- \leftrightarrow 4OH^-(aq) \tag{11b}$$

Associative 4e$^-$ pathway:

$$HO_{2,ad} + OH^-(aq) + e^- \leftrightarrow O_{ad} + 2OH^-(aq) \tag{12a}$$

$$O_{ad} + 2OH^-(aq) + H_2O(l) + e^- \leftrightarrow OH_{ad} + 3OH^-(aq) \tag{12b}$$

$$OH_{ad} + 3OH^- (aq) + e^- \leftrightarrow 4OH^- (aq) \tag{12c}$$
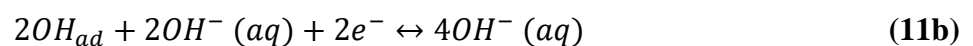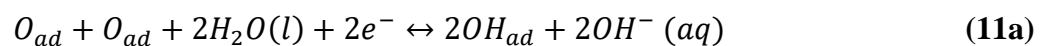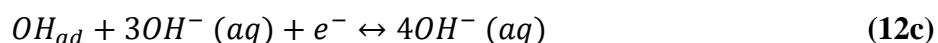
For the indirect 2e⁻ pathway, it firstly forms the HO_2^- (*Eqn.* 13a), which will subsequently occur through either 2e⁻ reduction to OH⁻ (*Eqn.* 13b) or the chemical disproportionation to O_2 and H_2O.[125] Since the HO_2^- cannot exist stably in an alkaline media, the disproportionation results in the sluggish kinetics and poor efficiency; therefore, most of ZABs rely on the 4e⁻ pathway. However, Wang *et al.* proposed a 2e⁻ $Zn-O_2/ZnO_2$ chemistry with higher reversibility and energy density, which provide the possibility for 2e⁻ pathway-based device design.[126] They reported that the unique water-poor and (Zn^{2+})-rich inner Helmholtz plane (IHP) on the air cathodes alleviated the 4e⁻ pathway and enable the stable existence of the ZnO_2 on the surface of cathodes.

Associative 2e⁻ pathway:

$$HO_{2,ad} + e^- \leftrightarrow HO_2^- (aq) \tag{13a}$$

$$2OH_{ad} + 2OH^- (aq) + 2e^- \leftrightarrow 4OH^- (aq) \tag{13b}$$

Unfortunately, both 2e⁻ and 4e⁻ pathways require high overpotentials to overcome sluggish kinetics, even at a very small current density; this leads to a much lower round-trip efficiency (up to 65%) for ZABs, compared to that of commercial LIBs (80% ~ 90%).[107] In addition, the overpotential increases sharply with the current density, which results in a low power density. To address these challenges, researchers focus on developing highly efficient ORR/OER bifunctional electrocatalysts, which include non-precious metal-based compounds (*e.g.*, layered hydroxides, nitrides, sulfides, phosphides, perovskite oxides) and carbon-based (*e.g.*, graphene, CNTs, and heteroatom doped-carbon) materials.[127,128] However, limited types of active sites are challenging to be efficient for both ORR and OER, since the desired adsorption energies of oxygen-containing species to achieve the optimized activity are different.[1] Defects engineering is an effective strategy, because it can (a) increase the number of active sites; (b) optimize the adsorption energy of reaction intermediates; (c) enhance the charge transfer.[129] Based on rational construction of atomic-scale interfaces, Chen *et al.* synthesized a hollow CoO bifunctional electrocatalyst with abundant O-vacancies in N, S co-doped

porous carbon.[130] The presence of O-vacancies formed a defect-rich interface and enhanced the adsorption capability for oxygen-related reactants, thus achieving a low OER overpotential (470 mV at 10 mA cm^{-2}) and a low ORR half-wave potential of 0.83 V. Moreover, the as-fabricated ZAB exhibits a high energy density (871 Wh kg^{-1} Zn) and a long cycling stability of 800 h at 10 mA cm^{-2}.

In addition to defects engineering, various strategies have been proposed to enhance the performance of air cathodes, such as cation/anion regulation, heteroatom doping, and binder-free configuration. He *et al.* synthesized a N, O-co-doped graphene nanoring-integrated box *via* high-temperature pyrolysis of CoCo-PBA, which exhibits high catalytic activity towards ORR/OER/HER.[131] Due to the unique hierarchically porous nanostructures on the hollow nanorings, the material possesses highly accessible active sites for electrocatalysis and facilitated the mass transport kinetics on the air cathode. In addition, the heteroatom doping strategy promotes the formation of "C+" active sites, which significantly improved the activity of OER/ORR. However, the relationship between active sites of electrocatalysts and OER/ORR has not been well interpreted; for example, the mechanism of catalytic activity in Fe-N-C electrocatalysts is still unclear. Therefore, more theoretical investigations should be conducted to better guide future air cathode design.

In general, in addition to high catalytic activities, an ideal air electrode should have strong mass and charge transfer capabilities.[132] Since the ORR/OER occurs among the gas-liquid-solid triple-phase boundaries, the air cathode requires a highly porous structure to promote the diffusion of air and liquid.[133] Meanwhile, electrode materials with suitable wettability and balanced hydrophobicity and hydrophilicity could suppress the evaporation loss of the electrolyte and avoid adverse effects[106]. Other systems involving gas conversion reactions, such as Zn-Cl$_2$ system, possess similar mechanisms, challenges and requirements for air cathodes; while the current research is relatively limited.[1]

5.2.2 Liquid phase

The liquid-liquid conversion-type cathodes usually act as current collectors and provide active sites for redox reactions, which generally exist in ZRFBs involving liquid-liquid conversion reactions and do not directly participate as reactants. Their physicochemical properties will significantly affect the performance of AZDs, such as electrocatalytic activity (affects activation polarization), pore structure and hydrophilicity (affects concentration polarization), and electrical conductivity (affects Ohmic polarization). Therefore, an ideal liquid-liquid conversion-type cathode is expected to possess good performance in electrical conductivity, electrocatalytic activity, (electro)chemical/mechanical stability, as well as appropriate hydrophilicity and pore structure.

At present, the most widely used electrode materials are commercial pure carbon materials, such as carbon plates, carbon felts and porous graphite.[134,135] However, carbon has a low redox potential ($CO_2(g) + 4H^+(aq) + 2e^- \leftrightarrow C(s) + 2H_2O(l)$, $E_C^0 = 0.205\ V\ vs.\ \text{SHE}$) and may be oxidized under working conditions, thus resulting in the carbon corrosion and a poor CE.[136] In addition, the number of catalytic active sites in commercial pure carbon materials is minimal. Zhang $et\ al.$ reported a bimodal highly ordered mesostructured carbon as the cathode for Zn-Br$_2$ flow battery, which is fabricated by an evaporation induced tri-constituent co-assembly method.[137] In addition, the highly ordered mesostructure with 2 nm pores on 5 nm pore walls is beneficial to Br$_2$ adsorption, thus providing more active sites for Br$_2$/Br$^-$ conversion. As a result, the assembled battery exhibits a good VE (82.9%) and EE (80.1%) at a high current density of 80 mA cm^{-2}. In addition to active sites, the pore structure design is crucial for liquid-liquid conversion-type cathodes. Zhang and colleagues designed cage-like porous carbon materials with a pore size of ~1.1 nm, which allow the free entrance of Br$^-$ (4.83 Å) and MEP$^+$ (9.25 Å) and entrap Br$_2$ complex (MEPBr$_3$, 12.40 Å) in the cage.[138] As this strategy effectively alleviates the bromine crossover and self-discharge issue, the as-fabricated battery demonstrates an outstanding CE (98%), EE (81%) and long durability (over 300 cycles) at a high current density of 80 mA cm^{-2}. Theoretically, these methods are universal for a variety of AZDs; however, specific materials and pore structures need to be developed according to specific chemical

environments. In addition, the electrode surface modification and heteroatom doping should be effective to improve the catalytic activity and stability of the electrode.

5.2.3 Solid phase

Cathodes involving solid-phase conversion reactions can be divided into two categories: a) liquid-solid reaction; b) solid-solid reactions. Similar to liquid-liquid conversion-type cathodes, the liquid-solid conversion-type cathodes act only as current collectors and provide active sites for redox reactions; therefore, they share similar requirements and design principles for cathode materials. While for the solid-solid reaction, cathodes are electrochemically active and directly participate in the conversion reactions. There are several long-established and mature reversible systems, such as Zn-Ni and Zn-Ag batteries, which use Zn metals as anodes and involve solid-phase conversion reactions (*Eqn.* 14 and 15).[8] Although these systems possess faster kinetics and higher power density than those with gas or liquid phase conversion-type mechanisms, their capacity is limited by cathode materials.[139,140] For instance, theoretical specific capacities of $Ni(OH)_2$ and AgO are 289 and 479 mAh g^{-1}, respectively, which are hard to satisfy the demands for future practical applications. Various strategies have been proposed to bring cathode materials closer to the theoretical capacity, such as heteroatom doping, defects engineering, composite fabrication, *etc*.[8]

$$NiOOH(s) + H_2O(l) + e^- \leftrightarrow Ni(OH)_2(s) + OH^-(aq) \tag{14}$$

$$2AgO(s) + H_2O(l) + 2e^- \leftrightarrow Ag_2O(s) + 2OH^-(aq) \tag{15a}$$

$$Ag_2O(s) + H_2O(l) + 2e^- \leftrightarrow 2Ag(s) + 2OH^-(aq) \tag{15b}$$
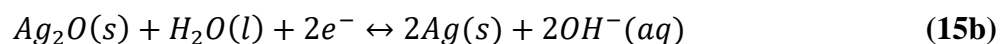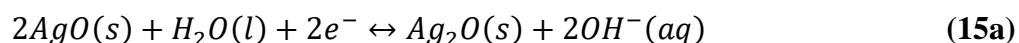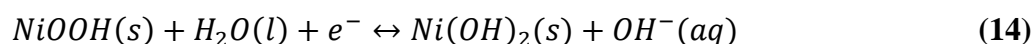
Cathodes with liquid-solid conversion reactions mainly achieve charge storage *via* the reversible electrochemical deposition/dissolution of active substances. In this case, cathodes generally serve only as current collectors and substrates for electrochemical deposition. Therefore, the specific capacity in such systems is not limited by the cathode materials, which provide the possibility of designing a semi-open device. For instance, Li and co-workers reported a Zn-MnO$_2$ redox flow

battery using a 3D porous graphite felt as a cathode, which demonstrated a high areal capacity (20 mA h cm^{-2} at 20 mA cm^{-2}) and CE (~99% after 400 cycles).[35] Electrodes for such systems are usually required with the following features: a) high electrical conductivity; b) good wettability with the electrolyte; c) high porosity to provide more surface area for deposition; d) high chemical and mechanical stability under working states. However, the inadequate areal capacity of current solid phase cathodes limits their practical applications. For instance, the poor electrical conductivity (10^{-6} S m^{-1}) and incomplete dissolution and exfoliation of MnO$_2$ deteriorate long-term cycling stability even at a low areal capacity (>2.0 mA h cm^{-2}).[82,141] This review recommends several methods to offset the damage caused by the low areal capacity to the energy density of the AZDs, including: (a) the deployment of flow systems to convert diffusion control to convection control, thereby improving the transport kinetics of Zn-ions in the conversion-type cathodes; (b) develop a series of electrolyte additives and redox mediators to improve device operation stability; (c) develop novel conversion-type cathode materials with high electrical conductivity and Zn-ion transport capability; (d) establish high-voltage system to get rid of the limitation of the narrow ESPW of aqueous electrolytes. These strategies will be discussed in detail in subsequent sections.

5.3 Electric double-layer capacitive (EDLC) cathodes

Although the 'Leyden jar' was reported as the first capacitor in 1746, the energy storage mechanism was not well understood until 1853, when von Helmholz proposed the electrical double-layer (EDL) model[142]. Subsequently, through the efforts from Gouy, Chapman, Stern, Grahame and other scientists, the modern EDLC mechanism was formed.[143–145] In the modern EDLC model (Figure 11a), due to electrostatic repulsion and thermodynamic diffusion, solvated ions will form a diffuse layer ($10^{-8} \sim 10^{-6}$ m) with a decreased ion concentration. As the distance from the electrode gets closer, partially solvated ions gradually formed in the outer Helmholtz plane (OHP, $10^{-9} \sim 10^{-8}$ m). Finally, the adsorption force in the inner Helmholtz plane (IHP, $< 10^{-9}$ m) is usually stronger than the electrostatic force; hence, the adsorption of solvent molecules and desolvated ions will be able to exist steadily. The potential distribution of the EDL interface depends on the ion(charge) distribution,

which can be estimated *via* the Poisson-Boltzmann equation.[146] As illustrated in Figure 11b, potential distributions in the IHP and OHP are both linear but with different slopes; while potential profiles in the diffuse layer is near linear and reach a plateau in the end (next to the bulk phase).

Generally, an ideal EDLC cathode should possess the following characteristics: a) large specific surface area and porosity; b) high electrical conductivity; c) high mechanical, chemical and thermodynamic stability; d) low cost and facile fabrication process. Currently, the most extensively investigated cathode candidates are carbon materials; however, they are facing several issues. For instance, compared to commercial AC, pristine CNTs are not suitable for EDLCs due to their low specific surface area (up to ~500 m^2 g^{-1}) and high cost (industrial grade multi-walled CNTs, ~400 USD per kg). Also, the agglomeration and restacking of the pristine graphene sheets limit their specific capacitance between 100~200 F g^{-1}.[147]

The pore size engineering is an important methodology to improve the EDLC cathode. In 2008, Gogotsi and Simon proposed that the EDL capacitance exhibits an anomalous increase when the pore size gets closer to the ion size; meanwhile, a lower capacitance will be obtained, when the pore is 50% larger than the optimum pore size.[148] Take EDLC cathodes in $ZnSO_4$ electrolyte as an example, the energy storage process is mainly achieved by physically adsorbed desolvated bare Zn^{2+} (0.74 nm) and SO_4^{2-} (0.73 nm) in the IHP; therefore, adjusting the pore size to 0.75~0.8 nm is expected to enhance the EDL capacitance. Zhang and colleagues synthesized a pencil shaving derived porous carbon, whose pore size is centered at 0.8, 1.1, and 1.2 nm.[149] The as-assembled ZHSC demonstrates a high power density (15.7 kW kg^{-1} at 65.4 Wh kg^{-1}) and good capacitance retention of 92.2% after 10,000 cycles at 10 A g^{-1}. However, as the mass loading of active materials increases to 17 mg /cm^2, the areal specific capacitance drops rapidly to 61.6% of that of low mass loading ones (2 mg cm^{-2}); this indicates that the diffusion of Zn-ion in the bulk phase of the material still encounters a large obstacle. The construction of hierarchically structured materials can boost the Zn-ion transport in the cathode. Yin *et al.* synthesized a hierarchically porous carbon cathode *via* acid etching, which makes full use of the advantages of micropores (enhanced ion adsorption), mesopores (providing smooth

ion transfer channels), and macropores (ion reservoir).[150] Hence, the assembled electrode exhibits a high capacitance of 340.7 F g^{-1} (at 0.1 A g^{-1}), excellent power density (48.8 kW kg^{-1} at 40.4 Wh kg^{-1}) and a high capacitance retention of 99.2% over 30,000 cycles at 20 A g^{-1}. In addition, other strategies, such as the construction of carbon composites, heteroatom doping, surface modification, can promote the performance of EDLC cathodes effectively.[151,152]

5.4 Pseudocapacitive cathodes

Different from EDLCs with the NFC process, the charge and energy storage of pseudocapacitive electrodes are deemed as CF processes, whose valence state of active materials changes during the cycling. As shown in Figure 8, Conway suggests three types of Faradaic mechanisms that can lead to pseudocapacitive behaviors, including underpotential deposition (UPD), redox pseudocapacitance and intercalation pseudocapacitance.[153] In essence, all three mechanisms are based on the rapid and reversible CF process on the surface or near-surface of active materials. Generally, a rechargeable battery involves the transfer of localized valence electrons (follows the Nernst Equation); while the charge storage in pseudocapacitors is achieved by the transfer of delocalized valence electrons, and the corresponding electrode potential is proportional to the electric charges passing through the electrode.

Compared with EDLC cathodes, pseudocapacitive cathodes could provide a superior specific capacitance and energy density; however, these merits are counterbalanced by the relatively poor cycling stability. This is mainly attributed to the undesired structural/morphological changes and the material degradation caused by redox reactions during the cycling. The electrochemical kinetics of pseudocapacitive materials are under surface-controlled and diffusion-controlled processes simultaneously; therefore, the requirements for pseudocapacitive materials are similar to EDLC materials (see section 5.3). Transition metal oxides (TMOs) are extensively studied pseudocapacitive cathodes, which undergo multiple oxidation states at specific potential ranges. One of the earliest TMO-based cathode materials to be investigated was RuO_2, which can achieve a specific capacitance

up to 1340 F g^{-1};[154] however, Ru is a precious metal (12,470 USD per kg), which introduces a barrier to commercialization for RuO_2-based pseudocapacitors. Therefore, researchers shifted their focus to lower-cost cathode candidates, including non-noble metal compounds (*e.g.* MnO_2, Co_3O_4 and V_2O_5), conducting polymers (*e.g.* polyaniline (PAN) and polypyrrole (PPy)) and MXene (2D transition metal carbides, carbonitrides and nitrides).[155–158]

The poor cycling stability, especially under high operation voltage window, is the most urgent issue to be solved for the commercialization of AZDs with pseudocapacitive cathodes. The construction of composites is an effective method, utilizing the synergistic effect of two components to improve the electrochemical performance, such as chemical stability, ion diffusion kinetics, electrical conductivity, and mechanical strength. Liu *et al.* reported a ZHSC using poly(4,4'-thiodiphenol, TDP)/AC composite cathode and Zn foil anode, which exhibits a high areal energy density (1.03 mWh cm^{-2}) and power density (9 mW cm^{-2}).[159] Since H$^+$ can bound to the carbonyl groups in poly(4,4'-TDP) molecules, the prepared cathodes successfully broaden the voltage window from 0.2–1.8 V to 0.1–1.9 V. In addition, several other composites demonstrate excellent electrochemical properties, such as GO/PANI (531 F g^{-1} at 200 mA g^{-1}), and Fe_2O_3/MnO_2 (838 F g^{-1} at 2 mV s^{-1}).[160–162]

6 Cell configurations

Besides electrode and electrolyte materials, different cell configurations will change the transport process of charge carriers or active substances in the electrolyte, thus affecting cell performance. As shown in Figure 12a and *Eqn.* 16, the flux of mass transfer of ions in a liquid electrolyte depends on the following three processes: a) the migration, driven by the potential differences; b) the diffusion, driven by the concentration gradient; c) the convection, driven by the external forces.

$$\textit{Migration: } J(x)_m = -\frac{qCD}{kT}\frac{dV}{dx}; \textit{ Diffusion: } J(x)_d = -D\frac{dC}{dx} \textit{ ; Convection: } J(x)_c = Cv_x \quad \textbf{(16a)}$$

$$\textit{Nernst-Planck equation: } J(x) = J(x)_m + J(x)_d + J(x)_c = Cv_x - \frac{qCD}{kT}\frac{dV}{dX} - D\frac{dC}{dx} \quad \textbf{(16b)}$$

Where C, v_x, q, D, k, T and V refer to concentration, convective velocity, unit charge, coefficient of diffusion, Boltzmann constant, temperature and electric potential, respectively. Generally, a cell configuration is a combination of the following two components: membranes and flow systems. In addition to avoiding a short circuit, membranes possess different permselectivity to different ions, which will affect the concentration gradient and potential differences during the migration and diffusion processes. The flow systems exert external forces that alter the convection process. This section will further discuss the operating principles of membranes and flow systems and summarize possible configurations.

6.1 Membranes

6.1.1 Electrochemistry

There are three main membrane configurations: a) membrane-free (separator/SE); b) single-membrane; c) double-membrane. The separator or single-membrane configuration (Figure 12b and c) divides the cell into two compartments. The main difference is that separators allow all active substances in the electrolytes to transport between two compartments; while membranes only partially allow active substances to pass through, thus partially separating working conditions of anodes and cathodes. Therefore, the choice between the separator or single-membrane configuration depends on whether active substances in two compartments are allowed to be mixed or not. For instance, as for conventional RFBs, both redox reactions mainly occur in the liquid phase, which leads to the necessity of using an ion-exchange membrane to separate electrolytes as the negative electrolyte (lower reduction potential) and the positive electrolyte (higher reduction potential)[1]. However, the electrolytes of ZABs, ZIBs, and ZHCSs usually do not contain active substances that can react with the Zn anode, so a membrane-free configuration is commonly used.[2,7,126]

The double-membrane configuration (Figure 12d) could entirely decouple the working conditions of anodes and cathodes and eliminate the electrolyte consistency issue, and thus elevate the cell cycling

stability and voltage window (2.5~3.5 V).[27,79] Generally, double-membrane configurations use a cation- and anion-exchange membrane and divide the cell into three compartments, thus allowing the use of electrolytes with large pH differences in anodic and cathodic compartments. However, this is hard to achieve by single-membrane or membrane-free configurations.[27]

Nevertheless, there are several substantial challenges to use membranes in AZDs. First, the high cost (*e.g.* Nafion[TM] 117, 1.33 USD per cm^2) and insufficient lifetime (3~8 years) of membranes may discourage large-scale deployment. Meanwhile, the ageing of the membrane can lead to the leakage of electrolytes in different compartments, which reduces the cell CE and raise the potential safety risks. In addition, the use of membranes and separators will inevitably affect the transport of electrolytes and ions and generate a Donnan overpotential, which will reduce the VE[163]. The resistances caused by membranes ($R_{i,m}$) is related to the thickness, which can be expressed by *Eqn. 17*.

$$R_{i,m} = \rho L = L/\delta \qquad (17)$$

Where *L*, ρ, and δ are thickness, resistivity (Ω cm) and conductivity (S cm^{-1}) of the material.

The ideal separator for AZDs should possess following electrochemical characteristics: (a) high ionic conductivity to minimize battery internal resistance; (b) excellent mechanical strength to suppress Zn dendrites growth; (c) high chemical stability and corrosion resistance; (d) high hydrophilicity. Based on the requirements for separators, membranes need to have high selectivity and permeability to specific ions to avoid self-discharge. Separators and membranes are of great significance to the electrochemical performance and reliability of AZDs, which will be discussed in the subsequent sections.

6.1.2 Separators for AZDs

In the current research, the commonly used separators for AZDs are glass fibers or filter papers, due to their high compatibility with aqueous electrolytes. However, the development of next-generation separators is crucial, because glass fibers or filter papers have following inherent disadvantages: (a)

high thickness (usually 100 ~ 500 μm) increases the weight, volume and internal resistance of the battery, thereby weakening the electrochemical performance; (b) large pore size and fragile nature lead to a weak inhibitory effect on Zn dendrites; (c) uneven pore distribution will result in uneven distribution of the electrolytes in different areas of the electrode surface, thereby reducing the utilization of cathode active materials and the uniform deposition/dissolution capability of Zn anodes. To achieve a more even electrolyte distribution inside the electrolyte and the electrode surface, Qin *et al.* proposed the use of a separator with a highly uniform pore distribution.[64] Then, they constructed a Zn//NaV$_3$O$_8$·1.5H$_2$O coin cell, demonstrating superior capacity retention (83.8% at 5 A g^{-1} after 5000 cycles) than that using glass fiber (~12.5% at 5 A g^{-1} after 5000 cycles). Recently, Srinivasan and colleagues innovatively synthesized a lignin@Nafion composite separator that can induce the beneficial Zn (002) lattice plane (parallel to the surface) deposition other than Zn (100) lattice plane (perpendicular to the surface).[164] Through density functional theory (DFT) calculation, they proved that the merits of this separator result from the interaction between SO$_3^-$ and Zn^{2+}, which modified Zn-ion coordination. Furthermore, considering the high cost of Nafion membranes, lignin derived from the biomass is introduced to form the composite separator, thereby increasing the commercial availability.

Therefore, this review suggests the development of next-generation separators can focus on following aspects: (a) further investigate the relationship among interfacial properties, functional groups in the separator and the deposition/dissolution/diffusion process of Zn ions; (b) improve the mechanical performance and reduce separator thickness in actual use; (c) further attempt to reduce the cost of high-performance separators.

6.1.3 Membranes for neutral and acidic systems

At present, commercialized Nafion series ion exchange membranes and porous Daramic membranes are most widely used in neutral and acidic AZDs. In fact, it is very challenging to develop new membrane materials because of the strong oxidizing nature and high potential environment of AZDs, such as Zn-Ce flow batteries ($Zn(s) + 2Ce^{4+}(aq) \leftrightarrow Zn^{2+}(aq) + 2Ce^{3+}(aq), E =$

2.48 $vs. SHE$).[78] The modification based on expensive commercial perfluorinated membranes (*e.g.*, Nafion) and porous membranes (*e.g.*, Daramic) is the mainstream technology of AZDs. For instance, to reduce the Ohmic losses in the Zn-Br$_2$ flow battery, Kim *et al.* proposed a Nafion-filled porous membrane with a low thickness (16 μm) and small areal resistance (3.12 Ω cm^2), which is superior to those for commercial SF-600 membrane (600 μm and 4.2 Ω cm^2).[165] More importantly, the Br$_2$ diffusivity of the as-prepared membrane (7.53 × 10^{-9} cm^2 min^{-1}) is two orders of magnitude lower than SF-600 membrane (2.67 × 10^{-7} cm^2 min^{-1}), which suppress the Br$_2$ crossover and alleviate the self-discharge issue. Moreover, Xie and colleagues synthesized a composite membrane by assembling an ultrathin layer of Nafion (7 μm) on porous polyolefin substrate, which achieved a good CE (97%) for Zn-I$_2$ flow battery at a high current density of 40 mA cm^{-2}. Even at a higher current density (80 mA cm^{-2}), the battery can operate stably within 500 cycles.[166] Although compositing commercial membrane with other economic materials has received many achievements in performance optimization and cost reduction, its ion transport mechanism is still unclear. For example, it is not yet clear whether the increase in ion selectivity is mainly due to the pore size exclusion of porous media or the Nafion. Therefore, advanced characterization and computational techniques should be applied to explore the underlying mechanism and further guide future membrane materials design.

6.1.4 Membranes for alkaline systems

Compared with neutral and acidic systems, the alkaline system is more corrosive; hence, it has put forward higher requirements on the stability of the membrane.[167] At present, perfluorinated ion-exchange membranes represented by Nafion are still mainstream membranes in alkaline AZDs; however, their poor VE and controversial ion transport mechanism limit the future application. This is because in alkaline media, hydroxide ions have higher mobility than Na$^+$/K$^+$; however, the ion transport in Nafion membranes mainly depends on the operation of the cation transport mechanism. This makes it difficult for hydroxide ions to pass through the Nafion membrane and severely reduces the ion conductivity and VE in alkaline media.[167] Li *et al.* prepared a cost-effective

polybenzimidazole (PBI) dense membrane for an alkaline Zn-Fe flow battery, which can guarantee fast transportation of hydroxyl ions in an alkaline electrolyte.[168] Moreover, the high mechanical strength of the PBI membrane could alleviate the Zn dendrite formation even at a very high current density (160 mA cm^{-2}). In addition to dense membranes such as PBI, another technological approach is to use porous membranes, which can isolate redox-active species from charge-balancing ions through pore size exclusion.[169] Based on an alkaline Zn-ferricyanide flow battery, Li *et al*. also prepared a nano-porous membrane with negative charges on the pore walls and surface, which is constructed by poly (ether sulfone) (PES) and negatively charged sulfonated poly (ether ether ketone) (SPEEK).[170] The negative charge in the membrane will induce the mutual repulsion between the negatively charged $[Zn(OH)_4]^{2-}$, thus converting the Zn dendrite direction and avoiding membrane failure. As a result, the fabricated Zn-ferricyanide flow battery exhibits a high durability (~240 cycles at 80 to 160 mA cm^{-2}) and remarkable areal capacity (154 mAh cm^{-2} Zn anode). In general, whether the use of dense or porous membrane technology is in its infancy, further exploration of materials and fundamental mechanisms is required.

6.2 Flow systems

Compared to natural convection, forced convection systems possess several merits. Firstly, even under a low flow rate (1 mm s^{-1}), a forced convection system is sufficient to convert the system from diffusion-controlled to convection-controlled processes, thus inhibiting concentration polarization and the formation of Zn dendrites (Figure 13a).[171,172] Meanwhile, the Zn dendrite growth direction would be deflected under the influence of the flow direction caused by the shear stress of flowing electrolytes, which reduces the possibility of internal short circuits.[24] In addition, as for convection-controlled system, the transport of Zn ions is greatly improved in the cathode; hence, the utilization of active materials and areal capacity of the cathode can also be significantly improved, especially for high loading scenarios. Secondly, a forced convection system could reduce the thickness of the electrolyte layer while enhancing the ionic flux, which will reduce the internal resistance to a

negligible scale, thus reducing the Ohmic losses and improving the VE (Figure 13b).[79] Thirdly, the forced convection system can make the composition of the electrode solution more stable, which is of great significance for pH-sensitive redox pairs (Figure 13c).[34,35] For instance, in a natural convection system based on Zn anodes and Mn^{2+}/MnO_2 liquid-solid conversion-type cathodes, a large pH change (1~3) during the cycling is sufficient to cause side reactions and unsatisfactory cycle stability. In addition, flow systems provide the possibility to decouple the energy and power: the battery capacity is determined by the charges stored in the electrolyte tank, while the power scales primarily with the rate of electrochemical reactions on the electrodes.[83]

However, there are some issues with cells using forced convection systems. Compared to a natural convection system, a flow system requires the use of one or more additional pumps and electrolyte tanks, which increases the fixed cost of the system and reduces the cell energy and power density. In addition, although the convection system could inhibit Zn dendrite growth and improve VE, additional energy is required to keep the electrolyte flowing, thus resulting in a lower EE. Therefore, to improve commercial viability, optimization based on the whole cell is necessary to determine the optimal flow rate and configuration.

6.3 Possible configurations

According to the number of membranes, cells can be divided into 1~3 compartments; in each compartment, the flow from the electrolyte could be either natural or forced convection. As a result, there are nine possible cell configurations (Figure 14). In general, as the number of membranes and forced convection systems increases, electrodes and electrolytes are more likely to work in a more suitable environment, which brings benefits in cell durability and working voltage window. However, more complex configurations often mean greater difficulty to offset the challenges brought by high costs.

Since AZDs are complex systems composed of multiple components, there is no universally optimal configuration suitable for all situations. The characteristics of specific cell configurations are often

only suitable for a certain range of applications. For instance, the cell configuration with a forced convection system is not suitable for applications with the volume limitations, such as hearing aid power supplies. Therefore, it is necessary to consider the optimization of cell configuration based on specific scenarios, which will be provided in the subsequent sections.

7 High-capacity applications

7.1 Conventional Devices

Stacking multiple battery modules is a common method to satisfy high-capacity demands; however, the lack of high energy density AZDs has hindered the further development of this strategy. Another candidate is RFBs (Figure 15a) that can store energy *via* liquid-liquid conversion reactions in both posi-electrolyte and nega-electrolyte, which decouple the linkage between energy and power. However, current RFBs face intrinsic issues, including high cost, limited service life, low CE/VE/EE, and low energy/power density.[173]

7.2 Novel Devices

ZRFBs are hybrid devices involving at least one solid-phase electrode reaction (Zn(II, aq)/Zn(s) redox pairs), which provide possibilities of the membrane-free and/or single-flow device design. The introduction of Zn anodes will make the areal capacity of the device limited by the anode, thus partially sacrificing the ability to decouple energy and power; however, the high volumetric charge density of the Zn metal (21053.22 C cm^{-3}) alleviates this defect to a certain degree, thereby achieving quasi-decoupling state under high DoD. Table 1 summarizes representative ZRFBs, in terms of their reaction mechanism, battery configuration and electrochemical performance. ZRFBs based on different chemical systems or different cell configurations exhibit various electrochemical characteristics. For instance, the EE of ZRFBs with two or more flow systems is usually lower (typically 40%~70%), while the single flow configuration can achieve higher EE (> 80%). In addition, ZRFBs involving solid-state cathodic reactions or O$_2$-related conversion reactions generally

possess much higher device energy or power density compared to that for ZRFBs relying on liquid-state or gaseous-state (except O_2) cathodic reactions. Currently, most ZRFBs have yet to reach the commercialization stage, while some ZRFBs have started commercialization attempts on the scale of hundreds of kWh to MWh level, such as Zn-Fe, Zn-Br$_2$ and Zn-O$_2$.[1]

When replacing the anode of conventional RFBs with Zn metals, single-flow single-membrane configurations could be realized (Figure 15b). Wang and colleagues reported a Zn-polyiodide flow battery using the Zn anode and posi-electrolyte containing highly soluble iodide/triiodide (I^-/I_3^-) redox couples, which demonstrates a high electrolyte energy density (167 Wh L^{-1}) close to that for low-end LIBs with the LiFePO$_4$ cathode.[174] They attributed this significant improvement to: a) the high solubility of the ZnI$_2$ (up to 7.0 M in the water); b) the use of Zn anodes allows the anodic chamber to have a flow-assisted system. However, as for (I^-/I_3^-) redox couples, one-third of the iodide ions act as a complexing agent to stabilize the iodine (I_2), which cannot contribute capacity and limited electrolyte energy density. To further improve the electrolyte energy density, Lu et $al.$ exploited Br$^-$ as the complexing agent to form I$_2$Br$^-$, which increases the electrolyte energy density to 202 Wh L$^-$ [189]. Meanwhile, the cell voltage is well-controlled to avoid the formation of toxic and corrosive Br$_2$.

It should be noted that in this review, flow-assisted systems are different from common flow systems in RFBs. Generally, the latter continuously provides active species as the sources for the energy conversion, which will be accompanied by the use of abundant amounts of electrolytes and large storage tanks; while the former merely conducts the forced convection of negligible amounts of electrolytes with a small-sized storage tank, which aims to reduce the internal resistance of the device and improve the cell durability.[24,175] Actually, with the further development of Zn dendrite suppression technology, flow-assisted systems could also be removed. A series of systems have been developed based on similar design principles, such as Zn-Br$_2$, Zn-Ce, Zn-Fe, Zn-ferricyanide and Zn-V.[78,80,176–178]

Based on the Zn anode, the use of cathodes involving solid-state conversion reactions allows ZRFBs to operate stably ($e.g.$ 98%~100% capacity retention after 1500 cycles) with faster kinetics in a

membrane-free configuration (Figure 15c). Generally, AZDs with solid-state conversion-type cathodes possess several merits, such as high power density (1500~6000 W kg^{-1}), non-flammability and low cost; however, they have been trapped by limited energy density (100~500 Wh kg^{-1} based on cathode active materials) and poor cycle life (typically 100~1000 cycles).[179] Chao *et al.* first proposed an electrolytic Zn-Mn battery with a high output voltage (1.95 V), remarkable gravimetric capacity (~570 mAh g^{-1} cathode), impressive device energy density (409 Wh kg^{-1}) and low cost (<US\$ 10 per kWh).[6] Subsequently, Cui *et al.* reported a membrane-free Zn/MnO$_2$ flow battery constructed with electrodeposition/dissolution reactions on both anodes (Zn^{2+}/Zn) and cathodes (Mn^{2+}/MnO$_2$), which exhibits a good rate capability (up to 10 C discharge) and an excellent durability (~100% capacity retention after 1000 cycles at 0.5 mAh cm^{-2}).[35] During the discharge process, the intercalation of Zn^{2+} and the dissolution of MnO$_2$ caused by H$^+$ are in a competitive relationship; usually, the latter has a higher reaction rate than the former; hence, only the MnO$_2$ deposition/dissolution could be observed during the relatively high rate cycling (6~10 C). However, the study on a hydrogen-manganese (H/MnO$_2$) battery has indicated that the conversion of Mn^{2+} to MnO$_2$ may involve two steps in sequence: a) oxidization of Mn^{2+} to Mn^{3+}; b) Mn^{3+} disproportionation generates Mn^{2+} and MnO$_2$.[180] To inhibit the Mn^{3+} disproportionation and improve the CE, Li and colleagues reported a soluble Mn(CH$_3$COO)$_2$ (Mn(AC)$_2$) neutral electrolyte, where the Mn^{2+} can directly deposit on the cathode in the form of MnO$_2$ due to the coordination effect of the AC$^-$.[34] The as-assembled ZRFB exhibits a high areal capacity (20 mAh cm^{-2}) and an excellent CE (99% after 400 cycles) at 40 mA cm^{-2}. Owning to the appropriate potential (0.536 V *vs.* SHE) of I$^-$/I$_3^-$ redox couples and their fast kinetics, Lu *et al.* proposed a mediator strategy that using I$^-$/I$_3^-$ redox couple to facilitate MnO$_2$ dissolution and recover 'lost capacity' caused by MnO$_2$ exfoliation, which achieved a record high areal capacity of 15 mAh cm^{-2} for over 50 cycles and excellent capacity retention (~100% after 225 cycles at 15 mAh cm^{-2}).[141] In addition to recovering the 'lost capacity', the I$^-$/I$_3^-$ redox mediator is effective in (a) improving cycling life and elevating CE; (b) reducing dead MnO$_2$ on the

electrode/membrane, thus decreasing overpotential, increasing VE, and suppressing electrode passivation.

ZRFBs using air cathodes (Zn-air flow batteries) are also considered promising devices for high-capacity applications. Unlike other ZRFBs, this system involves oxygen in the air during the cycling, thus removing the dependence on the flow system to continuously supply the electrolytes for the cathode reactions and significantly increasing the device energy density.[181] Generally, Zn-air flow batteries adopt a membrane-less single-flow configuration (Figure 15d), where the flow system is mainly used to improve the stability of the Zn anode. However, air cathodes are also accompanied by higher overpotential and slow reaction kinetics, which leads to a poor power density.

In addition, the use of ZRFBs with a double-membrane configuration (Figure 15e) could increase the operating voltage window and the device energy density. For instance, Yan *et al.* proposed a Zn-Fe RFB with a double-membrane multi-flow configuration, whose capital cost (100 USD per kWh) is estimated lower than the 2023 target set by the U.S. Department of Energy (150 USD per kWh).[79] The use of double-membrane configurations increases the operating voltage of Zn-Fe RFBs from 1.58 V to 1.99 V; however, this will also significantly increase the internal resistance of the device[176]. Therefore, flow-assisted systems are applied in anodic and middle compartments, thus reducing the internal resistance and enhancing the VE. Since the convection system may reduce the device EE, a series of optimizations were conducted to determine the optimum flow rates. To further enhance the energy density, Liu and coworkers first proposed a pH-decoupled ZRFB with Zn anode (in 2.4 M KOH + 0.1 M $Zn(CH_3COO)_2$) and MnO_2 (in 1.0 M $MnSO_4$ + 0.5 M H_2SO_4), which successfully broaden the operating potential to 2.44 V.[5] In addition, since the electrodes work in more suitable electrolytes, the as-fabricated ZRFB exhibits an ultrahigh specific capacity (616 mAh g^{-1} MnO_2 at 2 mA cm^{-2}), remarkable stability (99.5% capacity retention over 6000 cycles at 2 mA cm^{-2}), and an impressive energy density of 1503 Wh kg^{-1} (based on the total mass of anode and cathode).

Table 1. Representative Zn-based EES devices for high-capacity applications

ZRFBs	Discharge Cell Reaction	Cathodic Reaction State	Cell Configurations	Positive Electrolytes	Standard Potential (V vs. SHE)	System Efficiency at x mA cm⁻²	Capacity Retention at y mA cm⁻² after n Cycles	Ref.
Zn-Ce	$Zn(s) + 2Ce^{4+}(aq) \leftrightarrow Zn^{2+}(aq) + 2Ce^{3+}(aq)$	Liquid	Single-membrane, double-flow	0.8 M Ce(CH₃SO₃)₃ + 4.0 M CH₃SO₃H	2.04~2.48	E=46%, C=84% (x=50)	—	78
	Cathode: $MnO_2(s) + 4H^+(aq) + 2e^- \rightarrow Mn^{2+}(aq) + 2H_2O(l)$ Anode: $Zn(s) + 4OH^-(aq) - 2e^- \rightarrow Zn(OH)_4^{2-}(aq)$	Solid	Double-membrane, double-flow	1.0 M MnSO₄ + 0.5 M H₂SO₄	2.44	C=98.4% (x=2)	99.5% (n=6000, y=2)	5
	$Zn(s) + 2Mn^{4+}(aq) + 2H_2O(l) \leftrightarrow Zn^{2+}(aq) + Mn^{2+}(aq) + MnO_2(s) + 4H^+(aq)$	Solid	Single-membrane, single-flow	1.0 M MnAc₂	2.3	E=78%, C=99% (x=40)	~100% (n=100, y=40)	34
Zn-MnO₂	$Zn^{2+}(aq) + Mn^{2+}(aq) + 2H_2O(l) \leftrightarrow Zn(s) + MnO_2(s) + 4H^+(aq)$	Solid	Membrane-free, single-flow	4.0 M MnSO₄ + 4.0 M ZnSO₄	1.99	C=95% (2.0 mAh cm⁻²)	~100% (n=1000, at 0.5 mAh cm⁻²)	35
	$Zn^{2+}(aq) + Mn^{2+}(aq) + 2H_2O(l) \leftrightarrow Zn(s) + MnO_2(s) + 4H^+(aq)$	Solid	Membrane-free, single-flow	1.0 M MnAc₂ + 1.0 M ZnAc₂ + 2.0 M KCl + 0.1 M KI	1.99	—	~100% (n=225, at 15 mAh cm⁻²)	141
	$Zn^{2+}(aq) + Mn^{2+}(aq) + 2H_2O(l) \leftrightarrow 0.5Zn(s) + Zn_{0.5}MnO_2(s) + 4H^+(aq)$	Solid	Membrane-free, single-flow	1.0 M MnSO₄ + 1.0 M ZnSO₄	1.99	E=88%	92% (n=1800, y=30)	6
Zn-PbO₂	$Zn(s) + PbO_2(s) + 4H^+(aq) + SO_4^{2-}(aq) \leftrightarrow PbSO_4(s) + Zn^{2+}(aq) + 2H_2O(l)$	Solid	Membrane-free, single-flow	1.5 M ZnSO₄ + 0.5 M Na₂SO₄ + 0.5 M H₂SO₄	2.12	E>65%, C>80% (x=20)	~100% (n=90, y=20)	182
Zn-Cl₂	$Zn(s) + Cl_2(g) \leftrightarrow Zn^{2+}(aq) + 2Cl^-(aq)$	Gas	Membrane-less, single-flow	2.0 M ZnCl₂ + 4.0 M KCl	2.12	E=66%, C=84% (x=22)	—	183
Zn-Br₂	$Zn(s) + Br_2(aq) \leftrightarrow Zn^{2+}(aq) + 2Br^-(aq)$	Liquid	Single-membrane, single-flow	2.0 M ZnBr₂	1.85	E=82%, C=92% (x=20)	—	178
Zn-V	$Zn(s) + 2VO^+(aq) + 4H^+(aq) \leftrightarrow Zn^{2+}(aq) + 2VO^{2+}(aq) + 2H_2O(l)$	Liquid	Single-membrane, double-flow	1.7 M V³·⁵⁺ + 4 M H₂SO₄	1.76	E=72%, C=88%, V=82% (x=20)	99% (n=50, y=20)	80
Zn-Ni	$Zn(s) + 2NiO(OH)(s) + 2H_2O(l) + 2OH^-(aq) \leftrightarrow Zn(OH)_4^{2-}(aq) + 2Ni(OH)_2(s)$	Solid	Membrane-free, flow-assisted	ZnO in 45 w.t.% KOH	1.73	E>80%, C>90% (x=10)	~98% (n=1500, 3.7 Ah battery)	24
Zn-O₂	$Zn(s) + 1/2O_2(g) + H_2O(l) + 2OH^-(aq) \leftrightarrow Zn(OH)_4^{2-}(aq)$	Gas	Membrane-free, single-flow	0.7 M K₂Zn(OH)₄ + 7 M KOH + 0.7 M LiOH	1.59	E=72%, C=97% (x=20)	—	181
Zn-ferricyanide	$Zn(s) + 2Fe(CN)_6^{3-}(aq) + 4OH^-(aq) \leftrightarrow 2Fe(CN)_6^{4-}(aq) + Zn(OH)_4^{2-}(aq)$	Liquid	Single-membrane, double-flow	0.2 M K₃Fe(CN)₆	1.58	E=82.8%, C=99.5%, V=88.1% (x=160)	99.5% (y=100, n=210)	176
Zn-Fe	$Zn(s) + 2Fe^{3+}(aq) \leftrightarrow Zn^{2+}(aq) + 2Fe^{2+}(aq)$	Liquid	Double-membrane, multi-flow	1.0 M FeCl₂ + 1.0 M HCl	1.99	E=74%, C=99.9%, V=76% (x=40)	—	79
		Liquid	Single-membrane, double-flow	0.6 M FeCl₂ + 0.2 M FeCl₃	1.53	E=70%, C=60% (x=25)	—	177
Zn-I₂	$Zn(s) + I_2Br^-(aq) \leftrightarrow Zn^{2+}(aq) + 2I^-(aq) + Br^-(aq)$	Liquid	Single-membrane, double-flow	5.0 M ZnI₂ + 2.0 M ZnBr₂	1.35	E=88%, C=99% (x=10)	~100% (y=50, n=50)	89
	$Zn(s) + I_3^-(aq) \leftrightarrow Zn^{2+}(aq) + 3I^-(aq)$	Liquid	Single-membrane, double-flow	5.0 M ZnI₂	1.30	E=67%, C=96% (x=20)	92% (y=10, n=40)	174
Zn-Organic	$Zn(s) + 2TEPMO^+(aq) \leftrightarrow Zn^{2+}(aq) + 2TEPMO(aq)$	Liquid	Double-membrane, single-flow	1.0 M hydroxyl-TEMPO + 2.0 M NaCl + Na₂SO₄	1.595	E=74%, C=88% (x=10)	91.6% (y=3, n=1100)	85
		Liquid	Double-membrane, single-flow	poly(TEMPO) in 0.75 M Zn(ClO₄)₂	1.515	E=80%, C>90% (x=20)	81.0% (y=1.4, n=500)	184
	$Zn(s) + pBQ(aq) + 2H^+(aq) \leftrightarrow Zn^{2+}(aq) + HQ(aq)$	Liquid	Membrane-free, single-membrane	1.5 M ZnCl₂ + 0.05 M HQ	1.59	E=73%, C=74% (x=30)	—	185

* "E", "C" and "V" in the "system efficiency" column refer to the energy efficiency, Coulombic efficiency and voltage efficiency, respectively.

* TEPMO=(2,2,6,6-Tetramethylpiperidin-1-yl)oxyl, pBQ= parabenzoquinone, HQ=1,4-hydroquinone.

8 High power density applications

8.1 Conventional devices

Aqueous ZSCBs (Figure 16a) usually possess high power density (typically 1500~9000 W kg^{-1}), such as Zn-Ni and Zn-Ag systems.[8] Unfortunately, these rechargeable batteries have not succeeded in occupying the market of high power density applications. Although they have some advantages, such as high nominal voltage (1.65 V) and high discharge rate (up to 50 C), notable drawbacks are severe, including: a) a high self-discharge rate (> 1% capacity per day) after 30~50 cycles caused by the decomposition of active materials in a strongly alkaline environment; b) low specific capacity (< 300 mAh g^{-1}), narrow voltage window (1.0~1.6 V) and limited device energy density (< 60 Wh kg^{-1}); c) the formation of Zn dendrites.[139,140,186,187] To address these challenges, several start-up companies such as ZincFive optimizes the electrolyte composition to achieve high power density (3000 W kg^{-1}) while maintaining a good device energy density (70 Wh kg^{-1}) and cycling stability.[188] Nevertheless, this improvement is quite limited.

8.2 Novel devices

Unlike organic electrolytes with low ionic conductivity, the use of aqueous electrolytes allows AZDs to easily achieve high power density under safe operating conditions. Therefore, the development of next-generation high-power AZDs should focus on increasing the specific capacity of electrodes and device energy density while maintaining high power density. A variety of novel ZSCB systems (Figure 16b) have been developed in recent years (Table 2), such as Zn-S, Zn-Se, Zn-Se$_x$S$_y$ and Zn-I$_2$ batteries.[29–31,189] Liang and co-workers proposed a Zn-I$_2$ ZSCB involving highly reversible I$_2$/I$^+$ (1.83 V *vs.* Zn/Zn^{2+}) and I$^-$/I$_2$ (1.29 V *vs.* Zn/Zn^{2+}) couples.[189] Such a system possesses the following merits compared with the conventional I$_2$-based ZSCBs: a) the specific capacity (609 mAh g^{-1} at 0.2 A g^{-1}) is doubled due to a four-electron transfer process; b) a higher potential window increases the device energy density (495 Wh kg^{-1}). In addition, the solubility of ZnS (1.2×10^{-23} mg L^{-1}) and ZnSe (3.6×10^{-26} mg L^{-1}) in aqueous electrolytes is negligible, compared to that for Li$_2$S (>5 mg L^{-1}); therefore, chalcogen-based ZSCBs are viable in theory.[30] Recently, Zhi *et al.* reported the first

Zn/polysulfide system, which exhibits a high specific capacity (1148 mAh g^{-1}) and good energy density (724.7 Wh kg^{-1} cathode) at 0.3 A g^{-1};[29] this impressive specific capacity mainly results from the multi-electron transfer of S_6^{2-} and S^{2-} redox pairs. Later, they constructed a Zn-Se ZSCB, which achieved high capacity in both aqueous (611 mAh g^{-1} Se) and organic systems (551 mAh g^{-1} Se) at 0.1 A g^{-1}.[31] In addition, Wang and co-workers synthesized a Se-S composite solid-phase conversion-type cathode and achieved a record high specific capacity (1222 mAh g^{-1} at 0.2 A g^{-1}) and large energy density (867.6 Wh kg^{-1} SeS$_{5.76}$).[30] Subsequently, they conducted theoretical calculations and proved that the synergistic effect of Se and S could increase the electrical conductivity and reaction activity of the electrode materials, thereby promoting electrochemical kinetics.

The AZIB is an emerging EES device that was firstly reported in 2011, which has received widespread attention and numerous breakthroughs in the past decade. Benefit from the insertion-type cathodes, AZIBs are easier to achieve rapid electrode reaction kinetics and power density, which have been discussed in Section 5.1. Using organic cathode materials showing a weak intermolecular van der Waals force with Zn-ions can further improve the Zn-ion diffusivity and the device power density. However, the poor cycle life and narrow ESPW of most organic electrode materials limit the implementation of this strategy. For instance, although the AZIB using a ladder-like polymer (C$_6$S$_2$O$_2$)$_n$ has exhibited a high power density of 17433 W kg^{-1} (at 145.2 Wh kg^{-1}), its narrow voltage window (0.2~1.6 V) and insufficient durability (75.3% capacity retention after 10,000 cycles, at 20 A g^{-1}) hindered practical high-power applications.[190] Recently, Liu *et al.* developed a composite cathode *via* electrodepositing a poly(1,5-naphthalenediamine, NAPD) nanorods on the nanoporous carbon, which achieved a high capacity retention of 91% over 10,000 cycles at 10 A g^{-1}[191]. By analyzing the 3D molecular structures, they presumed that the superb cycling stability results from the aligned helix-shaped poly(1,5-NAPD) chains, which have ample spaces for Zn-ion (de)insertion and suppress the Zn-ion from trapping in the molecular chains.

Besides the extensively discussed challenges, such as narrow voltage window (1.0~1.9 V) and Zn anode issues, current AZIBs also face low areal specific capacity caused by sluggish Zn-ion diffusion

kinetics and poor conductivity of active materials. At present, the active material loading on the cathode materials used in most reports is 1~2 mg cm^{-2}, which is far lower than the loading used in commercial LIBs (10~20 mg cm^{-2}). As the loading increases, the utilization rate of the active material and the areal specific capacity of cathodes quickly drop to an unacceptable range. In addition to the innovation in electrode materials and electrolytes, this review suggests that following three aspects should be addressed in the future to solve this challenge: (a) develop next generation binders specifically for AZIBs; (b) optimize current electrode formula (active material: conductive additive: binder = 7:2:1 or 8:1:1); (c) optimize the electrode manufacturing process.

The double-membrane configuration (Figure 16d) could effectively decouple the electrolytes in anodic and cathodic compartments, thereby maximizing the operating voltage and enhancing the device energy density. Zhong *et al.* proposed a double-membrane Zn-MnO$_2$ conversion battery, whose anode (Zn-metal) and cathode (MnO$_2$) can work under alkaline (6 M KOH, 0.2 M ZnO and 5 mM vanillin) and acidic (3 M H$_2$SO$_4$ and 0.1 M MnSO$_4$) conditions, respectively.[27] This design increases the open circuit potential from 1.5 V (typical Zn-MnO$_2$ membrane-free conversion battery) to 2.83 V, which exhibits an impressive energy density (90 Wh kg^{-1}) and durability in a prototype scaled up to 3.3 Ah[187]. In addition, benefitting from working under the most suitable conditions, the utilization rate of MnO$_2$ is extremely high, which provides an impressive specific capacity and cycling stability. The utilization rate of MnO$_2$ working under the most suitable conditions is close to 100%, which provides a record high specific capacity (616 mAh g^{-1}) in a variety of current densities (100 mA g^{-1}~1000 mA g^{-1}), as well as remarkable capacity retention of 98% after 200 h cycling at 500 mA g^{-1}. To the best of our knowledge, this configuration is only attempted on a limited number of ZSCBs, while has not been applied in the AZIBs yet. It should be noted that the increase in energy density should not sacrifice huge power density. The double-membrane configuration inevitably increases the internal resistance, but this is within an acceptable range for high-power batteries. Although the employment of SEs is a highly effective method to enhance device energy density, the ion

conductivity of SEs is several orders of magnitude lower than that of LEs, which will cause rapid power density loss and is not recommended for high-power applications.

In addition, the use of flow-assisted systems may be an effective strategy to further enhance cycling stability and power performance (Figure 16e). Theoretically, this configuration only requires a negligible amount of electrolytes and forced convection at a very low flow rate (<0.1 mm s^{-1}), so it does not require a large storage tank and will not greatly sacrifice the device energy density and EE. However, current devices with the flow system are too large either in the laboratory or for practical applications, which will greatly deteriorate the device energy density and lose marketing competitiveness in applications with restrictions on volume or weight. Therefore, the development of devices with small-sized flow-assisted systems in the future could be promising for high-power applications.

Table 2. Representative Zn-based EES devices for high power density applications

Batteries	Configuration	Cathode Materials	Electrolyte	Working Potential (V)	Specific Capacity (mAh g^{-1}) at x A g^{-1}	Capacity Retention at y A g^{-1} after n Cycles	Rate Capability (Capacity Retention at z*x A g^{-1})	Maximal Power Density (W kg^{-1} at w Wh kg^{-1})	Ref.
Ni-based ZSCB	Membrane-free, natural convection	Ni-NiO@carbon cloth (CC)	6.0 M KOH + 0.5 M Zn(Ac)$_2$	0.0-0.75	237.1 (x=2.5)	87.5% (n=2000, y=31.25)	68.5% (z=40)	41600 (w=287.4)	140
Ag-based ZSCB	Membrane-free, natural convection	Ag$_2$O@rGO	ZnO saturated in 60 M KOH solution	0.8-2.05	42 (x=0.005)	100.0% (n=35, y=0.005)	—	—	139
MnO$_2$-based ZSCB	Membrane-free, natural convection	α-MnO$_2$	2.0 M ZnSO$_4$ + 0.1 M MnSO$_4$	1.0-1.9	285 (x=C/3)	92% (n=5000, 5C)	42.6% (z=10)	—	187
	Double-membrane, natural convection	MnO$_2$	Acidic (posi-electrolyte), alkaline (nega-trolyte)	0.0-2.85	>600 (x=0.1~1)	98% (n=200 hr, y=0.5)	99% (z=10)	—	27
I$_2$-based ZSCB	Membrane-free, natural convection	PAC-I$_2$	ZnCl$_2$: LiCl: CH$_3$CN=19:5:8	0.6-1.9	609 (x=0.2)	82% (n=6000, y=2)	64.9% (z=10)	1500 (w=400)	189
Chalcogenides-based ZSCB	Membrane-free, natural convection	poly(Li$_2$S$_6$-r-DIB) [a]	1 M Zn(TFSI)$_2$ + 21 M LiTFSI	0.0-1.95	1148 (x=0.3)	70% (n=300, y=0.3)	27.8% (z=16.7)	4800 (w=331)	29
	Membrane-free, natural convection	Se/CMK-3 [b]	1.0 M ZnSO$_4$	0.9-1.8	611 (x=0.1)	80.3% (n=1,000, y=1)	48.3% (z=50)	—	192
	Membrane-free, natural convection	Se$_x$S$_y$	3.0 M ZnSO$_4$ + 0.1 wt% I$_2$	0.2-1.3	1222 (x=0.2)	75% (n=500, y=4)	58.3% (z=25)	—	30
Mn-based AZIBs	Membrane-free, natural convection	α-MnO$_2$ @ graphene scrolls	2.0 M ZnSO$_4$ + 0.2 M MnSO$_4$	1.0-1.9	362.2 (x=0.3)	94% (n=3000, y=3)	55.1% (z=30)	9450 (w=109.2)	193
	Membrane-free, natural convection	MnO$_2$	4.0 M Zn(OTF)$_2$ + 0.5 M Me$_3$EtNOTF	1.0-1.9	150 (x=0.05)	88.5% (n=1000, y=2)	55% (z=40)	—	60
V-based AZIBs	Membrane-free, natural convection	δ-Ni$_{0.25}$V$_2$O$_5$·nH$_2$O	3.0 M Zn(TSFI)$_2$	0.3-1.7	402 (x=0.2)	98% (n=1200, y=5)	35.9% (z=25)	3920.8 (w=286.6)	108
	Membrane-free, natural convection	NH$_4$V$_4$O$_{10}$ nanobelt	1.0 M Zn(TSFI)$_2$	0.3-1.5	485 (x=0.1)	90% (n=3000, y=10)	38.1% (z=100)	6900 (w=90)	194
PBA-based AZIBs	Membrane-free, natural convection	Zinc hexacyanoferrate	1.0 M ZnSO$_4$	0.8-1.9	65.4 (x=0.06)	81% (n=100, y=0.3)	—	1700 (w=100)	195

	Configuration	Material	Electrolyte	Voltage	Specific capacity	Capacity retention		Power density	Ref
Organic AZIBs	Membrane-free, natural convection	Poly(1,5-NAPD)/AC	3.0 M ZnSO$_4$	0.0-1.8	315 (x=0.19)	91% (n=10000, y=10)	46.0% (z=77.9)	10000 (w=92)	[191]
	Membrane-free, natural convection	(C$_6$O$_2$S$_2$)$_n$	4.0 M Zn(TSFI)$_2$	0.2-1.6	205 (x=0.05)	75.3% (n=10000, y=20)	—	17433 (w=145.2)	[190]
	Membrane-free, natural convection	Polyaniline (PANI)	Ca(BH$_4$)$_2$ in Dimethylacetamide (DMAc)	0.5-1.5	200 (x=0.5)	92% (n=3000, y=5)	45% (z=100)	—	[196]

* The specific capacity, peak power density and energy density are based on the mass of cathodes.

^{a} poly(Li$_2$S$_6$-r-DIB) = poly(Li$_2$S$_6$-random-1,3-diisopropenylbenzene); ^{b} Se/CMK-3 = selenium-infused ordered mesoporous carbon.

9 Ultrahigh power density applications

9.1 Conventional devices

Traditional Zn-based SCs, including EDLCs and pseudocapacitors, are preferences for ultrahigh power applications. The characteristic structural feature of conventional SCs (Figure 17a and 17b) is that both cathodes and anodes only involve the NFC or CF process, other than NCF process.[9] Meanwhile, to facilitate the hydrated Zn^{2+} transfer and maximize the power density, membrane-less (separator) configuration and aqueous electrolytes are adopted. As a result, SCs usually possess ultrahigh power density (10^5~10^6 W kg^{-1}), long cycle life (<1% capacitance loss after 10,000 cycles) and fast response rate (millisecond-level); however, this also compromised energy density (< 5 Wh kg^{-1}).[197] Although a variety of high-performance electrode materials have been proposed, the energy density of SCs is still difficult to break the limitations of NFC and CF charge storage mechanisms.[198,199]

9.2 Novel devices

As shown in Figure 17c, when Zn anodes involving NCF processes are combined with EDLC or pseudocapacitive cathodes, ZHSCs are proposed. As an emerging concept, the first ZHSC device was proposed by Tian and colleagues in 2016.[200] Theoretically, ZHSCs are energy storage devices with characteristics of both batteries and supercapacitors. That is, they are expected to possess good energy density, high power density, short response time and long cycling stability.[32,201,202] However, the overall electrochemical performance of reported ZHSC devices (Table 3) has typically been significantly lower than expected. This is mainly due to the fact that the capacitance of cathode materials could not match with the Zn anode, which resulted in a low utilization rate of Zn and an

undesirable device energy/power density.[203] Therefore, the core optimization strategy of current cathode materials is to increase the energy density while ensuring high power density and long-term durability. A variety of strategies focusing on cathode material innovation have been discussed in Section 5.3 and 5.4, including the construction of hierarchical pore structure, heteroatom doping, surface morphology engineering, and the introduction of functional groups.[33,204–208] Theoretically, it is possible to construct ZHSCs with both high energy density and high power density by the employment of SEs and double-membrane configuration; however, this is not recommended by this review. Because this method may reduce the power density of ZHSC to a level similar to the high-power AZDs discussed in Section 8, but it cannot be compared with the latter in terms of energy density, due to the huge intrinsic gap in the specific capacity of the cathode material. In addition, the use of a flow system is not recommended, because: (a) the use of a flow system will inevitably increase the distance between cathode and anode and the amount of electrolyte used, which is not conducive to rapid ion transport; (b) ZHSCs are usually surface-controlled, and there is no significant benefits in using a flow system to convert diffusion-controlled to convection-controlled process.

Another method to construct hybrid devices is to adopt cathodes with a hybrid energy storage mechanism (Figure 17d), which has rarely been reported so far. Very recently, Sun *et al.* proposed an oxygen-bonded defective reduced graphene oxide (rGO) as the hybrid cathode for ZHSCs, which could simultaneously produce three types of electrochemical energy storage behaviors: pseudocapacitive, EDLC and gas-phase conversion-type reactions (ORR/OER).[209] During charge and discharge, the capacitance of the device is contributed to by: a) physical adsorption/desorption of anions on the rGO surface; b) electrochemical adsorption/desorption of Zn-ions on the oxygen-containing functional groups on cathodes; c) the ORR/OER catalysed by the defects of rGO exposed to electrodes/electrolyte/air triple phase interface. As a result, the assembled device exhibited a high specific capacitance (370.8 F g^{-1} at 0.1 A g^{-1}) and good durability (94.5% capacitance retention after 10,000 cycles at 5 A g^{-1}). More exploration of such devices will provide fresh inspiration for ultra-high power density applications.

Table 3. Representative ZHSCs for ultrahigh power density applications

Cathode Materials	Electrolyte	Working Potential (V)	Specific Capacity (mAh g⁻¹) at x A g⁻¹	Specific Capacitance (F g⁻¹) at x A g⁻¹)	Capacitance Retention at y A g⁻¹ after n Cycles	Maximal Power Density (W kg⁻¹ at w Wh kg⁻¹)	Maximal Energy Density (Wh kg⁻¹ at p W kg⁻¹)	Ref.
Activated carbon (AC), YP-80F	2.0 $_M$ ZnSO$_4$	0.5-1.5	—	259.4 (x=0.05)	~100% (n=10000, 1.56 mA cm⁻²)	3.9 mW cm⁻² at 89 µWh cm⁻²	115.4 µWh cm⁻² at 0.16 mW cm⁻²	32
AC	2.0 $_M$ ZnSO$_4$	0.2-1.8	121 (x=0.1)	272 (x=0.1)	91% (n=10000, y=1)	14900 (w=30)	85 (p=35)	201
AC, PSC-600	1.0 $_M$ Zn(TSFI)$_2$/PVA	0.2-2.2	85 (x=0.1)	413.3 (x=0.2)	92.2% (n=10000, y=10)	15700 (w=65.4)	147 (p=136.1)	204
Hierarchical porous carbon	3.0 $_M$ Zn(ClO$_4$)$_2$	0-1.9	179.8 (x=0.1)	340.7 (x=0.1)	99.2% (n=30000, y=20)	48800 (w=40.4)	104.8 (p=58)	150
Mesoporous hollow carbon sphere (MHCP)	2.0 $_M$ ZnSO$_4$	0.2-1.8	110 (x=1)	393 (x=0.1)	96% (n=10000, y=1)	13700 (w=36.8)	129.3 (p=266.4)	205
Layered B/N co-doped carbon	1.0 $_M$ ZnSO$_4$	0.2-1.8	127.7 (x=0.5)	287 (x=0.5)	81.3% (n=6500, y=5)	12200 (w=86.8)	101 (p=500)	206
Porous carbon nanoflake (PCNF)	1.0 $_M$ ZnSO$_4$	0.1-1.7	177.7 (x=0.5)	243 (x=0.5)	~90% (n=10000, y=10)	15390 (w=68.4)	142.2 (p=400.3)	207
Chemical activated graphene (aMEGO)	3.0 $_M$ Zn(TSFI)$_2$	0.0-1.9	—	210 (x=0.1)	93% (n=80000, y=8)	31400 (w=50)	106.3 (p=90)	33
MOFs derived carbon (MDC)	1.0 $_M$ ZnSO$_4$	0.1-1.7	—	123 (x=0.2)	99% (n=20000, y=1)	85500 (w=7.5)	36.4 (p=125)	208
Poly(4'4-TDP) [a]	2.0 $_M$ ZnSO$_4$	0.1-1.9	0.49 mAh cm⁻² (x=1 mA cm⁻²)	—	71% (n=2000, at 8 mA cm⁻²)	—	1.03 mWh cm⁻² (0.9 mW cm⁻²)	159
Graphene@polyaniline (PANI)	2.0 $_M$ ZnSO$_4$	0.0-0.8	154 (x=0.1)	414 (x=0.1)	80.5% (n=6000, y=5)	2455 (w=138)	205 (p=45.8)	210
Poly(3,3'-DHB)/AC [b]	2.0 $_M$ ZnSO$_4$	0.5-1.5	—	1.3 F cm⁻² (x=0.16 mA cm⁻²)	80.0% (n=5000, y=8 mA cm⁻²)	4.01 mW cm⁻² (~0.2 mWh cm⁻²)	0.18 mWh cm⁻² (p=0.26 mW cm⁻²)	211
RuO$_2$·xH$_2$O	2.0 $_M$ Zn(TSFI)$_2$	0.4-1.6	122 (0.1)	—	~100% (n=10000, y=1)	16700 (w=82)	102 (p=100)	202

* The specific capacity, peak power density and energy density are based on the mass of cathodes.
[a] Poly(4,4'-TDP) = poly(4,4'-thiodiphenol); [b] Poly(3,3'-DHB)/AC = poly(3,3'-dihydroxybenzidine)/activated carbon.

10 High energy density applications

10.1 Conventional devices

Devices with high energy density generally use insertion-type or solid-phase conversion-type cathodes, such as LiFePO$_4$-based LIBs. However, AZDs are difficult to achieve high energy density due to the narrow potential window, slow diffusion kinetics of Zn hydrated ions, limited areal capacity and low utilization rate of electrode materials.[4,7,116] Another viable candidate is the ZAB, which uses a Zn anode and an air cathode in a strongly alkaline electrolyte (Figure 18a).[69] Theoretically, ZAB is a special semi-open quasi-decoupling system, which is considered to possess high specific capacity (819 mAh g⁻¹ Zn) and energy density (1353 Wh kg⁻¹ Zn) due to: a) the oxygen in the surrounding air is used as active species, thus reducing the total mass and volume of the cathode; b) the specific

capacity and utilization rate of active materials are not limited by the slow diffusion kinetics of Zn-ions in the cathodes.[49,127] However, current commercialized rechargeable ZABs only demonstrated very limited device energy densities (35~50 Wh kg^{-1}).[212] The huge gap in energy density could be attributed to challenges in many aspects, mainly including: (a) low utilization rate and reversibility of Zn anode; (b) slow ORR/OER dynamics requires a larger air electrode to meet the power output requirements.; (c) narrow ESPW of aqueous electrolytes.

10.2 Novel devices

Table 4 summarizes representative ZABs and their electrochemical performance. The key to establish next-generation ZABs is the innovation in high-performance electrodes and electrolytes, which have been discussed in detail in Sections 3~5. In addition, the use of SEs can reduce the mass and volume of the entire device, thereby maximizing energy density. Lee et al. reported a realistic all-solid-state Zn–air pouch cell, which is fabricated by anti-freezing chitosan-biocellulosic (CBC) super-ionic electrolyte, 3D sponge copper phosphosulfide (CPS) cathode, and patterned Zn anodes[213]. The use of SEs reduced the mass ratio of electrolyte to anode and cathode to 1:1.4 and 1:0.55, respectively. As a result, the assembled 1-Ah-class ZAB exhibited unprecedented high device energy density (~ 523 Wh kg^{-1}, 1609 Wh L^{-1}), which is almost twice that of the most cutting-edge commercial LIBs. In addition, the battery also possesses a long cycle life (96% capacity retention over 6000 cycles at 25 mA cm^{-2}), good device power density (up to 1000 W kg^{-1}), wide operating temperature ($-20 \sim 80\,°C$), and mechanical flexibility. This work greatly reinvigorated the confidence in the development of high-energy AZDs.

Another universal method to increase the energy density of AZDs is to establish a high-voltage system. Although the double-membrane configuration can broaden the operating voltage, it is not suitable for ZABs. The widest operating voltage in the double-membrane configuration is achieved when the Zn anode and air cathode working in a strongly alkaline and strongly acidic environment, respectively; however, the current high-performance ORR/OER air cathode in strongly acidic media is highly dependent on noble-metal-based materials. When expensive noble-metal-based materials

and ion exchange membranes are used simultaneously, the exceptionally high cost will directly hinder the further commercialization of ZABs. In contrast, the WIS electrolyte that can also broaden the operating potential is more acceptable for ZABs, due to its ever-decreasing cost and the possibility of operating in a neutral/weakly acidic environment.[126] Also, the further research on molecular crowding electrolytes is highly recommended.[76]

The adopt of hybrid cathodes provide the possibility to construct AZDs with both high energy density and power density (Figure 18c). In addition to the hybrid cathodes discussed in the previous section, it is also promising to hybridize traditional air cathodes with insertion-type or solid-phase conversion-type cathodes. However, the current major challenge lies in the compatibility of working conditions; even electrodes with the same materials may demonstrate different charge storage mechanisms in different electrolytes. For instance, MnO_2 is a multifunctional active specie, whose optimal working condition for different scenarios are various: a) air cathodes (pH > 13); b) insertion-type cathodes (pH = 4.0~6.5); c) solid-phase conversion-type cathodes (pH < 3); d) pseudocapacitive cathodes (nano-sized, pH = 4.0~6.5 or pH > 13).[27,49,109,214] Fortunately, recent breakthroughs have increased the possibility of constructing hybrid cathodes. Very recently, Wang and colleagues have proven the 1 M $Zn(OTf)_2$ could construct a water-poor and (Zn^{2+})-rich IHP on the hydrophobic air cathode at a small current density (1 mA cm^{-2}), and for the first time achieved the reversible 2e$^-$ ORR/OER in the neutral condition for ZABs.[126] Rechargeable alkaline Zn-air batteries promise high energy density and safety but suffer from the sluggish 4-electron/oxygen (O_2) chemistry that requires participation of water, and from the electrochemical irreversibility originating from parasitic reactions caused by caustic electrolytes and atmospheric carbon dioxide. Wang *et al.* proposed a that proceeds through a 2e$^-$/O_2 process in nonalkaline aqueous electrolytes, which enables highly reversible redox reactions in Zn-air batteries. The nonalkaline Zn-air battery thus constructed not only tolerates stable operations in ambient air but also exhibits substantially better reversibility than its alkaline counterpart. In addition, they have also proposed a series of mildly acidic/near-neutral electrolyte systems, such as 1

м Zn(TFSI)$_2$ + 20 м LiTFSI and 0.5 м Zn(TSFI)$_2$ + 18 м Zn(ClO$_4$)$_2$, which could satisfy the requirements for insertion-type and air cathodes simultaneously.[28]

In addition to ZABs, AZIBs and ZSCBs with high specific capacity are also promising candidates for high energy density devices (Figure 18d). However, in addition to the narrow operating potential window and Zn anode issues, it still needs to solve the challenges brought about by the increase in the cathode active material loading, including: (a) the rapid decline in specific capacity and active material utilization rate, which has resulted in an areal specific capacity that cannot compete with commercial LIBs; (b) During the cycling, the cathode suffers a significant volume change due to phase transformation, which severely deteriorates the device durability. The currently reported cathode materials can only maintain high performance at a loading of 1~2 mg cm^{-2}, which is far from that of commercial LIBs (10-20 mg cm^{-2}). Therefore, subsequent improvements in the Zn-ion diffusivity and optimization of cathode formulations and manufacturing processes are urgently needed.

Although WIS electrolyte has become a hot spot in recent years as a strategy to increase the operating potential window and the reversibility of Zn anodes, its application in high energy density AZIBs or ZSCBs needs to be cautious. In addition to cost issues, following issues need to be considered: (a) this strategy increases the mass of the electrolyte, which damages the device energy density to a certain extent; (b) some cathode materials with low ESPW can not work stably in WIS electrolytes. Therefore, the future deployment of WIS electrolytes should be developed from full cell scales. In addition, other effective methodologies to increase the device energy density are effective, including the deployment of SEs, molecular crowding electrolytes, and double-membrane configuration (Figure 18e); but these still require more in-depth exploration.

Table 4. Representative ZABs for high energy density applications

Cathode Materials	Electrolyte	Potential Difference (E_{OER}-E_{ORR}, V)	Voltage Gap (ΔE, V)	Specific Capacity (mAh g^{-1}) at x A cm^{-2}	Durability (cycles at y A cm^{-2}, n min per cycle)	Maximal Power Density (mW cm^{-2} at z mA cm^{-2})	Maximal Energy Density (Wh cm^{-2} at p mW cm^{-2})	Round Trip Efficiency	Ref.
Co$_3$O$_4$	0.1 м KOH	1.117	0.72	—	175 (y=2, n=6.67)	—	—	62.7%	215
Co$_3$O$_4$@NiFe LDHs ^{a}	1.0 м KOH	0.78	0.80	667.5 (x=10)	1,200 (y=15, n=10)	—	797.6 (127.4 mW cm^{-2})	60%	216

Co-N-doped Carbon	0.1 M KOH	0.84	0.84	—	300 (y=10, n=11)	239.8 (z=1)	—	—	217
P-O-doped Fe-N-C	0.1 M KOH	0.74	0.77	—	450 (y=10, n=2.67)	232 (z=1)	—	61%	218
Co–Co$_3$O$_4$@NAC [b]	6.0 M KOH + 0.2 M Zn(AC)$_2$	1.042	0.773	721 (x=10)	105 (y=10, n=20)	164 (z=1)	—	—	219
Co$_3$O$_{4-x}$ nanosheets	6.0 M KOH + 0.2 M Zn(AC)$_2$	—	0.462	791 (x=5)	450 (y=5, n=20)	57 (z=1)	—	—	220
Pt-SCFP [c]	6.0 M KOH + 0.2 M ZnCl$_2$	0.73	0.77	790.4 (x=5)	240 (y=5, n=20)	122 (z=214)	—	61.9%	221

* The specific capacity, peak power density and energy density are based on the mass of Zn anodes.

[a] LDHs = layered double hydroxides; [b] NAC = nitrogen-doped carbon; [c] SCFP = $Sr(Co_{0.8}Fe_{0.2})_{0.95}P_{0.05}O_{3-\delta}$.

11 Conclusions and perspectives

This work adopts a holistic perspective to systematically review underlying mechanisms, development, and promising strategies of AZDs that have appeared since the 18th century. For the first time, this review uses the combination of key components to classify and summarize 15 types of promising AZDs, whose application scenarios include high capacity, high power, ultrahigh power, and high energy.

11.1 Overview of current AZDs

Figure 19a compares the performance of AZDs and other EES technologies in terms of energy density and power density (exclude devices with flow systems). Due to the use of aqueous electrolytes with high ionic conductivity, AZDs are easier to achieve high power density than other technologies that use organic electrolytes; however, this also causes a series of Zn anode issues and sacrifices operating voltage and energy density. When battery-typed cathodes are used, the best-performed AZIBs and ZSCBs can easily achieve much higher power densities than commercial LIBs and an energy density close to low-end LIBs, making them excellent substitutes for Ni-MH batteries and current high power density devices. The deployment of air cathodes in ZABs improves the capacity from breaking the cathode limitation; hence, rechargeable ZABs are promising candidates as next-generation high-energy-density devices. When replacing the cathode with a capacitive material, ZHSCs can achieve a much higher energy density than traditional EDLCs and pseudocapacitors with only a negligible sacrifice of power density, making them highly competitive in ultrahigh power density scenarios.

However, a major obstacle to the commercialization of rechargeable AZDs is their generally low areal capacity. Compared with traditional RFBs, the area capacity of ZRFBs is limited by Zn anodes, which increases the cost of stacks in high-capacity applications, such as grid-scale energy storage. For semi-open systems, the high areal capacity of ZABs can only be achieved when typical high-cost materials are employed, which is a challenge for the commercialization. In addition, for close systems, AZIBs, ZSCBs and ZHSCs face the problems of the low utilization rate of Zn anodes and rapid decline of surface capacity when the thickness of the cathode increases. Therefore, only a few AZDs start early industrialization attempts, such as ZABs, Zn-Br$_2$ flow batteries, and Zn-ferricyanide flow batteries. Most of the current research on emerging AZDs is still in the laboratory stage based on small (non-technological) systems, which cannot fully reflect the issues they may encounter in practical applications. For instance, the temperature distribution at the electrode will also affect the uniform deposition/dissolution behavior of the Zn-metal; however, most of the current evaluation systems (coin cells or Swagelok cells) do not involve the influence of thermal effects on the cell performance. Therefore, it is necessary to scale up the evaluation systems of AZDs to prototypes with kWh or Ah levels (*e.g.*, 18650 cells and pouch cells).

11.2 Next-generation AZDs

According to current major challenges of AZDs, various widely reported optimization strategies are evaluated from the perspectives of performance impact on key components and devices (Figure 20). Currently, no single strategy is perfect: each strategy can optimize several key performances but may negatively impact other properties. To meet the application requirements of specific scenarios, components and strategies with different characteristics need to be rationally combined in AZDs. For example, the strategy for high-power AZDs should try to avoid using methodologies that may deteriorate Zn-ion transport and device power density. The construction of next-generation AZDs requires joint efforts from the following six aspects, including anode, electrolyte, cathode, membrane, cell configuration and theoretical investigations.

11.2.1 Next-generation anodes

The uniform Zn deposition and the suppression of parasitic reactions are keys to solving severe Zn anode issues and improving anode reversibility and utilization rate. The *ex-situ* formed artificial SEI coatings have been shown to induce uniform electrolyte penetration and Zn-ion deposition, and inhibit dendrite growth. However, the *ex-situ* formed artificial SEI may cause failure during the cycling and lose its efficacy. Therefore, this review recommends the design of *in-situ* formed artificial SEI with self-healing ability. However, strategies involving artificial SEI layers should also mitigate their negative impacts on device power density and cost. The structural design of electrode is also a feasible strategy, whose future research direction should focus on increasing the areal loading of Zn, thereby increasing the cell areal capacity. In addition, the fundamental understanding of Zn dendrite growth, parasitic reaction and anode-electrolyte interface mechanisms is still insufficient, and more in-depth investigations are urgently needed.

11.2.2 Next-generation electrolytes

The current capacity degradation of most AZDs is caused by the consumption of liquid electrolytes, rather than short circuits caused by Zn dendrites. In AZDs, the electrolyte is the most critical factor that determines the cell operating voltage. WIS electrolyte and 'molecular crowding' electrolyte can effectively alter the solvation structure of Zn-ion and inhibit the activity of water, thus broadening ESPW and improving Zn anode reversibility. However, crowding agents and highly concentrated electrolytes may face the active materials decomposition and the precipitation of salts caused by water volatilization, respectively; these will lead to electrolyte consumption and device capacity decay. Meanwhile, WIS electrolyte is not suitable for semi-open systems represented by ZABs, owning to the water consumption from OER and evaporation. Therefore, in addition to reducing costs, these strategies also need to improve their long-term stability in various AZDs.

The development of SEs can also effectively suppress Zn dendrites, improve the reversibility of Zn anodes, increase device energy density, and provide the possibility of flexible device manufacturing. In future research, in addition to further enhancing the mechanical strength and ionic conductivity of

SEs, further in-depth investigations should be made on the interface properties and electrode/electrolyte compatibility. Moreover, improving the solubility of the active substances in electrolytes is extremely important for improving the electrolyte energy density and the electrode catalytic activity, which is crucial to improve the EE and areal capacity of ZRFBs.

11.2.3 Next-generation cathodes

Seven universal strategies for cathode improvement are evaluated in Figure 20. The current research and development of next-generation cathode materials for AZDs is to improve the transport kinetics of Zn-ion and other active species, thereby improving cathode utilization and catalytic activity. The current strategies can be divided into two categories: (a) reduce the intermolecular interactions between Zn-ion and cathode materials, such as pre-intercalation strategy and heteroatom doping; (b) altering the materials morphology (*e.g.*, increasing the specific surface area, shortening the diffusion path, and constructing favorable structures for Zn-ion transport), including pore size engineering, size regulation, defect engineering, *etc*. For cathodes involving electrocatalytic reactions, heteroatom doping and composite fabrication are effective methods for improving electrocatalytic activity; however, the synergy effects among different atoms or substances need to be further investigated. In addition, the employment of redox mediators could effectively enhance the materials utilization rate of electrode and the areal capacity; nevertheless, this is rarely studied in the current AZDs.

11.2.4 Next-generation membranes/separators

The basic principle of AZDs' separator/membrane optimization is to possess good chemical stability, uniform ion flux distribution, high ion conductivity, and good mechanical stability to suppress Zn dendrites. Perfluorinated cation exchange membranes are currently the most widely used membranes in AZDs, and most of them are suitable in acidic systems. Unfortunately, Zn anodes are thermodynamically unstable in strongly acidic media; therefore, AZDs urgently need high-performance membranes in near-neutral and alkaline media. Porous membranes are considered as one of the best candidates for AZDs, and a series of methodologies for pore size optimization and

pore distribution have been proposed. In addition, composite membrane engineering is an effective strategy to reduce membrane cost, thickness and improve electrochemical performances.

11.2.5 Device configuration innovation

The membrane-less configuration can maximize the power density of the device, and the presence of the membrane selectively permeates the active material, which improves CE and allows the electrode to work in a more favorable environment; the double-membrane configuration can also improve the device operating voltage. However, the use of the film must take into account the increase in cost and internal resistance. The flow system can transform diffusion-controlled into convection-controlled processes, thus improving Zn anode reversibility, cathode utilization rate and Zn-ion transport. However, the use of flow systems will inevitably reduce EE and increase the distance between the cathode and the anode, thereby leading to a larger device volume. Therefore, future research is required to find the optimal cell configuration for each AZD in specific application scenarios. Especially for AZDs using membranes and/or forced convection systems, it is particularly important to strike a balance between performance and cost. Meanwhile, it is promising to explore novel cell configurations, such as miniaturizing the flow-assisted system so that it can be used in scenarios with volume and/or weight restrictions.

11.2.6 Theoretical investigations

Multi-scale theoretical research is required to achieve deeper understanding of the underlying mechanisms; this will guide novel materials development, optimization, and the cell configuration design. For example, for AZDs involving solid-phase reactions (insertion-type or conversion-type), the cathodes may undergo a series of phase changes during the cycling, which are difficult to observe by *ex-situ* technologies. Therefore, conducting computational studies (*e.g.*, DFT, MD) combing with the use of advanced *in-situ* characterization techniques (*e.g.*, synchrotron X-ray tomography, SEM, neutron scattering, *etc.*) are recommended to understand critical mechanisms.

Reference

1. Khor, A., Leung, P., Mohamed, M.R., Flox, C., Xu, Q., An, L., Wills, R.G.A., Morante, J.R., and Shah, A.A. (2018). Review of zinc-based hybrid flow batteries: From fundamentals to applications. Mater. Today Energy *8*, 80–108.

2. Wang, M., Zheng, X., Zhang, X., Chao, D., Qiao, S., Alshareef, H., Cui, Y., and Chen, W. (2020). Opportunities of Aqueous Manganese-Based Batteries with Deposition and Stripping Chemistry. Adv. Energy Mater. *5*, 2002904.

3. Wu, K., Huang, J., Yi, J., Liu, X., Liu, Y., Wang, Y., Zhang, J., and Xia, Y. (2020). Recent Advances in Polymer Electrolytes for Zinc Ion Batteries: Mechanisms, Properties, and Perspectives. Adv. Energy Mater. *10*, 1903977.

4. Jia, H., Wang, Z., Tawiah, B., Wang, Y., Chan, C., Fei, B., and Pan, F. (2020). Recent advances in zinc anodes for high-performance aqueous Zn-ion batteries. Nano Energy *70*, 104523.

5. Liu, C., Chi, X., Han, Q., and Liu, Y. (2020). A High Energy Density Aqueous Battery Achieved by Dual Dissolution/Deposition Reactions Separated in Acid-Alkaline Electrolyte. Adv. Energy Mater. *12*, 1903589.

6. Chao, D., Zhou, W., Ye, C., Zhang, Q., Chen, Y., Gu, L., Davey, K., and Qiao, S. (2019). An Electrolytic Zn–MnO_2 Battery for High-Voltage and Scalable Energy Storage. Angew. Chem. Int. Ed. *3*, 7905-7910.

7. Liu, Y., He, G., Jiang, H., Parkin, I.P., Shearing, P.R., and Brett, D.J.L. (2021). Cathode Design for Aqueous Rechargeable Multivalent Ion Batteries: Challenges and Opportunities. Adv. Funct. Mater., *13*, 2010445.

8. Shang, W., Yu, W., Liu, Y., Li, R., Dai, Y., Cheng, C., Tan, P., and Ni, M. (2020). Rechargeable alkaline zinc batteries: Progress and challenges. Energy Storage Mater. *31*, 44–57.

9. Chen, G.Z. (2017). Supercapacitor and supercapattery as emerging electrochemical energy stores. Int. Mater. Rev. *62*, 173–202.

10. Xue, T., and Fan, H. (2021). From aqueous Zn-ion battery to Zn-MnO$_2$ flow battery: A brief story. J. Energy Chem. *54*, 194-201.

11. Potential Benefits of High-Power, High-Capacity Batteries (2020), US Department of Energy.

12. Yamato, T., and Shoji, T. (1986). Rechargeable Zn|ZnSO$_4$|MnO$_2$-type Cells. Inorganic Chim. Acta *2*, L27-L28.

13. Yang, Q., Liang, G., Guo, Y., Liu, Z., Yan, B., Wang, D., Huang, Z., Li, X., Fan, J., and Zhi, C. (2019). Do Zinc Dendrites Exist in Neutral Zinc Batteries: A Developed Electrohealing Strategy to In Situ Rescue In-Service Batteries. Adv. Mater. *31*, 1903778.

14. Electrochemistry Encyclopedia -- Volta and the "Pile" https://web.archive.org/web/20120716205546/http://electrochem.cwru.edu/encycl/art-v01-volta.htm.

15. History of the electrical units. - Association S-EAU-S http://seaus.free.fr/spip.php?article964.

16. Schumm, B. (2014). Carbon-Zinc Batteries. In Encyclopedia of Applied Electrochemistry (Springer New York), pp. 149–152.

17. Kordesch, K. (1981). Primary Batteries—Alkaline Manganese Dioxide-Zinc Batteries. In Comprehensive Treatise of Electrochemistry (Springer US), pp. 219–232.

18. Le, S., Zhang, L., Song, X., He, S., Yuan, Z., Liu, F., Zhang, N., Sun, K., and Feng, Y. (2019). Review—Status of Zinc-Silver Battery. J. Electrochem. Soc. *166*, A2980–A2989.

19. Reversible galvanic battery, US Patent (1900).

20. Zakoldaev, D.A., Shukalov, A.V., and Zharinov, I.O. (2019). From Industry 3.0 to Industry 4.0: Production modernization and creation of innovative digital companies. In IOP Conference Series: Materials Science and Engineering (Institute of Physics Publishing), p. 012206.

21. Shivkumar, R., Paruthimal Kalaignan, G., and Vasudevan, T. (1995). Effect of additives on zinc electrodes in alkaline battery systems. J. Power Sources *55*, 53–62.

22. Binder, L., Odar, W., and Kordesch, K. (1981). A study of rechargeable zinc electrodes for alkaline cells requiring anodic limitation. J. Power Sources *6*, 271–289.

23. Xu, C., Li, B., Du, H., and Kang, F. (2012). Energetic Zinc Ion Chemistry: The Rechargeable Zinc Ion Battery. Angew. Chemie Int. Ed. *51*, 933–935.

24. Clark, N., Eidler, P., and Lex, P. (1999). Development of Zinc/Bromine Batteries for Load-Leveling Applications : Phase 2 Final. 117.

25. Ito, Y., Nyce, M., Plivelich, R., Klein, M., Steingart, D., and Banerjee, S. (2011). Zinc morphology in zinc-nickel flow assisted batteries and impact on performance. J. Power Sources *196*, 2340–2345.

26. Song, J., Xu, K., Liu, N., Reed, D., and Li, X. (2021). Crossroads in the renaissance of rechargeable aqueous zinc batteries. Mater. Today. *45*, 191-212.

27. Zhong, C., Liu, B., Ding, J., Liu, X., Zhong, Y., Li, Y., Sun, C., Han, X., Deng, Y., Zhao, N., et al. (2020). Decoupling electrolytes towards stable and high-energy rechargeable aqueous zinc–manganese dioxide batteries. Nat. Energy *5*, 440–449.

28. Wang, F., Borodin, O., Gao, T., Fan, X., Sun, W., Han, F., Faraone, A., Dura, J.A., Xu, K., and Wang, C. (2018). Highly reversible zinc metal anode for aqueous batteries. Nat. Mater. *17*, 543–549.

29. Zhao, Y., Wang, D., Li, X., Yang, Q., Guo, Y., Mo, F., Li, Q., Peng, C., Li, H., and Zhi, C. (2020). Initiating a Reversible Aqueous Zn/Sulfur Battery through a "Liquid Film." Adv. Mater. *32*, 2003070.

30. Li, W., Ma, Y., Li, P., Jing, X., Jiang, K., and Wang, D. (2021). Synergistic Effect between S and Se Enhancing the Electrochemical Behavior of Se_xS_y in Aqueous Zn Metal Batteries. Adv. Funct. Mater. *20*, 2101237.

31. Chen, Z., Mo, F., Wang, T., Yang, Q., Huang, Z., Wang, D., Liang, G., Li, Q., Chen, A., Guo, Y., et al. (2021). Zinc/Selenium Conversion Battery: A System Highly Compatible to both Organic and Aqueous Electrolytes. Energy Environ. Sci. *14*, 2441-2450.

32. Zhang, P., Li, Y., Wang, G., Wang, F., Yang, S., Zhu, F., Zhuang, X., Schmidt, O.G., and Feng, X. (2019). Zn-Ion Hybrid Micro-Supercapacitors with Ultrahigh Areal Energy Density and Long-Term Durability. Adv. Mater. *31*, 1806005.

33. Wu, S., Chen, Y., Jiao, T., Zhou, J., Cheng, J., Liu, B., Yang, S., Zhang, K., and Zhang, W. (2019). An Aqueous Zn-Ion Hybrid Supercapacitor with High Energy Density and Ultrastability up to 80 000 Cycles. Adv. Energy Mater. *9*, 1902915.

34. Xie, C., Li, T., Deng, C., Song, Y., Zhang, H., and Li, X. (2020). A highly reversible neutral zinc/manganese battery for stationary energy storage. Energy Environ. Sci. *13*, 135–143.

35. Li, G., Chen, W., Zhang, H., Gong, Y., Shi, F., Wang, J., Zhang, R., Chen, G., Jin, Y., Wu, T., et al. (2020). Membrane-Free Zn/MnO_2 Flow Battery for Large-Scale Energy Storage. Adv. Energy Mater. *10*, 1902085.

36. Simon, P., and Gogotsi, Y. (2008). Materials for electrochemical capacitors. Nat. Mater. *7*, 845–854.

37. Okubo, M., Hosono, E., Kim, J., Enomoto, M., Kojima, N., Kudo, T., Zhou, H., and Honma, I. (2007). Nanosize effect on high-rate Li-ion intercalation in $LiCoO_2$ electrode. J. Am. Chem. Soc. *129*, 7444–7452.

38. Fleischmann, S., Mitchell, J.B., Wang, R., Zhan, C., Jiang, D., Presser, V., and Augustyn, V. (2020). Pseudocapacitance: From Fundamental Understanding to High Power Energy Storage Materials. Chem. Rev. *120*, 6738–6782.

39. Levi, M.D., and Aurbach, D. (1999). Frumkin intercalation isotherm — a tool for the description of lithium insertion into host materials: a review. Electrochim. Acta *45*, 167–185.

40. Levi, M.D., Lukatskaya, M.R., Sigalov, S., Beidaghi, M., Shpigel, N., Daikhin, L., Aurbach, D., Barsoum, M.W., and Gogotsi, Y. (2015). Solving the Capacitive Paradox of 2D MXene using Electrochemical Quartz-Crystal Admittance and In Situ Electronic Conductance Measurements. Adv. Energy Mater. *5*, 1400815.

41. Mathis, T.S., Kurra, N., Wang, X., Pinto, D., Simon, P., and Gogotsi, Y. (2019). Energy Storage Data Reporting in Perspective—Guidelines for Interpreting the Performance of Electrochemical Energy Storage Systems. Adv. Energy Mater. *9*, 1902007.

42. Simon, P., Gogotsi, Y., and Dunn, B. (2014). Where do batteries end and supercapacitors begin? Science, *343*, 1210–1211.

43. Jiang, Y., and Liu, J. (2019). Definitions of Pseudocapacitive Materials: A Brief Review. Energy Environ. Mater. *2*, 30–37.

44. Dong, H., Li, J., Guo, J., Lai, F., Zhao, F., Jiao, Y., Brett, D.J.L., Liu, T., He, G., and Parkin, I.P. (2021). Insights on Flexible Zinc-Ion Batteries from Lab Research to Commercialization. Adv. Mater. *20*, 2007548.

45. Banerjee, A., Wang, X., Fang, C., Wu, E., and Meng, Y. (2020). Interfaces and Interphases in All-Solid-State Batteries with Inorganic Solid Electrolytes. Chem. Rev. *120*, 6878–6933.

46. Li, D., Cao, L., Deng, T., Liu, S., and Wang, C. (2021). Design of a Solid Electrolyte Interphase for Aqueous Zn Batteries. Angew. Chemie Int. Ed. *60*, 13035–13041.

47. Dawson, J.A., Canepa, P., Famprikis, T., Masquelier, C., and Islam, M.S. (2017). Atomic-Scale Influence of Grain Boundaries on Li-Ion Conduction in Solid Electrolytes for All-Solid-State Batteries. J. Am. Chem. Soc. *140*, 362–368.

48. Guo, X., Sigle, W., and Maier, J. (2003). Blocking Grain Boundaries in Yttria-Doped and Undoped Ceria Ceramics of High Purity. J. Am. Ceram. Soc. *86*, 77–87.

49. Mainar, A.R., Iruin, E., Colmenares, L.C., Kvasha, A., de Meatza, I., Bengoechea, M., Leonet, O., Boyano, I., Zhang, Z., and Blazquez, J.A. (2018). An overview of progress in electrolytes for secondary zinc-air batteries and other storage systems based on zinc. J. Energy Storage *15*, 304–328.

50. Yufit, V., Tariq, F., Eastwood, D.S., Biton, M., Wu, B., Lee, P.D., and Brandon, N.P. (2019). Operando Visualization and Multi-scale Tomography Studies of Dendrite Formation and Dissolution in Zinc Batteries. Joule *3*, 485–502.

51. Wang, R.Y., Kirk, D.W., and Zhang, G. (2006). Effects of Deposition Conditions on the Morphology of Zinc Deposits from Alkaline Zincate Solutions. J. Electrochem. Soc. *153*, C357.

52. Borchers, N., Clark, S., Horstmann, B., Jayasayee, K., Juel, M., and Stevens, P. (2021). Innovative zinc-based batteries. J. Power Sources *484*, 229309.

53. Shin, J., Lee, J., Park, Y., and Choi, J.W. (2020). Aqueous zinc ion batteries: Focus on zinc metal anodes. Chem. Sci. *11*, 2028–2044.

54. Guo, X., Zhang, Z., Li, J., Luo, N., Chai, G.-L., Miller, T.S., Lai, F., Shearing, P., Brett, D.J.L., Han, D., et al. (2021). Alleviation of Dendrite Formation on Zinc Anodes via Electrolyte Additives. ACS Energy Lett. *6*, *2*, 395–403.

55. Yang, Q., Li, Q., Liu, Z., Wang, D., Guo, Y., Li, X., Tang, Y., Li, H., Dong, B., and Zhi, C. (2020). Dendrites in Zn-Based Batteries. Adv. Mater. *32*, 2001854.

56. Zheng, J., Zhao, Q., Tang, T., Yin, J., Quilty, C.D., Renderos, G.D., Liu, X., Deng, Y., Wang, L., Bock, D.C., et al. (2019). Reversible epitaxial electrodeposition of metals in battery anodes. Science *366*, 645–648.

57. Kang, Z., Wu, C., Dong, L., Liu, W., Mou, J., Zhang, J., Chang, Z., Jiang, B., Wang, G., Kang, F., et al. (2019). 3D Porous Copper Skeleton Supported Zinc Anode toward High Capacity and Long Cycle Life Zinc Ion Batteries. ACS Sustain. Chem. Eng. *7*, 3364–3371.

58. Kang, L., Cui, M., Jiang, F., Gao, Y., Luo, H., Liu, J., Liang, W., and Zhi, C. (2018). Nanoporous $CaCO_3$ Coatings Enabled Uniform Zn Stripping/Plating for Long-Life Zinc Rechargeable Aqueous Batteries. Adv. Energy Mater. *8*, 1801090.

59. Zhao, Z., Zhao, J., Hu, Z., Li, J., Li, J., Zhang, Y., Wang, C., and Cui, G. (2019). Long-life and deeply rechargeable aqueous Zn anodes enabled by a multifunctional brightener-inspired interphase. Energy Environ. Sci. *12*, 1938–1949.

60. Cao, L., Li, D., Pollard, T., Deng, T., Zhang, B., Yang, C., Chen, L., Vatamanu, J., Hu, E., Hourwitz, M.J., et al. (2021). Fluorinated interphase enables reversible aqueous zinc battery chemistries. Nat. Nanotechnol. *16*, 1–9.

61. Turney, D.E., Gallaway, J.W., Yadav, G.G., Ramirez, R., Nyce, M., Banerjee, S., Chen-Wiegart, Y.C.K., Wang, J., D'Ambrose, M.J., Kolhekar, S., et al. (2017). Rechargeable Zinc Alkaline Anodes for Long-Cycle Energy Storage. Chem. Mater. *29*, 4819–4832.

62. Zhang, T., Tang, Y., Guo, S., Cao, X., Pan, A., Fang, G., Zhou, J., and Liang, S. (2020). Fundamentals and perspectives in developing zinc-ion battery electrolytes: A comprehensive review. Energy Environ. Sci. *13*, 4625–4665.

63. Krężel, A., and Maret, W. (2016). The biological inorganic chemistry of zinc ions. Arch. Biochem. Biophys. *611*, 3–19.

64. McMahon, M.E., Santucci, R.J., and Scully, J.R. (2019). Advanced chemical stability diagrams to predict the formation of complex zinc compounds in a chloride environment. RSC Adv. *9*, 19905–19916.

65. Jindra, J., Mrha, J., and Musilová, M. (1973). Zinc-air cell with neutral electrolyte. J. Appl. Electrochem. *3*, 297–301.

66. Baugh, L.M. (1979). Corrosion and polarization characteristics of zinc in neutral-acid media - I. Pure zinc in solutions of various sodium salts. Electrochim. Acta *24*, 657–667.

67. Leclanché, G. (1839-1882). A. du texte (1867). Quelques observations sur l'emploi des piles électriques / par Georges Leclanché.

68. Clark, S., Mainar, A.R., Iruin, E., Colmenares, L.C., Blázquez, J.A., Tolchard, J.R., Latz, A., and Horstmann, B. (2019). Towards rechargeable zinc-air batteries with aqueous chloride electrolytes. J. Mater. Chem. A *7*, 11387–11399.

69. R. Mainar, A., Leonet, O., Bengoechea, M., Boyano, I., de Meatza, I., Kvasha, A., Guerfi, A., and Alberto Blázquez, J. (2016). Alkaline aqueous electrolytes for secondary zinc-air batteries: an overview. Int. J. Energy Res. *40*, 1032–1049.

70. Sapkota, P., and Kim, H. (2010). An experimental study on the performance of a zinc air fuel cell with inexpensive metal oxide catalysts and porous organic polymer separators. J. Ind. Eng. Chem. *16*, 39–44.

71. Zhang, X.G. (2009). Secondary Batteries - Zinc Systems | Zinc Electrodes: Overview. Encyclopedia of Electrochemical Power Sources (Elsevier), 454–468.

72. Lee, J.-S., Tai Kim, S., Cao, R., Choi, N.-S., Liu, M., Lee, K.T., and Cho, J. (2011). Metal-Air Batteries with High Energy Density: Li-Air versus Zn-Air. Adv. Energy Mater. *1*, 34–50.

73. Nathan, T., Cloke, M., and Prabaharan, S.R.S. (2008). Electrode Properties of Mn_2O_3 Nanospheres Synthesized by Combined Sonochemical/Solvothermal Method for Use in Electrochemical Capacitors. J. Nanomater. *948183*.

74. Huang, S., Zhu, J., Tian, J., and Niu, Z. (2019). Recent Progress in the Electrolytes of Aqueous Zinc-Ion Batteries. Chem. – A Eur. J. *25*, 14480–14494.

75. Ma, L., Chen, S., Li, N., Liu, Z., Tang, Z., Zapien, J.A., Chen, S., Fan, J., and Zhi, C. (2020). Hydrogen-Free and Dendrite-Free All-Solid-State Zn-Ion Batteries. Adv. Mater. *32*, 1908121.

76. Xie, J., Liang, Z., and Lu, Y. (2020). Molecular crowding electrolytes for high-voltage aqueous batteries. Nat. Mater. *19*, 1006–1011.

77. Kwabi, D.G., Ji, Y., and Aziz, M.J. (2020). Electrolyte Lifetime in Aqueous Organic Redox Flow Batteries: A Critical Review. Chem. Rev. *120*, 6467–6489.

78. Leung, P.K., Ponce-De-León, C., Low, C.T.J., Shah, A.A., and Walsh, F.C. (2011). Characterization of a zinc-cerium flow battery. J. Power Sources *196*, 5174–5185.

79. Gong, K., Ma, X., Conforti, K.M., Kuttler, K.J., Grunewald, J.B., Yeager, K.L., Bazant, M.Z., Gu, S., and Yan, Y. (2015). A zinc-iron redox-flow battery under $100 per kWh of system capital cost. Energy Environ. Sci. *8*, 2941–2945.

80. Ulaganathan, M., Suresh, S., Mariyappan, K., Periasamy, P., and Pitchai, R. (2019). New Zinc-Vanadium (Zn-V) Hybrid Redox Flow Battery: High-Voltage and Energy-Efficient Advanced Energy Storage System. ACS Sustain. Chem. Eng. *7*, 6053–6060.

81. Qiu, C., Zhu, X., Xue, L., Ni, M., Zhao, Y., Liu, B., and Xia, H. (2020). The function of Mn^{2+} additive in aqueous electrolyte for $Zn/\delta-MnO_2$ battery. Electrochim. Acta *351*, 136445.

82. Julien, C.M., and Mauger, A. (2017). Nanostructured MnO_2 as electrode materials for energy storage. Nanomaterials *7*, 396.

83. Yao, Y., Lei, J., Shi, Y., Ai, F., and Lu, Y. (2021). Assessment methods and performance metrics for redox flow batteries. Nat. Energy *6*, 582–588.

84. Soloveichik, G.L. (2015). Flow Batteries: Current Status and Trends. Chem. Rev. *115*, 11533–11558.

85. Winsberg, J., Stolze, C., Schwenke, A., Muench, S., Hager, M.D., and Schubert, U.S. (2017). Aqueous 2,2,6,6-Tetramethylpiperidine-N-oxyl Catholytes for a High-Capacity and High Current Density Oxygen-Insensitive Hybrid-Flow Battery. ACS Energy Lett. *2*, 411–416.

86. Bryans, D., McMillan, B.G., Spicer, M., Wark, A., and Berlouis, L. (2017). Complexing Additives to Reduce the Immiscible Phase Formed in the Hybrid $ZnBr_2$ Flow Battery. J. Electrochem. Soc. *164*, A3342.

87. Schneider, M., Rajarathnam, G.P., Easton, M.E., Masters, A.F., Maschmeyer, T., and Vassallo, A.M. (2016). The influence of novel bromine sequestration agents on zinc/bromine flow battery performance. RSC Adv. *6*, 110548–110556.

88. Weber, N., O, J.P., and No, B. (2016). Electrolyte for rechargeable electrochemical cell, US patent.

89. Weng, G.-M., Li, Z., Cong, G., Zhou, Y., and Lu, Y. (2017). Unlocking the capacity of iodide for high-energy-density zinc/polyiodide and lithium/polyiodide redox flow batteries. Energy Environ. Sci. *10*, 735–741.

90. Xie, C., Duan, Y., Xu, W., Zhang, H., and Li, X. (2017). A low-cost neutral zinc–iron flow battery with high energy density for stationary energy storage. Angew. Chemie Int. Ed. *56*, 14953–14957.

91. Dong, H., Li, J., Zhao, S., Zhao, F., Xiong, S., Brett, D.J.L., He, G., and Parkin, I.P. (2020). An anti-aging polymer electrolyte for flexible rechargeable zinc-ion batteries. J. Mater. Chem. A *8*, 22637–22644.

92. Manthiram, A., Yu, X., and Wang, S. (2017). Lithium battery chemistries enabled by solid-state electrolytes. Nat. Rev. Mater. *2*, 1–16.

93. Zhao, Q., Stalin, S., Zhao, C., and Archer, L.A. (2020). Designing solid-state electrolytes for safe, energy-dense batteries. Nat. Rev. Mater. *5*, 229–252.

94. Farrington, G.C., and Dunn, B. (1982). Divalent beta″-aluminas: High conductivity solid electrolytes for divalent cations. Solid State Ionics *7*, 267–281.

95. Ikeda, S., Kanbayashi, Y., Nomura, K., Kasai, A., and Ito, K. (1990). Solid electrolytes with multivalent cation conduction (2) zinc ion conduction in $ZnZrPO_4$ system. Solid State Ionics *40*, 79–82.

96. Martinolich, A.J., Lee, C., Lu, I., Bevilacqua, S.C., Preefer, M.B., Bernardi, M., Schleife, A., and See, K.A. (2019). Solid-State Divalent Ion Conduction in $ZnPS_3$. Chem. Mater. *31*, 3652–3661.

97. Xiao, Y., Wang, Y., Bo, S.-H., Kim, J.C., Miara, L.J., and Ceder, G. (2019). Understanding interface stability in solid-state batteries. Nat. Rev. Mater. *5*, 105–126.

98. Ma, L., Chen, S., Li, N., Liu, Z., Tang, Z., Zapien, J.A., Chen, S., Fan, J., and Zhi, C. (2020). Hydrogen-Free and Dendrite-Free All-Solid-State Zn-Ion Batteries. Adv. Mater. *32*, 1908121.

99. Zhang, Q., Li, C., Li, Q., Pan, Z., Sun, J., Zhou, Z., He, B., Man, P., Xie, L., Kang, L., et al. (2019). Flexible and High-Voltage Coaxial-Fiber Aqueous Rechargeable Zinc-Ion Battery. Nano Lett. *19*, 4035–4042.

100. Xiong, B., Loss, R.D., Shields, D., Pawlik, T., Hochreiter, R., Zydney, A.L., and Kumar, M. (2018). Polyacrylamide degradation and its implications in environmental systems. npj Clean Water *1*, 1–9.

101. Mohamad, A.A., Mohamed, N.S., Yahya, M.Z.A., Othman, R., Ramesh, S., Alias, Y., and Arof, A.K. (2003). Ionic conductivity studies of poly(vinyl alcohol) alkaline solid polymer electrolyte and its use in nickel–zinc cells. Solid State Ionics *156*, 171–177.

102. Liu, J., Hu, M., Wang, J., Nie, N., Wang, Y., Wang, Y., Zhang, J., and Huang, Y. (2019). An intrinsically 400% stretchable and 50% compressible NiCo//Zn battery. Nano Energy *58*, 338–346.

103. Weston, J.E., and Steele, B.C.H. (1982). Effects of inert fillers on the mechanical and electrochemical properties of lithium salt-poly(ethylene oxide) polymer electrolytes. Solid State Ionics *7*, 75–79.

104. Croce, F., Appetecchi, G.B., Persi, L., and Scrosati, B. (1998). Nanocomposite polymer electrolytes for lithium batteries. Nature *394*, 456–458.

105. Dong, L., Yang, W., Yang, W., Li, Y., Wu, W., and Wang, G. (2019). Multivalent metal ion hybrid capacitors: A review with a focus on zinc-ion hybrid capacitors. J. Mater. Chem. A *7*, 13810–13832.

106. Caramia, V., and Bozzini, B. (2014). Materials science aspects of zinc-air batteries: A review. Mater. Renew. Sustain. Energy *3*, 1–12.

107. Tomboc, G.M., Yu, P., Kwon, T., Lee, K., and Li, J. (2020). Ideal design of air electrode-A step closer toward robust rechargeable Zn-air battery. APL Mater. *8*, 50905.

108. Li, J., McColl, K., Lu, X., Sathasivam, S., Dong, H., Kang, L., Li, Z., Zhao, S., Kafizas, A.G., Wang, R., et al. (2020). Multi-Scale Investigations of δ-$Ni_{0.25}V_2O_5 \cdot nH_2O$ Cathode Materials in Aqueous Zinc-Ion Batteries. Adv. Energy Mater. *10*, 2000058.

109. Jiao, Y., Kang, L., Berry-Gair, J., McColl, K., Li, J., Dong, H., Jiang, H., Wang, R., Corà, F., Brett, D.J.L., et al. (2020). Enabling stable MnO_2 matrix for aqueous zinc-ion battery cathodes. J. Mater. Chem. A *8*, 22075–22082.

110. Li, J., Luo, N., Wan, F., Zhao, S., Li, Z., Li, W., Guo, J., Shearing, P.R., Brett, D.J.L., Carmalt, C.J., et al. (2020). Defected vanadium bronzes as superb cathodes in aqueous zinc-ion batteries. Nanoscale *12*, 20638–20648.

111. Pan, H., Shao, Y., Yan, P., Cheng, Y., Han, K.S., Nie, Z., Wang, C., Yang, J., Li, X., Bhattacharya, P., et al. (2016). Reversible aqueous zinc/manganese oxide energy storage from conversion reactions. Nat. Energy *1*, 16039.

112. Ni, G., Han, B., Li, Q., Ji, Z., Huang, B., and Zhou, C. (2016). Instability of Zinc Hexacyanoferrate Electrode in an Aqueous Environment: Redox-Induced Phase Transition, Compound Dissolution, and Inhibition. ChemElectroChem *3*, 798–804.

113. Zhang, N., Cheng, F., Liu, Y., Zhao, Q., Lei, K., Chen, C., Liu, X., and Chen, J. (2016). Cation-Deficient Spinel $ZnMn_2O_4$ Cathode in $Zn(CF_3SO_3)_2$ Electrolyte for Rechargeable Aqueous Zn-Ion Battery. J. Am. Chem. Soc. *138*, 12894–12901.

114. Gao, X., Wu, H., Li, W., Tian, Y., Zhang, Y., Wu, H., Yang, L., Zou, G., Hou, H., and Ji, X. (2020). H^+-Insertion Boosted α-MnO_2 for an Aqueous Zn-Ion Battery. Small *16*, 1905842.

115. Sun, W., Wang, F., Hou, S., Yang, C., Fan, X., Ma, Z., Gao, T., Han, F., Hu, R., Zhu, M., et al. (2017). Zn/MnO_2 Battery Chemistry with H^+ and Zn^{2+} Coinsertion. J. Am. Chem. Soc. *139*, 9775–9778.

116. Huang, J., Guo, Z., Ma, Y., Bin, D., Wang, Y., and Xia, Y. (2019). Recent Progress of Rechargeable Batteries Using Mild Aqueous Electrolytes. Small Methods *3*, 1800272.

117. Chao, D., Zhou, W., Xie, F., Ye, C., Li, H, Jaroniec, M., Qiao, S. (2020) Roadmap for advanced aqueous batteries: From design of materials to applications. Sci. Adv. *21*, aba4098.

118. Ramaswamy, N., and Mukerjee, S. (2012). Fundamental mechanistic understanding of electrocatalysis of oxygen reduction on Pt and non-Pt surfaces: Acid versus alkaline media. Adv. Phys. Chem. *2012,* 491604.

119. Ramaswamy, N., and Mukerjee, S. (2011). Influence of inner- and outer-sphere electron transfer mechanisms during electrocatalysis of oxygen reduction in alkaline media. J. Phys. Chem. C *115*, 18015–18026.

120. Wan, K., Yu, Z., Li, X., Liu, M., Yang, G., Piao, J., and Liang, Z. (2015). pH Effect on Electrochemistry of Nitrogen-Doped Carbon Catalyst for Oxygen Reduction Reaction. ACS Catal. *5*, 4325–4332.

121. Blizanac, B.B., Ross, P.N., and Markovic, N.M. (2007). Oxygen electroreduction on Ag(111): The pH effect. Electrochim. Acta *52*, 2264–2271.

122. Jiao, Y., Zheng, Y., Jaroniec, M., and Qiao, S. (2014). Origin of the electrocatalytic oxygen reduction activity of graphene-based catalysts: A roadmap to achieve the best performance. J. Am. Chem. Soc. *136*, 4394–4403.

123. Wang, J.X., Zhang, J., and Adzic, R.R. (2007). Double-trap kinetic equation for the oxygen reduction reaction on pt(111) in acidic media. J. Phys. Chem. A *111*, 12702–12710.

124. Nørskov, J.K., Rossmeisl, J., Logadottir, A., Lindqvist, L., Kitchin, J.R., Bligaard, T., and Jónsson, H. (2004). Origin of the overpotential for oxygen reduction at a fuel-cell cathode. J. Phys. Chem. B *108*, 17886–17892.

125. Ma, R., Lin, G., Zhou, Y., Liu, Q., Zhang, T., Shan, G., Yang, M., and Wang, J. (2019). A review of oxygen reduction mechanisms for metal-free carbon-based electrocatalysts. npj Comput. Mater. *5*, 1–15.

126. Sun, W., Wang, F., Zhang, B., Zhang, M., Küpers, V., Ji, X., Theile, C., Bieker, P., Xu, K., Wang, C., et al. (2021). A rechargeable zinc-air battery based on zinc peroxide chemistry. Science *371*, 46–51.

127. Wang, H.F., and Xu, Q. (2019). Materials Design for Rechargeable Metal-Air Batteries. Matter *1*, 565–595.

128. Guo, J., Kang, L., Lu, X., Zhao, S., Li, J., Shearing, P.R., Wang, R., Brett, D.J.L., He, G., Chai, G., et al. (2021). Self-activated cathode substrates in rechargeable zinc–air batteries. Energy Storage Mater. *35*, 530–537.

129. Suen, N., Hung, S., Quan, Q., Zhang, N., Xu, Y., and Chen, H. (2017). Electrocatalysis for the oxygen evolution reaction: recent development and future perspectives. Chem. Soc. Rev. *46*, 337–365.

130. Jiang, Y., Deng, Y., Fu, J., Lee, D.U., Liang, R., Cano, Z.P., Liu, Y., Bai, Z., Hwang, S., Yang, L., et al. (2018). Interpenetrating Triphase Cobalt-Based Nanocomposites as Efficient Bifunctional Oxygen Electrocatalysts for Long-Lasting Rechargeable Zn–Air Batteries. Adv. Energy Mater. *8*, 1702900.

131. Hu, Q., Li, G., Li, G., Liu, X., Zhu, B., Chai, X., Zhang, Q., Liu, J., and He, C. (2019). Trifunctional Electrocatalysis on Dual-Doped Graphene Nanorings–Integrated Boxes for Efficient Water Splitting and Zn–Air Batteries. Adv. Energy Mater. *9*, 1803867.

132. Dai, Y., Yu, J., Cheng, C., Tan, P., and Ni, M. (2020). Mini-review of perovskite oxides as oxygen electrocatalysts for rechargeable zinc–air batteries. Chem. Eng. J. *397*, 125516.

133. Wu, J., Liu, B., Fan, X., Ding, J., Han, X., Deng, Y., Hu, W., and Zhong, C. (2020). Carbon-based cathode materials for rechargeable zinc-air batteries: From current collectors to bifunctional integrated air electrodes. Carbon Energy *2*, 370–386.

134. Zhao, Y., Si, S., and Liao, C. (2013). A single flow zinc//polyaniline suspension rechargeable battery. J. Power Sources *241*, 449–453.

135. Jorné, J., Kim, J.T., and Kralik, D. (1979). The zinc-chlorine battery: half-cell overpotential measurements. J. Appl. Electrochem. *9*, 573–579.

136. Eifert, L., Jusys, Z., Banerjee, R., Behm, R.J., and Zeis, R. (2018). Differential Electrochemical Mass Spectrometry of Carbon Felt Electrodes for Vanadium Redox Flow Batteries. ACS Appl. Energy Mater. *1*, 6714–6718.

137. Wang, C., Li, X., Xi, X., Zhou, W., Lai, Q., and Zhang, H. (2016). Bimodal highly ordered mesostructure carbon with high activity for Br_2/Br^- redox couple in bromine based batteries. Nano Energy *21*, 217–227.

138. Wang, C., Lai, Q., Xu, P., Zheng, D., Li, X., and Zhang, H. (2017). Cage-Like Porous Carbon with Superhigh Activity and Br_2-Complex-Entrapping Capability for Bromine-Based Flow Batteries. Adv. Mater. *29*, 1605815.

139. Ozgit, D., Hiralal, P., and Amaratunga, G.A.J. (2014). Improving performance and cyclability of zinc-silver oxide batteries by using graphene as a two dimensional conductive additive. ACS Appl. Mater. Interfaces *6*, 20752–20757.

140. Li, L., Jiang, L., Qing, Y., Zeng, Y., Zhang, Z., Xiao, L., Lu, X., and Wu, Y. (2020). Manipulating nickel oxides in naturally derived cellulose nanofiber networks as robust cathodes for high-performance Ni-Zn batteries. J. Mater. Chem. A *8*, 565–572.

141. Lei, J., Yao, Y., Wang, Z., and Lu, Y. (2021). Towards high-areal-capacity aqueous zinc–manganese batteries: promoting MnO_2 dissolution by redox mediators. Energy Environ. Sci. *14*, 4418–4426.

142. Helmholtz, H. (1853). Ueber einige Gesetze der Vertheilung elektrischer Ströme in körperlichen Leitern mit Anwendung auf die thierisch-elektrischen Versuche. Ann. der Phys. und Chemie *165*, 211–233.

143. Stern, O. (1924). ZUR THEORIE DER ELEKTROLYTISCHEN DOPPELSCHICHT. Zeitschrift für Elektrochemie und Angew. Phys. Chemie *30*, 508–516.

144. Grahame, D.C. (1947). The electrical double layer and the theory of electrocapillarity. Chem. Rev. *41*, 441–501.

145. Ojha, K., Arulmozhi, N., Aranzales, D., and Koper, M.T.M. (2020). Double Layer at the Pt(111)–Aqueous Electrolyte Interface: Potential of Zero Charge and Anomalous Gouy–Chapman Screening. Angew. Chemie Int. Ed. *59*, 711–715.

146. Netz, R.R., and Orland, H. (2000). Beyond Poisson-Boltzmann: Fluctuation effects and correlation functions. Eur. Phys. J. E *1*, 203–214.

147. Kim, B.K., Sy, S., Yu, A., and Zhang, J. (2015). Electrochemical Supercapacitors for Energy Storage and Conversion. In Handbook of Clean Energy Systems (John Wiley & Sons, Ltd), 1–25.

148. Largeot, C., Portet, c., Chmiola, J., Taberna, P., Gogotsi, Y. and, and Simon, P. (2008). Relation between the Ion Size and Pore Size for an Electric Double-Layer Capacitor. J. Am. Chem. Soc. *130*, 2730–2731.

149. Li, Z., Chen, D., An, Y., Chen, C., Wu, L., Chen, Z., Sun, Y., and Zhang, X. (2020). Flexible and anti-freezing quasi-solid-state zinc ion hybrid supercapacitors based on pencil shavings derived porous carbon. Energy Storage Mater. *28*, 307–314.

150. Yin, J., Zhang, W., Wang, W., Alhebshi, N.A., Salah, N., and Alshareef, H.N. (2020). Electrochemical Zinc Ion Capacitors Enhanced by Redox Reactions of Porous Carbon Cathodes. Adv. Energy Mater. *10*, 2001705.

151. Hassan, F.M., Chabot, V., Li, J., Kim, B.K., Ricardez-Sandoval, L., and Yu, A. (2013). Pyrrolic-structure enriched nitrogen doped graphene for highly efficient next generation supercapacitors. J. Mater. Chem. A *1*, 2904–2912.

152. Wang, Y., Wu, Y., Huang, Y., Zhang, F., Yang, X., Ma, Y., and Chen, Y. (2011). Preventing graphene sheets from restacking for high-capacitance performance. J. Phys. Chem. C *115*, 23192–23197.

153. Conway, B.E. (1999). Electrochemical Supercapacitors (Springer US).

154. Hu, C., Chen, W., and Chang, K. (2004). How to Achieve Maximum Utilization of Hydrous Ruthenium Oxide for Supercapacitors. J. Electrochem. Soc. *151*, A281.

155. Li, H., Wang, J., Chu, Q., Wang, Z., Zhang, F., and Wang, S. (2009). Theoretical and experimental specific capacitance of polyaniline in sulfuric acid. J. Power Sources *190*, 578–586.

156. Conway, B.E., Birss, V., and Wojtowicz, J. (1997). The role and utilization of pseudocapacitance for energy storage by supercapacitors. J. Power Sources *66*, 1–14.

157. Toupin, M., Brousse, T., and Bélanger, D. (2004). Charge storage mechanism of MnO_2 electrode used in aqueous electrochemical capacitor. Chem. Mater. *16*, 3184–3190.

158. Shao, Y., El-Kady, M., Sun, J., Li, Y., Zhang, Q., Zhu, M., Wang, H., Dunn, B., and Kaner, R.B. (2018). Design and Mechanisms of Asymmetric Supercapacitors. Chem. Rev. *118*, 9233–9280.

159. Xin, T., Wang, Y., Wang, N., Zhao, Y., Li, H., Zhang, Z., and Liu, J. (2019). A high-capacity aqueous Zn-ion hybrid energy storage device using poly(4,4′-thiodiphenol)-modified activated carbon as a cathode material. J. Mater. Chem. A *7*, 23076–23083.

160. Huang, M., Li, F., Dong, F., Zhang, Y., and Zhang, L. (2015). MnO_2-based nanostructures for high-performance supercapacitors. J. Mater. Chem. A *3*, 21380–21423.

161. Wang, H., Hao, Q., Yang, X., Lu, L., and Wang, X. (2009). Graphene oxide doped polyaniline for supercapacitors. Electrochem. Commun. *11*, 1158–1161.

162. Sarkar, D., Khan, G.G., Singh, A.K., and Mandal, K. (2013). High-performance pseudocapacitor electrodes based on α-Fe_2O_3/MnO_2 core-shell nanowire heterostructure arrays. J. Phys. Chem. C *117*, 15523–15531.

163. Boettcher, S.W., Oener, S.Z., Lonergan, M.C., Surendranath, Y., Ardo, S., Brozek, C., and Kempler, P.A. (2021). Potentially Confusing: Potentials in Electrochemistry. ACS Energy Lett. *6*, 261–266.

164. Yuan, D., Manalastas, W., Zhang, L., Chan, J., Meng, S., Chen, Y., and Srinivasan, M. (2019). Lignin@Nafion Membranes Forming Zn Solid–Electrolyte Interfaces Enhance the Cycle Life for Rechargeable Zinc-Ion Batteries. ChemSusChem *12*, 4889–4900.

165. Kim, R., Kim, H.G., Doo, G., Choi, C., Kim, S., Lee, J.-H., Heo, J., Jung, H.-Y., and Kim, H.-T. (2017). Ultrathin Nafion-filled porous membrane for zinc/bromine redox flow batteries. Sci. Rep. *7*, 1–8.

166. Xie, C., Liu, Y., Lu, W., Zhang, H., and Li, X. (2019). Highly stable zinc–iodine single flow batteries with super high energy density for stationary energy storage. Energy Environ. Sci. *12*, 1834–1839.

167. Yuan, Z., Zhang, H., and Li, X. (2018). Ion conducting membranes for aqueous flow battery systems. Chem. Commun. *54*, 7570–7588.

168. Yuan, Z., Duan, Y., Liu, T., Zhang, H., and Li, X. (2018). Toward a Low-Cost Alkaline Zinc-Iron Flow Battery with a Polybenzimidazole Custom Membrane for Stationary Energy Storage. iScience *3*, 40–49.

169. Yuan, Z., Yin, Y., Xie, C., Zhang, H., Yao, Y., and Li, X. (2019). Advanced Materials for Zinc-Based Flow Battery: Development and Challenge. Adv. Mater. *31*, 1902025.

170. Yuan, Z., Liu, X., Xu, W., Duan, Y., Zhang, H., and Li, X. (2018). Negatively charged nanoporous membrane for a dendrite-free alkaline zinc-based flow battery with long cycle life. Nat. Commun. *9*, 1–11.

171. Zhang, L., Cheng, J., Yang, Y., Wen, Y., Wang, X., and Cao, G. (2008). Study of zinc electrodes for single flow zinc/nickel battery application. J. Power Sources *179*, 381–387.

172. Cheng, J., Zhang, L., Yang, Y., Wen, Y., Cao, G., and Wang, X. (2007). Preliminary study of single flow zinc-nickel battery. Electrochem. Commun. *9*, 2639–2642.

173. Choi, C., Kim, S., Kim, R., Choi, Y., Kim, S., Jung, H., Yang, J.H., and Kim, H.T. (2017). A review of vanadium electrolytes for vanadium redox flow batteries. Renew. Sustain. Energy Rev. *69*, 263–274.

174. Li, B., Nie, Z., Vijayakumar, M., Li, G., Liu, J., Sprenkle, V., and Wang, W. (2015). Ambipolar zinc-polyiodide electrolyte for a high-energy density aqueous redox flow battery. Nat. Commun. *6*, 1–8.

175. Turney, D.E., Shmukler, M., Galloway, K., Klein, M., Ito, Y., Sholklapper, T., Gallaway, J.W., Nyce, M., and Banerjee, S. (2014). Development and testing of an economic grid-scale flow-assisted zinc/nickel-hydroxide alkaline battery. J. Power Sources *264*, 49–58.

176. Yuan, Z., Duan, Y., Liu, T., Zhang, H., and Li, X. (2018). Toward a Low-Cost Alkaline Zinc-Iron Flow Battery with a Polybenzimidazole Custom Membrane for Stationary Energy Storage. iScience *3*, 40–49.

177. Selverston, S., Savinell, R.F., and Wainright, J.S. (2017). Zinc-Iron Flow Batteries with Common Electrolyte. J. Electrochem. Soc. *164*, A1069–A1075.

178. Lai, Q., Zhang, H., Li, X., Zhang, L., and Cheng, Y. (2013). A novel single flow zinc-bromine battery with improved energy density. J. Power Sources *235*, 1–4.

179. Zhang, N., Cheng, F., Liu, J., Wang, L., Long, X., Liu, X., Li, F., and Chen, J. (2017). Rechargeable aqueous zinc-manganese dioxide batteries with high energy and power densities. Nat. Commun. *8*, 1–9.

180. Chen, W., Li, G., Pei, A., Li, Y., Liao, L., Wang, H., Wan, J., Liang, Z., Chen, G., Zhang, H., et al. (2018). A manganese-hydrogen battery with potential for grid-scale energy storage. Nat. Energy *3*, 428–435.

181. Pan, J., Ji, L., Sun, Y., Wan, P., Cheng, J., Yang, Y., and Fan, M. (2009). Preliminary study of alkaline single flowing Zn-O_2 battery. Electrochem. Commun. *11*, 2191–2194.

182. Leung, P.K., Xu, Q., and Zhao, T.S. (2012). High-potential zinc-lead dioxide rechargeable cells. Electrochim. Acta *79*, 117–125.

183. Jorné, J., Kim, J.T., and Kralik, D. (1979). The zinc-chlorine battery: half-cell overpotential measurements. J. Appl. Electrochem. *9*, 573–579.

184. Winsberg, J., Janoschka, T., Morgenstern, S., Hagemann, T., Muench, S., Hauffman, G., Gohy, J.-F., Hager, M.D., and Schubert, U.S. (2016). Poly(TEMPO)/Zinc Hybrid-Flow Battery: A Novel, "Green," High Voltage, and Safe Energy Storage System. Adv. Mater. *28*, 2238–2243.

185. Leung, P.K., Martin, T., Shah, A.A., Mohamed, M.R., Anderson, M.A., and Palma, J. (2017). Membrane-less hybrid flow battery based on low-cost elements. J. Power Sources *341*, 36–45.

186. Beard, K.W., and Reddy, T.B. (2019). LINDEN'S HANDBOOK OF BATTERIES, Fifth Edition (McGraw-Hill Education).

187. Pan, H., Shao, Y., Yan, P., Cheng, Y., Han, K.S., Nie, Z., Wang, C., Yang, J., Li, X., Bhattacharya, P., et al. (2016). Reversible aqueous zinc/manganese oxide energy storage from conversion reactions. Nat. Energy *1*, 16039.

188. Nickel-Zinc Chemistry Overview — ZincFive https://www.zincfive.com/nickelzinc-overview.

189. Zou, Y., Liu, T., Du, Q., Li, Y., Yi, H., Zhou, X., Li, Z., Gao, L., Zhang, L., and Liang, X. (2021). A four-electron Zn-I$_2$ aqueous battery enabled by reversible I$^-$/I$_2$/I$^+$ conversion. Nat. Commun. *12*, 1–11.

190. Xie, J., Yu, F., Zhao, J., Guo, W., Zhang, H.L., Cui, G., and Zhang, Q. (2020). An irreversible electrolyte anion-doping strategy toward a superior aqueous Zn-organic battery. Energy Storage Mater. *33*, 283–289.

191. Zhao, Y., Wang, Y., Zhao, Z., Zhao, J., Xin, T., Wang, N., and Liu, J. (2020). Achieving high capacity and long life of aqueous rechargeable zinc battery by using nanoporous-carbon-supported poly(1,5-naphthalenediamine) nanorods as cathode. Energy Storage Mater. *28*, 64–72.

192. Chen, Z., Mo, F., Wang, T., Yang, Q., Huang, Z., Wang, D., Liang, G., Li, Q., Chen, A., Guo, Y., et al. (2021). Zinc/Selenium Conversion Battery: A System Highly Compatible to both Organic and Aqueous Electrolytes. Energy Environ. Sci. *14*, 2441-2450.

193. Wu, B., Zhang, G., Yan, M., Xiong, T., He, P., He, L., Xu, X., and Mai, L. (2018). Graphene Scroll-Coated α-MnO$_2$ Nanowires as High-Performance Cathode Materials for Aqueous Zn-Ion Battery. Small *14*, 1703850.

194. Li, Q., Rui, X., Chen, D., Feng, Y., Xiao, N., Gan, L., Zhang, Q., Yu, Y., and Huang, S. (2020). A High-Capacity Ammonium Vanadate Cathode for Zinc-Ion Battery. Nano-Micro Lett. *12*, 3.

195. Zhang, L., Chen, L., Zhou, X., and Liu, Z. (2015). Towards High-Voltage Aqueous Metal-Ion Batteries Beyond 1.5 V: The Zinc/Zinc Hexacyanoferrate System. Adv. Energy Mater. *5*, 1400930.

196. Wan, F., Zhang, L., Wang, X., Bi, S., Niu, Z., and Chen, J. (2018). An Aqueous Rechargeable Zinc-Organic Battery with Hybrid Mechanism. Adv. Funct. Mater. *28*, 1804975.

197. Dubal, D.P., Ayyad, O., Ruiz, V., and Gómez-Romero, P. (2015). Hybrid energy storage: The merging of battery and supercapacitor chemistries. Chem. Soc. Rev. *44*, 1777–1790.

198. Zhang, Y.Z., Wang, Y., Cheng, T., Yao, L.Q., Li, X., Lai, W.Y., and Huang, W. (2019). Printed supercapacitors: Materials, printing and applications. Chem. Soc. Rev. *48*, 3229–3264.

199. Shao, Y., El-Kady, M.F., Sun, J., Li, Y., Zhang, Q., Zhu, M., Wang, H., Dunn, B., and Kaner, R.B. (2018). Design and Mechanisms of Asymmetric Supercapacitors. Chem. Rev. *118*, 9233–9280.

200. Tian, Y., Amal, R., and Wang, D.-W. (2016). An Aqueous Metal-Ion Capacitor with Oxidized Carbon Nanotubes and Metallic Zinc Electrodes. Front. Energy Res. *4*, 34.

201. Dong, L., Ma, X., Li, Y., Zhao, L., Liu, W., Cheng, J., Xu, C., Li, B., Yang, Q.H., and Kang, F. (2018). Extremely safe, high-rate and ultralong-life zinc-ion hybrid supercapacitors. Energy Storage Mater. *13*, 96–102.

202. Dong, L., Yang, W., Yang, W., Wang, C., Li, Y., Xu, C., Wan, S., He, F., Kang, F., and Wang, G. (2019). High-Power and Ultralong-Life Aqueous Zinc-Ion Hybrid Capacitors Based on Pseudocapacitive Charge Storage. Nano-Micro Lett. *11*, 94.

203. Liu, Q., Zhang, H., Xie, J., Liu, X., and Lu, X. (2020). Recent progress and challenges of carbon materials for Zn-ion hybrid supercapacitors. Carbon Energy *2*, 521–539.

204. Li, Z., Chen, D., An, Y., Chen, C., Wu, L., Chen, Z., Sun, Y., and Zhang, X. (2020). Flexible and anti-freezing quasi-solid-state zinc ion hybrid supercapacitors based on pencil shavings derived porous carbon. Energy Storage Mater. *28*, 307–314.

205. Liu, P., Liu, W., Huang, Y., Li, P., Yan, J., and Liu, K. (2020). Mesoporous hollow carbon spheres boosted, integrated high performance aqueous Zn-Ion energy storage. Energy Storage Mater. *25*, 858–865.

206. Lu, Y., Li, Z., Bai, Z., Mi, H., Ji, C., Pang, H., Yu, C., and Qiu, J. (2019). High energy-power Zn-ion hybrid supercapacitors enabled by layered B/N co-doped carbon cathode. Nano Energy *66*, 104132.

207. Pan, Z., Lu, Z., Xu, L., and Wang, D. (2020). A robust 2D porous carbon nanoflake cathode for high energy-power density Zn-ion hybrid supercapacitor applications. Appl. Surf. Sci. *510*, 145384.

208. Xiong, T., Shen, Y., Lee, W.S.V., and Xue, J. (2020). Metal Organic framework derived carbon for ultrahigh power and long cyclic life aqueous Zn ion capacitor. Nano Mater. Sci. *2*, 159–163.

209. Sun, G., Xiao, Y., Lu, B., Jin, X., Yang, H., Dai, C., Zhang, X., Zhao, Y., and Qu, L. (2020). Hybrid Energy Storage Device: Combination of Zinc-Ion Supercapacitor and Zinc-Air Battery in Mild Electrolyte. ACS Appl. Mater. Interfaces *12*, 7239–7248.

210. Han, J., Wang, K., Liu, W., Li, C., Sun, X., Zhang, X., An, Y., Yi, S., and Ma, Y. (2018). Rational design of nano-architecture composite hydrogel electrode towards high performance Zn-ion hybrid cell. Nanoscale *10*, 13083–13091.

211. Wang, N., Xin, T., Zhao, Y., Li, Q., Hu, M., and Liu, J. (2019). Boosting the Capacitance of an Aqueous Zinc-Ion Hybrid Energy Storage Device by Using Poly(3,3′-dihydroxybenzidine)-Modified Nanoporous Carbon Cathode. ACS Sustain. Chem. Eng. *7*, 14195–14202.

212. Zhang, J., Zhou, Q., Tang, Y., Zhang, L., and Li, Y. (2019). Zinc-air batteries: Are they ready for prime time? Chem. Sci. *10*, 8924–8929.

213. Shinde, S.S., Jung, J.Y., Wagh, N.K., Lee, C.H., Kim, D.-H., Kim, S.-H., Lee, S.U., and Lee, J.-H. (2021). Ampere-hour-scale zinc–air pouch cells. Nat. Energy *6*, 592–604.

214. Yao, B., Chandrasekaran, S., Zhang, J., Xiao, W., Qian, F., Zhu, C., Duoss, E.B., Spadaccini, C.M., Worsley, M.A., and Li, Y. (2019). Efficient 3D Printed Pseudocapacitive Electrodes with Ultrahigh MnO_2 Loading. Joule *3*, 459–470.

215. He, Y., Zhang, J., He, G., Han, X., Zheng, X., Zhong, C., Hu, W., and Deng, Y. (2017). Ultrathin Co_3O_4 nanofilm as an efficient bifunctional catalyst for oxygen evolution and reduction reaction in rechargeable zinc-air batteries. Nanoscale *9*, 8623–8630.

216. Guo, X., Hu, X., Wu, D., Jing, C., Liu, W., Ren, Z., Zhao, Q., Jiang, X., Xu, C., Zhang, Y., et al. (2019). Tuning the Bifunctional Oxygen Electrocatalytic Properties of Core-Shell Co_3O_4@NiFe LDH Catalysts for Zn-Air Batteries: Effects of Interfacial Cation Valences. ACS Appl. Mater. Interfaces *11*, 21506–21514.

217. Chen, S., Cheng, J., Ma, L., Zhou, S., Xu, X., Zhi, C., Zhang, W., Zhi, L., and Zapien, J.A. (2018). Light-weight 3D Co-N-doped hollow carbon spheres as efficient electrocatalysts for rechargeable zinc-air batteries. Nanoscale *10*, 10412–10419.

218. Sun, H., Liu, S., Wang, M., Qian, T., Xiong, J., and Yan, C. (2019). Updating the Intrinsic Activity of a Single-Atom Site with a P-O Bond for a Rechargeable Zn-Air Battery. ACS Appl. Mater. Interfaces *11*, 33054–33061.

219. Zhong, X., Yi, W., Qu, Y., Zhang, L., Bai, H., Zhu, Y., Wan, J., Chen, S., Yang, M., Huang, L., et al. (2020). Co single-atom anchored on Co_3O_4 and nitrogen-doped active carbon toward bifunctional catalyst for zinc-air batteries. Appl. Catal. B Environ. *260*, 118188.

220. Li, M., Luo, F., Zhang, Q., Yang, Z., and Xu, Z. (2020). Atomic layer Co_3O_{4-x} nanosheets as efficient and stable electrocatalyst for rechargeable zinc-air batteries. J. Catal. *381*, 395–401.

221. Wang, X., Sunarso, J., Lu, Q., Zhou, Z., Dai, J., Guan, D., Zhou, W., and Shao, Z. (2020). High-Performance Platinum-Perovskite Composite Bifunctional Oxygen Electrocatalyst for Rechargeable Zn–Air Battery. Adv. Energy Mater. *10*, 1903271.

List of Figures

Figure 1. Ragone plot of application scenarios of EES devices.

Figure 2. The adaptability of various EES technologies in representative application scenarios.

In this figure: LIBs = Li-ion batteries, Pb-acid = lead-acid batteries, Ni-MH = Ni-metal hydride batteries, VRFBs = all-vanadium redox flow batteries, AZIBs = aqueous Zn-ion batteries, ZSCBs = Zn solid-state conversion-type batteries, ZRFBs = Zn-based redox flow batteries, and ZHSCs = Zn hybrid supercapacitors.

Figure 3. The development history of representative Zn-based EES devices.

Figure 4. Energy storage mechanism of aqueous Zn-based EES devices.

Schematic of typical electrochemical charateristics of electrodes with capacitive, capacitive-Faradaic and Faradaic processes in a) cyclic voltammogram (CV), b) galvanostatic charge-discharge (GCD) profile, and c) Nyquist plot; d) capacity-potential (CP) curve for $LiCoO_2$ particles with different sizes[37]; e) band model for charge storage mechanisms. Reprinted with permission from Chen *et al.*[9] Copyright 2017 Taylor & Francis.

Figure 5. Interfaces and interphases in AZDs.

Band diagrams of the HOMO and LUMO of batteries with a) non-aqueous electrolytes and b) aqueous electrolytes. Schematic illustration of interfacial phenomena experienced in aqueous batteries with c) liquid electrolytes and d) solid-state electrolytes.

Figure 6. Electrochemistry and challenges of Zn deposition/dissolution.

a) Pourbaix diagram for Zn-H_2O system at $[Zn]_t = 0.1$ M; schematical diagram of b) homogeneous Zn deposition, and c) inhomogeneous Zn deposition with the dendrite growth; schematical diagram of the formation of d) HER, and e) the passivation. In this figure: Grey ball = Zn^{2+} near the Zn anode, blue ball = electrodeposited Zn atoms, green ball = H_2 molecules, and yellow ball = passivation products.

Figure 7. Electrolyte pH value selection.

a) Molar fraction distribution of particular Zn species as a function of pH values; b) the pH dependence of the solubility of Zn(II) species (the concentration of total Zn(II) species is 10^{-6} M); Reprinted from Maret *et al.*[63] c) the pH values of electrolytes with different compositions; d) Zn^{2+}-solvation structures in the electrolytes with 1 M Zn(TFSI)$_2$ and 5 M, 10 M, 20 M LiTFSI. Reprinted with permission from Wang *et al.*[28] Copyright 2018 Springer Nature.

Figure 8. Classification of cathodes for aqueous Zn-based EES devices.

Figure 9. Schematic diagram of energy storage mechanisms and promising strategies of insertion-type cathodes.

Schematical diagram of a) reversible Zn^{2+} (de)insertion; b) conversion reaction; c) Zn^{2+} and H^+ co-(de)insertion.

Figure 10. Schematical diagram of ORR reaction pathways in alkaline electrolytes.

Figure 11. Schematic diagram of energy storage mechanisms for EDLC cathodes.

a) EDLC model; b) the potential distribution of a EDLC model.

Figure 12. Electrochemistry of membrane.

a) Ion mass transfer in liquid electrolytes; membrane configurations: b) membrane-free, c) single-membrane, and d) double-membrane.

Figure 13. Electrochemistry of flow system.

a) Convert diffusion-controlled to convection-controlled process; b) reduce internal resistance; c) maintain stable electrolyte composition.

Figure 14. Possible cell configurations.

Figure 15. Aqueous Zn-based EES devices for high-capacity applications.

a) Configuration of conventional all-liquid phase redox flow batteries (RFBs); configuration of Zn based hybrid redox flow batteries (ZRFBs) with b) single-membrane, single/double-flow, c) membrane-free, single flow, d) membrane-free, flow assisted and e) double-membrane, single/double/multi-flow.

Figure 16. Aqueous Zn-based EES devices for high power density applications.

a) Conventional Zn-based solid-phase conversion-type batteries (ZSCBs): b) novel ZSCBs; c) aqueous Zn-ion batteries (AZIBs); ZSCBs or AZIBs with d) double-membrane, e) membrane-free, flow-assisted system.

Figure 17. Aqueous Zn-based EES devices for ultrahigh power density applications.

Configuration of a) electro-double layer capacitors (EDLCs) and b) pseudocapacitors; configuration of Zn based hybrid supercapacitors (ZHSCs) with c) EDLC or pseudocapacitive cathodes, and d) hybrid cathodes.

Figure 18. Aqueous Zn-based EES devices for high energy density applications.

a) Configuration of conventional Zn-air batteries (ZABs); b) ZABs with hybrid cathodes. a) Conventional Zn-air batteries (ZABs): b) improved ZABs; c) ZABs with hybrid cathodes; d) novel ZSCBs; e) ZSCBs or AZIBs with double membranes.

Figure 19. Performance comparison of AZDs and other EES devices.

a) Ragone plot of AZDs and other EES devices (exclude devices with flow systems); b) areal capacity of state-of-the-art AZDs and other EES devices.

Figure 20. Multi-angle evaluation of strategies for AZDs.